STABILIZATION STUDY OF SURFACE MODIFIED MAGNETITE NANOPARTICLES IN NITRILE BUTADIENE RUBBER LATEX

TAI MUN FOONG

DISSERTATION SUBMITTED IN FULFILMENT OF THE REQUIREMENTS FOR THE DEGREE OF MASTER OF PHILOSOPHY

INSTITUTE OF GRADUATE STUDIES
UNIVERSITY OF MALAYA
KUALA LUMPUR

2016

UNIVERSITY OF MALAYA
ORIGINAL LITERARY WORK DECLARATION

Name of Candidate: TAI MUN FOONG

Registration/Matric No: HGA130010

Name of Degree: Master of Philosophy

Title of ~~Project Paper/Research Report/Dissertation/~~Thesis ("this Work"):

Stabilization Study of Surface Modified Magnetite Nanoparticles in Nitrile Butadiene Rubber Latex

Field of Study: Material Engineering (Nanotechnology)

I do solemnly and sincerely declare that:

(1) I am the sole author/writer of this Work;
(2) This Work is original;
(3) Any use of any work in which copyright exists was done by way of fair dealing and for permitted purposes and any excerpt or extract from, or reference to or reproduction of any copyright work has been disclosed expressly and sufficiently and the title of the Work and its authorship have been acknowledged in this Work;
(4) I do not have any actual knowledge nor do I ought reasonably to know that the making of this work constitutes an infringement of any copyright work;
(5) I hereby assign all and every rights in the copyright to this Work to the University of Malaya ("UM"), who henceforth shall be owner of the copyright in this Work and that any reproduction or use in any form or by any means whatsoever is prohibited without the written consent of UM having been first had and obtained;
(6) I am fully aware that if in the course of making this Work I have infringed any copyright whether intentionally or otherwise, I may be subject to legal action or any other action as may be determined by UM.

    Candidate's Signature   Date:

Subscribed and solemnly declared before,

    Witness's Signature   Date:

Name:

Designation:

ABSTRACT

In the present study, magnetite nanoparticles (<50 nm) with high saturation magnetization (80.23 emu/g) was successfully synthesized through co-precipitating technique by co-precipitating iron (II) and iron (III) chloride salts in the presence of 3.00 M ammonium hydroxide at final pH 9.5. It was found that increasing the final pH and total iron salts concentration increased saturation magnetization, but the variation of ammonium hydroxide concentration did not change the saturation magnetization. In contrast, the saturation magnetization decreased from 80.23 emu/g to 64.83 emu/g when the addition rate of ammonium hydroxide was increased from 5 ml/min to 20 ml/min. The reduction of saturation magnetization for these samples was due to decrease in the crystallite size of the particles with increasing addition rate.

Additional continuous efforts were made to further improve the dispersion stability of magnetite nanoparticles in aqueous media by modifying the magnetite surface using surface modifiers (e.g., polyethylene glycol, oleic acid) to generate an effective repulsive force in between particles. It was found that the resultant MNPs incorporated with oleic acid demonstrated a maximum stability in maintaining good colloidal dispersion. This MNPs colloidal suspension performance was approximately 7 times higher (21 days) than the uncoated MNPs (3 days). The reason can be mainly attributed to the formation of oleate secondary layer in the bilayer oleic acid coated MNPs that enabled the MNPs to be well dispersed in polar (acrylonitrile) and non-polar (butadiene) parts of the building block of nitrile latex. In addition, the oleic acid coating layer could reduce the oxidation reaction that trigger phase transition as compared with PEG coating. Thermogravimetric analysis (TGA) measurements suggested that there was two kinds of binding between molecules of oleic acid and magnetite. The coating density of PEG and oleic acid on the MNPs particle surface increased with increasing loading amount.

The mechanical properties of nitrile butadiene rubber latex film were reduced by the addition of oleic acid coated MNPs but it is within the acceptable range. Lastly, the results proved that NBR latex film incorporated with oleic acid coated MNPs has improved magnetic properties and thermal stability. The saturation magnetization of NBR latex film was increased from 0.19 emu/g to 1.85 emu/g. Based on the results, oleic acid coated MNPs is the ideal magnetic additive for metal detectable glove application.

ABSTRAK

Dalam kajian ini, nanozarah magnetit (< 50 nm) yang mempunyai pemagnetan tepu yang tinggi (80.23 emu/g) telah berjaya disediakan melalui kaedah pemendakan kimia. Dalam cara ini, garam ferum (II) dan ferum (III) klorida akan mendak di bawah kehadiran 3.00 M ammonium hidroksida pada pH 9.5. Pemagnetan tepu nanozarah magnetit didapati meningkat apabila menggunakan pH dan jumlah kepekatan garam yang tinggi tetapi tiada perubahan bagi kepekatan ammonium hidroksida. Pemagnetan tepu bagi kadar penambahan ammonium hidroksida adalah berbeza, kekuatannya berkurangan dari 80.23 emu/g ke 64.83 emu/g apabila kadar ini meningkat dari 5 ml/min ke 20 ml/min. Penurunan pemagnetan tepu nanozarah adalah disebabkan oleh pengurangan saiz kristalit.

Kestabilan sebaran nanozarah dalam media akueus telah diwujudkan dengan menggunakan pengubah permukaan (polyethylen glikol, asid oleik) supaya daya tolakan wujud di antara zarah. MNPs yang bersalut asid oleik telah mencapai kestabilan yang maksimum. Prestasi ampaian kolloid MNPs bersalut asid oleik ini adalah tujuh kali ganda (21 hari) lebih tinggi daripada MNPs yang tidak bersalut (3 hari). Hal ini demikian kerana dua lapisan asid oleik ini membolehkannya bersebar dalam bahagian berkutub dan bahagian tidak berkutub yang terdapat dalam blok binaan latek nitril. Selain itu, lapisan asid oleik ini dapat mengurangkan tindak balas pengoksidaan yang akan menyebabkan transformasi fasa magnetit. Analisa thermogravimetrik menunjukkan dua jenis ikatan di antara molekul asid oleik dan magnetit. Di samping itu, kepadatan salutan pada permukaan zarah meningkat apabila jumlah muatannya meningkat.

Kekuatan mekanikal filem latek nitril didapati menurun selepas penambahan MNPs bersalut asid oleik tetapi ia masih dalam julat yang boleh diterima. Akhir sekali, sifat magnetik dan kestabilan haba bagi filem latek nitril yang mengandungi MNPs bersalut

asid oleik telah meningkat. Sifat pemagnetan tepu filem latek ini telah bertambah dari 0.19 emu/g ke 1.85 emu/g. Berdasarkan hasil kajian ini, MNPs bersalut asid oleik adalah pengisi magnetik yang paling sesuai bagi aplikasi sarung tangan magnetik.

ACKNOWLEDGEMENTS

First and foremost, I would like to thank my supervisors, Prof. Dr. Sharifah Bee Abd Hamid and Dr. Lai Chin Wei for their patient guidance, support and invaluable advice provided throughout my master studies at University of Malaya.

Special thanks go to Dr. Orathai Boodamnoen and Dr. Roshasnorlyza Hazan for their encouragement, and helpful discussion throughout my research. Then, I would like to give a grateful thank to all the research assistant and friends in NANOCAT who helped me along the way. My research cannot be completed smoothly without their assistance and I really appreciate their help. Moreover, I would like to convey thanks to Ministry of Higher Education Malaysia for providing me with MyMaster fund.

Last but not least, I wish to thank my family for unconditional support during my master studies and other people who lent me a hand throughout my master study and gave a full cooperation to make every loading a success. Thank you.

TABLE OF CONTENTS

LIST OF FIGURES

LIST OF TABLES

LIST OF SYMBOLS AND ABBREVIATIONS

EPDM	:	Ethylene propylene diene monomer
FDA	:	Food and Drug Administration
FESEM	:	Field Scanning Electron Microscope
FTIR	:	Fourier Transform Infrared Spectroscopy
HRTEM	:	High-resolution Transmission Electron Microscope
MNPs	:	Magnetite nanoparticles
MRI	:	Magnetic resonance imaging
NBR	:	Nitrile butadiene rubber
OA	:	Oleic acid
PEG	:	Polyethylene glycol
PFCA	:	Perfluorocarboxylic acid
SDBS	:	Sodium Dodecyl Benzene Sulphonate
SPIONs	:	Superparamagnetic iron oxides
TGA	:	Thermogravimetric analysis
USD	:	United States dollar
USPIONs	:	Ultra-small superparamagnetic iron oxides
UTM	:	Universal Testing Machine
VSM	:	Vibrating sample magnetometer
XRD	:	X-ray diffraction
ZDBC	:	Zinc Dibutyldithiocarbamate
α	:	Alpha-form crystal structure
β	:	Beta-form crystal structure
γ	:	Gamma-form crystal structure
H_c	:	Coercivity

M_s	:	Saturation magnetization
M_r	:	Remanence/Retentivity
phr	:	Part per hundred of rubber
Tc	:	Curie temperature
TSC	:	Total solid content
μ_r	:	Relative permeability
χ	:	Magnetic susceptibility

LIST OF APPENDICES

CHAPTER 1: INTRODUCTION

1.1   Overview

This chapter contains the introduction to the nitrile gloves and the food safety issues in which the research is concerned with, the aims and objectives of the study, and the scope of the thesis.

1.2   Introduction

The total world rubber glove demand is estimated to be 160 billion pieces per year. Based on this customer's estimation, the percentage of total rubber glove used for food processing and handling is approximately 5-10%. This relates to a total of 8-16 billion pieces. This may represent another USD 146 million to USD 438 million. Gloves for food processing and handling in Japan are a competitive business due to cheap imports from China. Manufacturing or packaging line employees in prepared food and pharmaceuticals industries are generally required to wear sealed gloves for hygiene purpose (Rajasekar et al., 2009).

Gloves are commonly made from latex, vinyl, nitrile or polyethylene co-polymer, with vinyl and polyethylene gloves being the cheaper options. Nitrile butadiene rubber (NBR) gloves are more durable and have good elasticity, which provides comfort and dexterity. During the course of manufacturing or packaging, small pieces of the glove may become torn off or separated from the glove and become contaminant to the food product. Research on rubber nano-composites can be both fundamental and applied, and has attracted growing attentions to increase the mechanical and detectable properties of the rubber glove.

Numerous studies have demonstrated that the uniform distribution of nano-scaled filler particles into a rubber matrix, with reasonably good interfacial bonding strength, could lead to a rubber nano-composite with significantly improved properties (Lu et al., 2008). For example, by distributing 10 phr of organically modified montmorillonite into NBR, the tensile strength of the resulting rubber nano-composite could exceed 18 MPa, which was 9 times higher than that of the neat NBR (Ramesan et al, 2005). It was also reported that when the particle size of magnesium hydroxide ($Mg(OH)_2$) was reduced from micron-level to nano-level, both the mechanical and the fire retardation properties of its filled ethylene propylene diene monomer (EPDM) rubber could be substantially improved (Lu et al.,2008). Theoretical analyses have suggested that properties of nano-filler particles, interfacial bonding strength of filler/matrix, and uniform distribution of nano-filler particles were the most important factors on the properties of rubber nano-composites.

Nowadays, magnetic field is an important parameter for studying the physical properties of materials (L évy et al., 2005; Na et al., 2006)-. Recently, magnetic field, similar to the conventional reaction parameters such as temperature and pressure, has been introduced as a new tool to control chemical reactions, materials synthesis in several systems, such as electrochemical process, solid state reactions, hydrothermal synthesis, sol-gel synthesis and precipitation synthesis (Qi et al, 2009).

Superparamagnetic nanoparticles are currently used as contrast agent in magnetic resonance imaging (MRI) (Sonvico et al., 2005). They are originally ferromagnetic substances which have lost their permanent magnetism due to their small size. The magnetization of such nanoparticles follows an external magnetic field without any hysteresis and they are better known as "superparamagnetic" due to their large magnetic susceptibility (Corot et. al, 2006). These nanoparticles consist of a coated iron oxide core

(magnetite, maghemite or other insoluble ferrites) characterized by a large magnetic moment in the presence of a static external magnetic field.

They are classified into two main groups according to their size (Mornet et al., 2005; Roch et al., 2005). SPIONs (superparamagnetic iron oxides) have a hydrodynamic size greater than 50 nm (coating included). They show interesting properties such as superparamagnetism, high field irreversibility, high saturation field, extra anisotropy contributions or shifted loops after field cooling (Marghussian, 2015). USPIONs (ultra-small superparamagnetic iron oxides), whose nanoparticles are smaller than 50 nm included the hydrodynamic size coating (Esterlrich et al., 2015).

Magnetite (Fe_3O_4), maghemite (γ-Fe_2O_3) and hematite (α-Fe_2O_3) are three main iron oxides that fall under the category of SPIONs. Ferrites, which are mixed oxides of iron and other transition metal ions (e.g. Cu, Co, Mn, and Ni), have also been reported to be superparamagnetic (Spaldin, 2010). Hematite is the oldest known of the iron oxides and is widespread in rocks and soils. It is also known as ferric oxide, iron sesquioxide, red ochre, specularite, specular iron ore, kidney ore, or martite. Hematite is extremely stable at ambient conditions, and often is the end product of the transformation of other iron oxides. Magnetite is also known as black iron oxide, magnetic iron ore, loadstone, ferrous ferrite, or Hercules stone. It exhibits the strongest magnetism of any transition metal oxide (Majewski & Thierry, 2007).

The precipitation technique is the simplest and most efficient chemical pathway to obtain iron oxide particles. Iron oxides (FeOOH, Fe_3O_4 or γ-Fe_2O_3) are usually prepared by addition of alkali to iron salt solutions and keeping the suspensions for ageing. The main advantage of the precipitation process is that a large amount of nanoparticles can be synthesized. However, the control of particle size distribution is limited, because only kinetic factors are controlling the growth of the crystal (Mohapatra & Anand, 2010).

In the precipitation process, two stages are involved i.e., a short burst of nucleation occurs when the concentration of the species reaches critical super saturation, and then, there is a slow growth of the nuclei by diffusion of the solutes to the surface of the crystal. To produce monodisperse magnetite nanoparticles, these two stages should be separated; i.e., nucleation should be avoided during the period of growth (Tartaj et. al., 2006). A wide variety of factors can be adjusted in the synthesis of magnetite nanoparticles to control size, magnetic characteristics, or surface properties. The size and shape of the nanoparticles can be tailored with relative success by adjusting pH, ionic strength, temperature, nature of the salts (perchlorates, chlorides, sulfates, and nitrates), or the Fe(II)/Fe(III) concentration ratio (Mohapatra & Anand, 2010).

A great variety of polymers with hydroxyl, carboxylate, carboxyl, styrene or vinyl alcohol groups have been used in magnetite nanoparticles production. Coating or encapsulation of particles with polymers is the oldest and simplest method of magnetite nanoparticles preparation. Other methods include e. g. suspension, dispersion or emulsion polymerization (Utkan et al., 2011). The most common polymers used to stabilize bare magnetic nanoparticles are starch and dextran and its derivatives, polyethylene glycol, alginate, polyvinyl alcohol, chitosan, polylactide, poly (ethylene imine), and dendrimers (Garcá-Jimeno & Estelrich, 2013). Stabilization can be achieved by several approaches, including *insitu* coatings and post synthesis coatings (Laurent et al.,2008). Nanoparticles are coated during synthesis for *in situ* coatings, while post-synthesis coating method consists of grafting the polymer onto the magnetic nanoparticles once synthesized.

1.3   Problem Statement

Nitrile butadiene rubbers (NBR) are copolymer of a diene and a vinyl-unsaturated nitrile. It was obtained by emulsion polymerization of acrylonitrile and butadiene (Roff & Scott, 2013). Recently, many gloves are made by nitrile rubber, used in home and

industrial cleaning and medically as examination and disposable gloves. Nitrile gloves offer greater puncture resistance compared to natural rubber gloves (Carraher, 2012). However, nitrile gloves have limitation to strength and hence it can be broken easily. During the manufacturing, small pieces of the glove may become torn off or separated from the glove. The small pieces of glove may become contaminants in the food or pharmaceutical product being handled. As there are some parts of glove missing, the production comes to a halt to trace back the missing part in the product. If the missing part of the glove is not traced, then the whole shift food production will be disposed.

The white or light flesh-colour glove pieces are often difficult to discern from the product and, therefore, become very difficult to remove prior to packaging and shipping the product. Detecting glove pieces may be solved by use of gloves of a colour that distinctively contrasts the colour of the product. However, reliance upon visual detection alone leaves room for human error and missed contaminants may be packaged with the food product (Haddock et al., 2006). To overcome this situation, magnetite nanoparticles (MNPs) will be incorporated to nitrile butadiene rubber glove.

The goal is to deliver a glove where broken parts of the glove can be detected via a metal detectable device. The magnetic response of magnetite nanoparticles (MNPs) in magnetic field provides a chance to manipulate or assemble the MNPs via *in situ* method or in a controlled manner. Therefore, the magnetic nanoparticles has been focus of much recently as a detectable agent with the modulation of its composition, size and magnetic properties that can permits its use in variety format of detectable device. Magnetite nanoparticles (MNPs) has high superparamagnetic properties, low Curie temperature, high magnetic susceptibility, non-toxic and good antibacterial properties. Magnetite nanoparticles are the only FDA approved nanoparticles used in the pharmaceutical industry. As far as the size and size-dispersivity control are concerned, tendency to isolate

magnetic nanostructures for aggregating into bigger cluster, driven by particle-particle interaction and /or by reduction of energy associated to the high surface to volume ratio has represented a critical major problem due to the properties of MNPs.

To improve the dispersion stability of MNPs in aqueous media, strategies to modify the MNPs surface by modifiers (small organic molecules, surfactants and polymers) to generate an effective repulsive force have been conducted. Besides that, protecting shells not only to stabilize the magnetic properties but it can be used for further protection of magnetic nanoparticles against oxidation by oxygen, or erosion by acid or base. Coating agent, either small organic molecules or polymer, which could provide sufficient repulsive interactions to prevent agglomeration must be able to balance the magnetic and the van der Waals attractive forces acting on the nanoparticles. In addition, the coating agent must not contain environmentally and harmful elements, not impair interaction between magnetite and binder, and it has to be cheap.

Coating of magnetite nanoparticles can prevent the agglomeration of the magnetite particles in aqueous solution effectively, and obtain stable magnetic suspension which can easily be blended together with others latex compounding ingredients when initially introduces in the formulation process giving homogenized latex compound. Then, the final product, a metal detectable glove which contain the magnetite particles in its entire shape of glove can be produced.

1.4 Objectives

The objectives of this research are listed as below:

i. To develop synthesis methodology of magnetite nanoparticles (MNPs) by co-precipitation method, yielding particle size < 100 nm.

ii. To stabilize magnetite nanoparticles (MNPs) in nitrile butadiene rubber latex by incorporation of coating agents from chemical oxidation and agglomeration.

1.5 Outline of Research Work

Generally, this research studies can be divided into four stages, namely, synthesis of magnetite nanoparticles (MNPs), synthesis of coated MNPs, characterization of MNPs and coated MNPs, and performance test on nitrile butadiene rubber latex film loaded with MNPs.

Part I: Synthesis of Magnetite Nanoparticles (MNPs)

In this stage, magnetite nanoparticles was primarily synthesized through co-precipitation method. Operational parameters such as final pH, precipitating agent concentration, iron salt concentration, and addition rate were optimized to produce the required size and magnetic properties for MNPs.

Part II: Synthesis of Coated MNPs

The synthesis of coated MNPs were carried out based on the reaction condition of MNPs with the highest saturation magnetization in previous section (**Part I**). Coated MNPs were fabricated using *in situ* coating technique, where coating agents (e.g., polyethylene glycol, oleic acid) with different loading amount were introduced into the iron salts solution before the addition of ammonium hydroxide solution. In this stage, sedimentation test was carried out to evaluate the stability of MNPs in nitrile butadiene

rubber latex. Sediment of coated MNPs were observed and recorded at 3 hours, 3 days, 7 days, 14 days and 21 days.

Part III: Characterization of MNPs and coated MNPs

The structural, morphological, chemical, magnetic properties of uncoated and coated MNPs were characterized via various characterization techniques. The characterization techniques are X-ray diffraction (XRD), Raman spectroscopy, Field Scanning Electron Microscope-Energy Dispersive Spectroscopy (FESEM-EDS), High-resolution Transmission Electron Microscope (HRTEM), and Fourier Transform Infrared Spectroscopy (FTIR). Meanwhile, the magnetic properties of the MNPs were measured by Vibrating Sample Magnetometer (VSM) operated at room temperature. In addition of that, Zeta Sizer was used to measure the particle size distribution and zeta-potential of the nanoparticles produced. Lastly, the formation of coating and estimation of binding efficiency on the surface of MNPs were investigated via Thermogravimetric analysis (TGA). The principle and the measuring conditions of each measurement are discussed in **Chapter 3-Research Methodology**.

Part IV: Performance Test of MNPs loaded nitrile butadiene rubber latex films

In this final stage, the performance test of the prepared nitrile butadiene rubber films modified with MNPs was carried out. Firstly, the nitrile butadiene rubber latex compound was incorporated with optimized oleic acid coated MNPs during the compounding process. Then, latex films were formed by a series of dipping process. The measurement of magnetic properties as well as mechanical properties of nitrile butadiene rubber latex films incorporated with MNPs were measured by Vibrating Sample Magnetometer (VSM) and Universal Testing Machine (UTM). In addition, thermal stability of the nitrile butadiene rubber latex films was investigated via Thermogravimetric analysis (TGA).

CHAPTER 2: LITERATURE REVIEW

2.1 Introduction and Overview

This chapter contains the introduction of the nitrile gloves, detection of glove fragments, and development of magnetic detectable gloves. Next, magnetic behaviour of magnetite nanoparticles begin with the fundamentals of magnetism and their deviations from respective bulk properties. Lastly, the stabilization of magnetite nanoparticles by surfactants (e.g., polyethylene glycol and oleic acid) was also presented in this chapter.

2.2 Nitrile Butadiene Rubber

Nitrile butadiene rubber, also known as acrylonitrile butadiene rubber or as nitrile rubber, is an unsaturated synthetic rubber copolymer of acrylonitrile and butadiene (NCPS Board, 2013). It was invented in a German program to substitute natural rubber during 1930s.
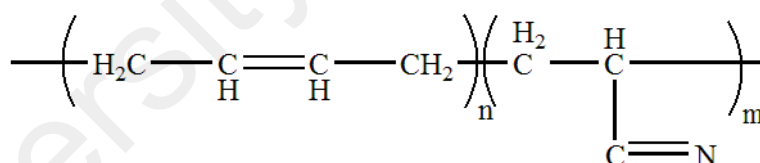
Figure 2.1: Chemical structure of nitrile butadiene rubber

Nitrile butadiene rubber is produced either by hot or cold emulsion polymerization (Kent, 2010). Most of the nitrile butadiene rubber is produced by cold emulsion polymerization at about 5 ℃, and this result in more linear polymer which are easier to process than 'hot' polymers. Hot nitrile butadiene rubber polymers are polymerized at 40 ℃ to produce highly branched polymers. As a matter of fact, branching not only can provide good tack and a strong bond in adhesive applications but also offer better tear strength (Klingender, 2008).

As the Acrylonitrile content is increased, the molecules becomes less hydrophilic and more polar. The primary properties affected are the glass transition temperature and solubility parameter and both increase with increasing acrylonitrile content. The acrylonitrile content in commercially available nitrile rubber are ranges from 18 % to 50 %. The grade of Nitrile rubber used is determined by the final properties required, and by the percentage of acrylonitrile present (Whelan, 2012).

Table 2.1: Grade of nitrile butadiene rubber

Grade of nitrile rubber	Percentage of acrylonitrile (%)
Low	18-24
Medium low	26-28
Medium	34
Medium high	38-40
High	50

The acrylonitrile content of the nitrile rubber has an important effect on the physical properties of the Nitrile rubber. As acrylonitrile content increases, the oil and fuel resistance, tensile strength, hardness, heat resistance, abrasion resistance, and compatibility with polar materials increases while low temperature flexibility, resilience, compression set, and gas permeability reduces (Whelan, 2012).

2.2.1   Nitrile Butadiene Rubber Latex

Nitrile butadiene rubber was available as a latex, which is widely used in glove manufacturing industry. A latex is any polymer emulsified in an aqueous medium, it refer to any synthetic polymers "dispersed" or "emulsified" in water (Rapra Technology Limited, 2006). Nitrile butadiene rubber latex is also used in the application of paper saturation, abrasive, leather finishing, nonwoven binders and tape release coating (Kent , 2010).

2.2.2 Nitrile Glove

In the late 1980s, Neil E. Tillotson and Luc G. DeBecker invented the disposable Nitrile Latex Glove. They filed for a patent in May 11th of 1990 and the patent was finally granted to the Tillotson Corporation in May 14th of 1991. This invention aims to produce a latex glove that does not numb or fatigue the wearer's hand when worn continuously for extended period of time.

Nitrile gloves are mainly made from carboxylated nitrile (XNBR) latex, which can be synthesized from monomers of acrylonitrile, butadiene and carboxylic acid. Each composition variation of the monomers will provide a specific function for the synthetic latex gloves. Acrylonitrile imparts penetration resistance from chemicals such as fats, hydrocarbon oils, and solvents. The stiffness and chemical resistance of the nitrile gloves increased with the concentration of acrylonitrile. Butadiene incorporate softness and flexibility and contributes to the elasticity of the glove. Carboxylic acid contributes to the tensile strength, or the tear resistance of the glove but reduce in water resistance, resilience, compression set, and low temperature properties. The characteristics of the glove can modified by changing the composition of these monomers (Gaza & Zaborski, 2016).

Generally, nitrile gloves possess greater puncture resistant than natural rubber latex gloves. They provide superior resistance to puncture and also used for protection against various chemicals (Neville, 2013). However, nitrile gloves are stiffer and more expensive than natural rubber latex gloves (Lipinski & Tang, 2010). It also exhibit inferior tensile strength when compared to natural rubber latex gloves. Table 2.2 shows the different between nitrile gloves and natural rubber latex gloves (Jayanthy & Sankaranarayanan, 2005; Galpaya & Dona, 2009).

11

Table 2.2: The comparison of nitrile gloves and natural rubber latex gloves

Nitrile gloves	Natural rubber latex gloves
Durables	Not as durable as nitrile gloves
Consistent in latex composition	Latex composition depending on many factors (season, soil, weather)
Synthetic product without natural latex proteins	High risk of Type I hypersensitivity (latex protein allergens)
Excellent chemical resistance	Limited protection over range of chemicals
Longer shelf life (5 years)	Shorter shelf life (3 years)
Odour free	Unpleasant odour

2.2.3   Detection and Tracing of Nitrile Gloves Fragments

Food borne hazards include all undesirable biological, chemical and physical substances and contaminants that can be found in food and that pose a health risk to consumers. Physical hazards that are often found in food and drug include: metal fragments, screws, machine filings, glass pieces, stones, insulation/paint, plastic material fragments, personal effects such as jewellery, buttons and nail fragments, insect parts and fragments (Weston, 2014).

To overcome this issues, effective inspection system was developed by utilising fast and non-destructive methods for sensing the safety situation of food produce (Feng & Sun, 2012). Metal detector, and x-ray technology seem to be the most effective methods to identify contaminant in food. Metal detector are a cost-effective solution for identifying metallic foreign object contaminant, but it has a major drawback that only metal can be detected. X-ray detection systems are able to find metal contaminants, and other solid contaminants with different densities than metal. The x-ray detection equipment produces an image of the food product that can be analysed for contamination (Haff & Toyofuku, 2008). The comparison between X-ray and Metal detection system is shown in Table 2.3. Plastic contaminant present the most serious detection challenges as they are unable to be detected by metal detection and the density of plastic is most likely similar to the product

it is within, which makes detecting through x-ray inspection difficult. Most commonly found plastics in food are low-density polyethylene and polyethylene films used in packaging and rubber/plastic gloves (Lewis, 2014).

Table 2.3: Comparison between X-ray and Metal detection system (Ries, 2014)

Metal detection	X-ray inspection
Long lifetime even in the harshest environments.	Moderate lifetime in harsh environments.
Dry products, small products, piped or bulk products have best sensitivity.	Large packaged products and cases can be inspected.
Conductive (wet/salty) products are the most difficult to ignore.	Dense products with a lot of texture are the most difficult to achieve good performance.
Operates over a wide range of speeds.	Speed must be constant within a limited range.
Performance dependent on aperture size, and coil configuration.	Performance dependent on X-ray source, receiver, and power.

The wearing of gloves by worker in manufacturing or packaging line in the prepared–food pharmaceutical, and agri-food industries are important to protect products from contamination and to maintain a high standard of hygiene and cleanliness (Lucas et al., 2006). In this case, the tiny fragment of glove that is torn due to manufacturing defect or failure during usage will mix into food or drug as a foreign body which pose risks of injury or choking to consumers. The conventional methods to identify a glove fragments are visual inspection. It is accepted practice that operatives' gloves should be coloured blue and it is now a requirement in many countries that this procedure be followed so that gloves can be detected visually. However, reliance upon visual detection alone leaves room for human error and missed contaminants may be packaged with the product, particularly where small glove pieces are concerned (Lucas et al., 2006).

By incorporating detectable additives during manufacturing to magnetize the glove, broken pieces or fragments of glove mixed in with food products can be detected by a

standard metal detector in food processing plants. This enable the identification of glove fragments in food and prevent contaminated products from reaching the market. However, in order to produce a detectable glove, there are a few requirements to be met. Firstly, the entire shape of the gloves should contain the detectable material, it being possible for an accidental cut in the glove to occur at any point. Secondly, the method of detection must be sufficiently sensitive in order to detect small fragments of the glove. Lastly, there is no impairment of the mechanical properties of the glove (De Ricci & Phalip, 1999).

The first metal detectable glove was invented by De Ricci and Phalip in 1996, they filed for a patent in November 1996 and the patent was granted to the Hutchinson, France in July 1999. In this invention, the glove is made of nitrile latex and compose of multilayer. As shown in Figure 2.2, the middle layer of the glove is comprise of metals, iron oxide or ferrites particle, with strong hysteresis loop and low coercivity uniformly distributed throughout the layer. These layer is sandwich between two layers of latex which do not contain any detectable material. In accordance with the invention, the said polymeric glove has maximum slope greater than 0.05 $m^3.kg^{-1}$ and coercive field about 1294 Oe. The fragment (5$\times$5 mm) of glove was able to detect by Safeline® S35 metal detector (De Ricci & Phalip, 1999).
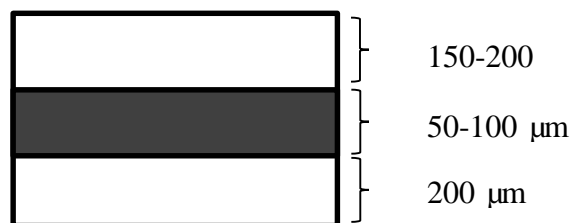
Figure 2.2: Sectional view of a multilayer glove article
(De Ricci & Phalip, 1999)

14

In year 2001, Dennis Connor has dispersed 3-6 % by volume of iron oxide with particle size of 1 to 200 μm into natural latex, nitrile latex and polyvinylchloride. The patent filed was granted under him together with Ck European Safety Equipment Ltd. (Connor, 2001). Currently, metal detectable gloves with trade name of "detect-a-gloves" (shown in Figure 2.3) is available in market. This glove is made from polyvinyl chloride, which is meant for food handling purpose in food industry, detectable in the electromagnetic range of 50 kHz up to 1 MHz, and made from Food and Drug Administration (FDA) accepted materials (Superior Glove Works ltd, n.d.).

Figure 2.3: Blue vinyl metal detectable glove
(Superior Glove Works ltd, n.d.)

Ansell Healthcare Products Llc was granted for its invention of magnetically detectable latex articles made of nitrile, natural rubber, polyurethane, and polychloroprene latex in 2006. The glove may include multiple cured latex layers having chromium oxide or magnetite dispersed throughout the cured latex layers. The outer and inner latex layer comprising 10 phr of chromium oxide dispersed throughout the latex layer while the middle latex layer comprising 25 phr of magnetite dispersed throughout the latex layer. The glove and pieces (100 mm^2) cut from the glove were detectable using a Safeline® metal detector (Lucas et al., 2006).

Recently, a patent was granted to Hainan University for the invention of magnetic latex composite. In this invention, 60 to 80 weight percentage of iron oxide nanoparticle and 20-40 weight percentage of natural latex are subjected to emulsion blending and co-

15

condensation by a nano-compounding technique to prepare the magnetic composite latex films. The magnetic composite latex films prepared has favourable magnetic properties, high comprehensive mechanical properties and can be molded later. It can be used for preparing sealing strips, electronic memory elements, television sound equipment, teaching aids, toys and medical appliances, and has wide application prospects ("Nano ferroferric oxide/natural composite magnetic latex and preparation method thereof," 2013).

Table 2.4: Summary of patents

Type of materials	Size	Type of Latex	Title	Publication Number	Assignee
Iron Oxide (Fe_3O_4, γFe_2O_3)	0.1-200 μm	Nitrile Butadiene Rubber (NBR)	Detectable polymeric protection goods, their preparation procedure and their applications	US 5922482 A (1996) EP 0773455 A1 (1997)	Hutchinson
Iron oxide (Fe_3O_4, γFe_2O_3)	1-200 μm	Nitrile Butadiene Rubber (NBR), Natural rubber (NR), Polyvinyl chloride (PVC).	Gloves	US 20040154072 A1 (2001) WO 2002071876 (2002) EP 1365665 (2003)	Dennis Frederick Connor
Chromium oxide ($Cr_2O_{3,}$ CrO_2) Iron oxide (Fe_3O_4)	0.3-15 μm	Nitrile Butadiene Rubber (NBR), Natural rubber (NR), etc.	Magnetically detectable latex articles	WO 2003076476 (2003) CA 2472184 (2004) US 7122593 (2006)	Ansell Healthcare Products Inc.
Iron oxide (Fe_3O_4)	100 nm	Natural rubber (NR)	Nano ferroferric oxide/natural composite magnetic latex and preparation method thereof	CN 103289144 A (2013)	Hainan University

2.3   Magnetite Nanoparticles

2.3.1   Background of Magnetic Nanoparticles

Magnetic nanoparticles are nanomaterials with particle size less than 100 nm. They can be manipulated by an external magnetic field (Gao et al., 2009; Indira & Lakshmi, 2010). Magnetic nanoparticles has been investigated thoroughly due to its widespread applications in the field of biomedical, engineering, material science, and environmental. They are usually composed of pure metal, typical examples are iron, nickel, cobalt and their oxides like magnetite, maghemite, chromium dioxide, and ferrite.

2.3.2   Magnetism of Materials

The magnetic properties of all matters originate from atoms and in turn atoms are composed of protons, neutrons and electrons. The protons and neutrons are packed together in the atom's nucleus while electrons are constantly in motion surrounding the nucleus. Ampere suggest that a magnetic field is produced whenever an electrical charge is in motion (Alex Duthie, 2012). Negative electrical charge of the electron produce a magnetic field when spinning and orbiting surround the nucleus of an atom. The spin and orbit direction determine the direction of the magnetic field, and magnetic moment is the strength of these magnetic field. According to Sattler (2010), all materials under the action of a magnetic field, H will acquire a magnetic moment. The magnetization, M is a vector quantity and defined as total magnetic moment per unit volume.

$$M = \frac{m}{v} \qquad \text{(Equation 2.1)}$$

Magnetization can be considered as a continuous vector field without considering the atomic structure of the materials. Magnetization is proportional to an external magnetic field as follow:

$$\chi_v = \frac{M}{H} \qquad \text{(Equation 2.2)}$$

Where χ_v is magnetic susceptibility (volume) of a material. This shows that magnetization of a material is dependent on susceptibility and magnetic field strength. Magnetic susceptibility is commonly used to determine the category of different magnetic materials. For example, paramagnetic material possesses magnetic susceptibility, $\chi > 0$ while diamagnetic material behave oppositely. The responses of a material to an applied external magnetic field H is called magnetic induction or magnetic flux density, B (Getzlaff, 2007).

$$B = \mu_0(H+M) \qquad \text{(Equation 2.3)}$$

Where μ_0 is the permeability of vacuum, a universal constant with value of $4\pi \times 10^{-7}$ (1.257×10^{-6}) H/m (Sattler, 2010). A material with χ as the magnetic susceptibility is called linear material. The relationship between B and H for a linear material present:

$$B = \mu_0(1+\chi)H \qquad \text{(Equation 2.4)}$$

$$B = \mu_0\mu_r H \qquad \text{(Equation 2.5)}$$

The relative permeability, $\mu_r = (1 + \chi)$ of a material is a measurement of the degree to which the material can be magnetized, or the ease with which can be induced in an external field. Typical values for the relative permeability are:

In vacuum : $\mu_r = 1$

In matter generally : $\mu_r \geq 1$

Possible in matter : $\mu_r \approx 100,000$

The common magnetic terms in international system units (SI) or centimeter, gram, second units (CGS) systems and conversion factors have been summarized in Table 2.5.

**Table 2.5: Magnetic term and conversion between SI and CGS unit**

Magnetic Term	Symbol	SI unit	CGS unit	Conversion (SI/CGS)
Magnetic induction	B	Tesla (T)	Gauss (G)	10^4
Magnetic field	H	A/m	Oersted (Oe)	$4\pi/10^3$
Magnetization	M	A/m	emu/cm^3	10^{-3}
Mass magnetization	σ	Am^2/kg	emu/g	1
Magnetic moment	m	Am^2	emu	10^3
Volume susceptibility	χ_v	dimensionless	dimensionless	$(4\pi)^{-1}$
Mass susceptibility	χ	m^3/kg	emu/Oe.g	$10^3/4\pi$
Vacuum permeability	μ_0	H/m	dimensionless	$(4\pi\times10^{-7})^{-1}$

2.3.2.1 Classification of Magnetic Behaviour

According to Indira and Lakshmi (2010), materials are classified by their response to an external magnetic field. They can be categorized into five groups:

a) Diamagnetism

According to Merhari (2009), diamagnetism is natural property of all materials. It is a feeble magnetism, and made up of atoms that have no net magnetic moments. Therefore, diamagnetic materials are often assume as non-magnetic. However, the diamagnetic properties is due to a slight electron rearrangement under external magnetic field that opposes the applied field (Williams, 2014). Diamagnetic susceptibility are negative, and small ($\chi = 10^{-5}$) when exposed to a magnetic field, and it is temperature independent (Chikazumi & Graham, 2009). The example of diamagnetic materials are mercury, silver, copper, lead, silicone and water (Ida, 2015). Superconductor is another type of diamagnetic materials, it repel the magnetic field entirely and act as a perfect diamagnetism due to the Meissner effect (Poole et al., 2007).
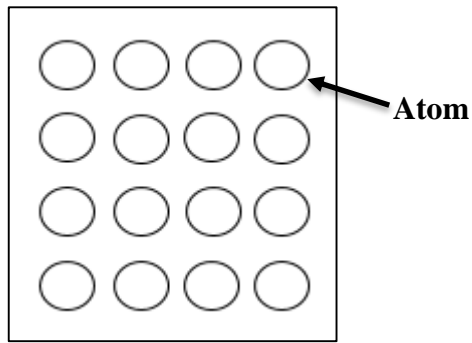
Figure 2.4: Magnetic ordering of diamagnetic material
(Murad &Cashion, 2011)

b) Paramagnetism

In contrast with diamagnetic materials, paramagnetic materials have a feeble positive susceptibility when exposed to the magnetic fields. The susceptibility of a paramagnetic material is inversely proportional to temperature as it follows the Curie Law. Similar to diamagnetic materials, their magnetism disappears when the external field is removed (Merhari, 2009). The magnetic moment arises from unpaired electron spins, and the alignment of the electron spin moment under external magnetic field (Jangid et al., 2014). Paramagnetic materials are magnesium, tantalum, and many others iron containing mineral (Williams, 2014).
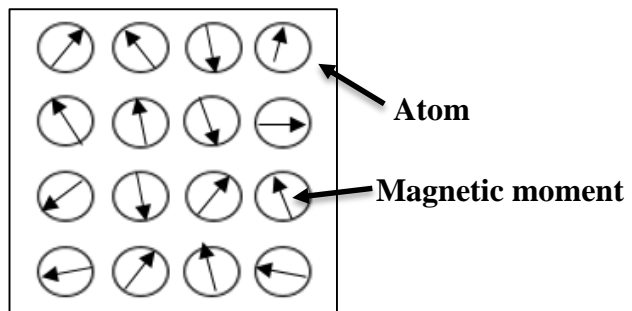
Figure 2.5: Magnetic ordering of paramagnetic material
(Murad & Cashion, 2011)

c) Ferromagnetism

Ferromagnetism is a very important type of magnetism. Unlike paramagnets, ferromagnets have a very strong atomic moment. The magnetization is permanently retained in the material, and it will turned into a permanent magnet (Williams, 2014). Their strength are related to the magnetic domains existed in the materials. When a magnetic field is applied, the near random organization of domains are aligned, and grow of this alignment will produced a large magnetic forces within a domains.
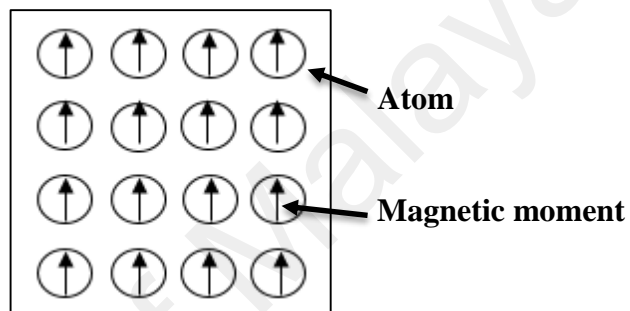
Figure 2.6: Magnetic ordering of ferromagnetic material
(Murad & Cashion, 2011)

The two prominent characteristic of ferromagnetic material are spontaneous magnetization, and magnetic ordering temperature. The saturation magnetization goes to zero at the Curie temperature. At higher temperature, the magnetic orientation of ferromagnetic materials will become disordered. The susceptibility for ferromagnetic materials is very large as compared to paramagnetic materials, and achieving magnetization saturation at room-temperature under moderate magnetic fields (Merhari, 2009). In addition, ferromagnets preserves a memory of an applied field upon removal. This behaviour is called hysteresis and hysteresis loop is a plot of the variation of magnetization with magnetic field. Coercive force or coercivity of the material is the force required to remove the residual magnetism from the material. When the magnetizing force is reduced to zero, some magnetic flux remains in the material even though the magnetizing force is zero. This is called retentivity, and it indicates the level of residual

magnetism in the material (Spaldin, 2010). Typical examples of ferromagnets are nickel, iron and cobalt and their alloys (Ida, 2015).
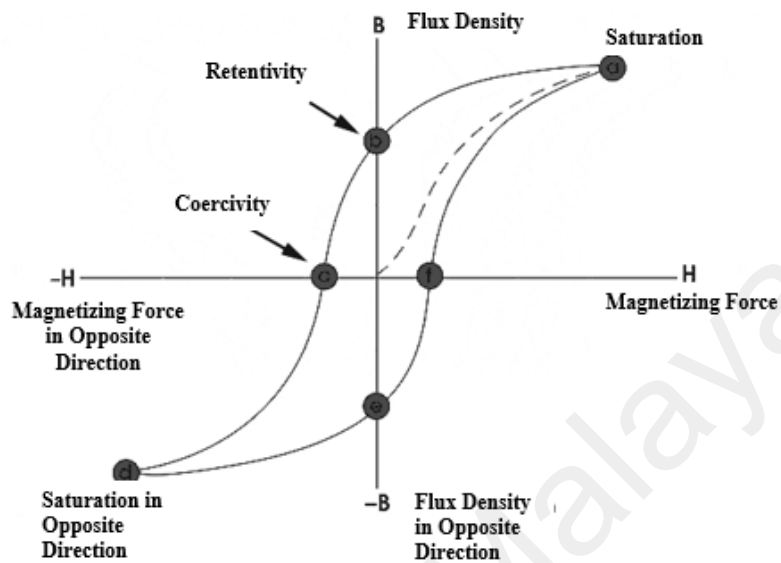
Figure 2.7: Hysteresis loop of a ferromagnet
(Schodek et al., 2009)

d) Ferrimagnetism

Ferrimagnetism is a magnetic properties that is normally found in ionic compounds (Williams, 2014). In these ionic materials, the magnetic moments of ion on lattice site in the crystal are aligned antiparallel to those of ions on another lattice site. The electron spin and the magnetic moments of these two sub-lattices are not equal, they partially cancel each other and therefore produce a net magnetic moment (Carter & Norton, 2007). The susceptibility of ferrimagnet is small and positive. Ferrimagnetism is similar to ferromagnetism, it exhibits Curie temperatures, spontaneous magnetization, remanence, and hysteresis. However, they have very different magnetic ordering (John, 2014).

e) Antiferromagnetism

In an antiferromagnet, there are two sub-lattices having equal spin magnetic moment but in opposite direction, result in zero net magnetic moment. Besides that, antiferromagnet has zero remanence and no hysteresis. The susceptibility of antiferromagnetic materials are small, positive and follows Curie-Weiss law for paramagnets above the Néel temperature (Merhari, 2009). Deviation from ideal antiferromagnetism occur when the anti-parallelism is unequal. Canted antiferromagnet with a small net magnetization can be produce and it possesses many typical magnetic characteristic of ferro- and ferrimagnets. Hematite is a well-known example of canted antiferromagnetism (Murad & Cashion, 2011).
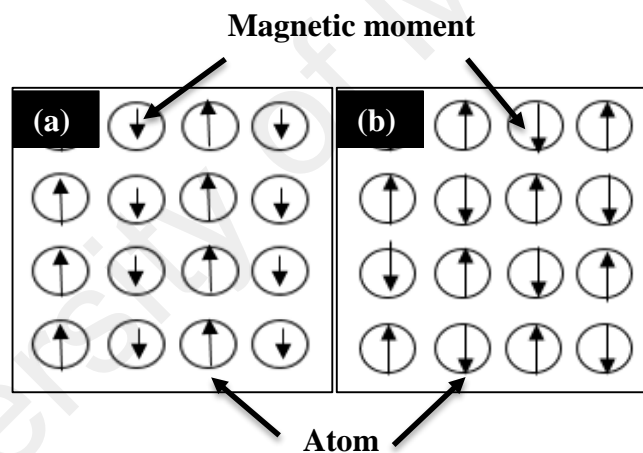
Figure 2.8: Magnetic ordering of (a) ferrimagnetic and (b) antiferromagnetic material

2.3.3   Magnetic Iron Oxides

The magnetic particle obtained from magnetic transition metals (iron, nickel, and cobalt) oxidized readily whereas iron oxide like magnetite are more stable against oxidation. Iron oxide is an important transition metal oxide, and it usually exists in nature in three phases of magnetite (Fe_3O_4), maghemite (γ-Fe_2O_3) and hematite (α-Fe_2O_3) (Khalil, 2015). Nano-magnetite particles possess strong ferrimagnetic behaviour and

lower sensitivity to oxidation have attracted much interest because they belong to the class of materials having no-toxic and biological compatibility by the presence of Iron ions (Kandpal et al., 2014).

Table 2.6: Various Iron Oxides
(Schwertmann & Cornell, 2008)

Class	Name	Formula
Oxides	Magnetite	Fe_3O_4
	Maghemite	γ-Fe_2O_3
	Hematite	α-Fe_2O_3
	-	β-Fe_2O_3
	-	ε-Fe_2O_3
	Wustite	FeO
Oxyhydroxides	Goethite	α-FeOOH
	Alkaganeite	β-FeOOH
	Lepidocrocite	γ-FeOOH
	Feroxyhyte	δ'-FeOOH
	Ferrihydrite	$Fe_5HO_8.4H_2O$
Hydroxide	Bernalite	$Fe(OH)_3$
	-	$Fe(OH)_2$
	Green Rusts	$Fe_x^{III}Fe_y^{II}(OH)_{3x+2y-z}(A^-)_z$; $A^- = Cl^-$; ½ SO_4^{2-}

2.3.3.1 Crystal Structure of Magnetic Iron Oxides

a) Magnetite

Magnetite is one of the most important class of iron oxides, it is black in colour and ferromagnetic (Ramimoghadam et al., 2014). Magnetite possess an inverse spinel structure with oxygen forming a face-centered cubic closed packing along [111] (Hasany et al., 2012). This unit cell belongs to the Fd3m space group and the unit cell edge of magnetite, a, has a value of 0.8396 nm (Cornell & Schwertmann, 2008). There are eight formula units per unit cell for magnetite. Unit cell formula of Magnetite can be written as $[Fe^{3+}]_A [Fe^{3+}, Fe^{2+}]_B O^{2-}_4$ and iron cations will occupy either tetrahedral (site A) or octahedral (site B) sites . Although magnetite in stoichiometry has the ratio of cations, Fe

$^{(II)}$/Fe $^{(III)}$ = 0.5 but magnetite is commonly non-stoichiometric resulting a Fe^{3+} deficient sub lattice (Ramimoghadam et al., 2014).

b) Maghemite

Maghemite also has the spinel structure, but differ from magnetite with the presence of cationic vacancies in the octahedral sites (Ramimoghadam et al., 2014). The structure of maghemite is cubic, and each unit of maghemite contains 32 O^{2-} ions, 21⅓ Fe^{3+} ions and 2⅓ vacancies. Oxygen anions give rise to a cubic close-packed array while ferric ions are distributed over tetrahedral sites (eight Fe ions per unit cell) and octahedral sites (the remaining Fe ions and vacancies). Maghemite has the similar structure of magnetite, the only different is that all or most of the Fe in maghemite is in the trivalent state (Wu et al., 2015).

2.3.3.2 Phase Transformation of Magnetite

Magnetite is not very stable and sensitive to oxidation. In the presence of oxygen, magnetite might transform into maghemite and/or hematite (Laurent, 2008). Maghemite can be obtained by heating at lower temperature while hematite is obtained when magnetite is heated to high temperature in oxidizing environment. The oxidation process of magnetite to maghemite is topotactic and isomorphic process, the crystal structure remain the same. The magnetite is oxidized to maghemite or hematite according to the following reaction:

$$4Fe_3O_4 + O_2 \rightarrow 6Fe_2O_3 \qquad \textbf{(Equation 2.6)}$$

On the other hand, it can be reduced to wustite or iron in a reducing atmosphere (e.g. carbon):

$$Fe_3O_4 + C \rightarrow 3FeO + CO \qquad \textbf{(Equation 2.7)}$$
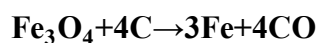
$$Fe_3O_4+4C \rightarrow 3Fe+4CO \qquad \textbf{(Equation 2.8)}$$

2.3.3.3 Magnetic Properties of Magnetite Nanoparticles

Different phases of iron oxides display different magnetic ordering depend on the alignment of the electron spin. At room temperature, both magnetite and maghemite are ferrimagnetic (Bououdina, 2014). Table 2.7 shows saturation magnetization and the crystalline parameter defining the magnetism of magnetite and maghemite at 300 K (Rajan & Lekkala, 2013).

**Table 2.7: Physical and magnetic properties of magnetic iron oxides**

Magnetic Iron Oxides	Magnetite (Fe_3O_4)	Maghemite (γ-Fe_2O_3)
Density (g cm^{-1})	5.21	4.86
Colour	Black	Reddish-brown
Structure	Inverse spinel	Defect spinel
Crystal system	Cubic	Cubic; Tetragonal
Space group	Fd3m	$P4_332$ (cubic); $P4_12_12$ (tetragonal)
Lattice parameter (nm)	a = 0.8387	a = 0.8352 (cubic), a = b = 0.8330, c = 2.490 (tetragonal)
Type of magnetism	Ferrimagnetic	Ferrimagnetic
Curie Temperature, Tc (K)	850	820-986
Saturation Magnetization, Ms (300K) (emu/g)	92-100	60-80
Single domain critical diameter, d_{SD} (nm)	~103.5	~85
Superparamagnetic critical diameter, d_{SPM} (nm)	~24	~35

According to Lowrie (2007), the transition between single domain and multi-domain behaviour occurs when the reduction of magnetotstatic energy is balanced by the energy associated with the addition of domain wall. The transition occur in magnetite grain about 0.05-0.1 μm diameter. Magnetite grain larger than few micrometre in diameter are considers multi domain. However, true multi domain behaviour in magnetite are observed if the grain size is larger than 15-20 μm.

The characteristic of nano-magnetic particle are different from the bulk ones. The surface-to-volume ratio increases when the size of the nanoparticles decreases. This ratio become the important factor for their unique physical and chemical properties compared to those of the bulk material (Issa et al., 2013). Magnetic nanoparticles show new phenomena such as high saturation field, superparamagnetism, extra anisotropy contributions, or shifted loops after field cooling that arise from narrow and finite-size effects and surface effects that dominate the magnetic behaviour of individual nanoparticles (Majewski & Thierry, 2007).

The ferromagnetic behaviour of a material can be represented in term of magnetic domains. Magnetic domain is a small region where all the magnetic dipoles are perfectly aligned in the same direction (Bakshi, 2009). Magnetic domains exist in order to reduce the magnetostatic energy of the system. The domain structure of a ferromagnetic material determines the size dependence of its magnetic behaviour (Fojtik et al., 2009). For a larger grain size, the coercivity of a material decrease as the grain subdivides into domains. Grain with two or more domains are called multi domains. The internal magnetization of each domain is equal to the saturation magnetization, but the net magnetization for the grain is much less than the saturation magnetization, or to an average magnetization close to zero due to different directions of atomic magnetic moments (Guimar ães, 2009).

When the grain size is reduced below a critical value, it becomes a single magnetic domain, where all magnetic moment are aligned along the same direction. The maximum coercivity of a material occurs within its single domain range. Coercivity of a substances decreases with the particles size and it preserve a net magnetization in the absence of applied magnetic field. According to the magnetic domain theory, the critical size of the single domain is affected by a few factors. These factors are magnetic saturation value, the strength of the crystal anisotropy and exchange forces, surface or domain-wall energy, and the particles shape (Akbarzadeh et al., 2012). When the size of single domain particles further reduces below a critical diameter, the coercivity becomes zero, and such particles said to exhibit superparamagnetism behaviour. Superparamagnetism is caused by thermal effect, and it happened when typical ferromagnetic materials diameter less than 50 nm. The simple magnetization reversal energy become equal to the energy at room temperature in this size scale. The thermal fluctuations at room temperature are sufficiently strong to overcome the magnetic interaction between the magnetic domains and demagnetize spontaneously, therefore they exhibit zero coercivity and no hysteresis (Fojtik et al., 2009). Superparamagnetic materials can only be magnetized in the presence of external field and they are intrinsically non-magnetic (Faraji et al., 2011;Varanda et al., 2011).
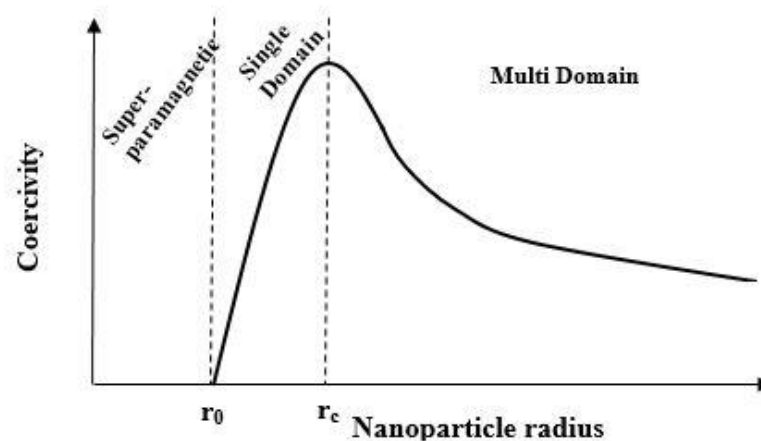
Figure 2.9: The relationship between size and coercivity of small particles (Fojtik et al., 2009)

In addition, surface effect such as oxidation, existence of surfactants, and surface strain are the other features that dominates the magnetic properties of magnetic nanoparticles (Issa et al., 2013). Oxidation can easily happen on the surface of magnetic nanoparticle when they are exposed in the atmosphere. Wu, He, and Jiang (2009) reviewed that the coercivity of magnetic nanoparticles increases for core diameter smaller than 10 nm after oxidation while the coercivity remains the same for sample with core diameter of 50 nm. Magnetic characteristic such as saturation magnetization decrease proportionally with reduction of size of magnetic substances. The relationship between the particle size and saturation magnetization of magnetite is shown in Figure 2.11. The reduction of saturation magnetization is not preferable, therefore a lot of studies have been conducted either surface coating or modification of composition in order to find out excellent magnetic particles which maintains higher magnetic property (Nogi et al., 2012).
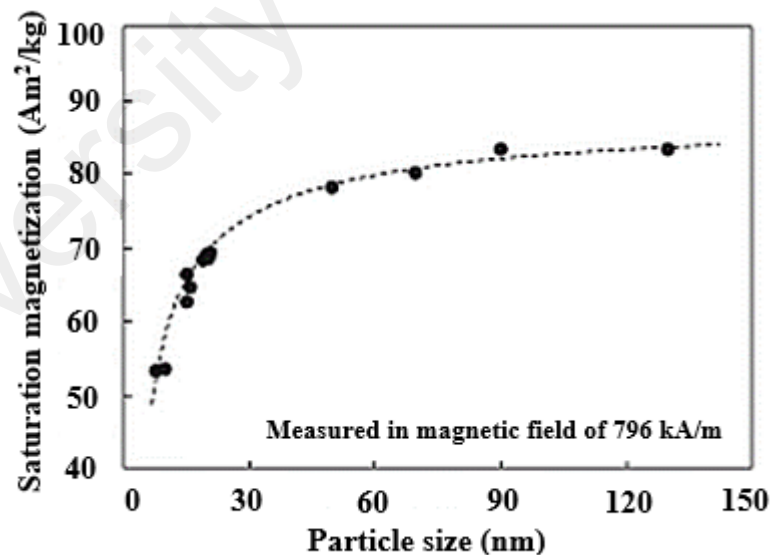
Figure 2.10: The relationship between particle size of spherical magnetite and saturation magnetization
(Nogi et al., 2012)

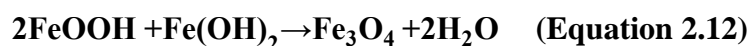### 2.3.3.4   Preparation of Magnetite Nanoparticles

Numerous methods can be used to synthesis magnetic particles in nano-scales, for example chemical methods such as co-precipitation of hydroxide, hydrothermal synthesis, and sol-gel transformation etc (Haw et al., 2010;Laurent & Mahmoudi, 2011; Wahajuddin, 2012;Zhao et al., 2012;Filippousi et al., 2014) .

Table 2.8: Comparison of different chemical methods to synthesis iron oxide nanoparticles

Synthesis method	Advantages	Disadvantages
Co-precipitation	Simple synthesis High yield Scalable	Wide particle size distribution Expose to oxidation Aggregation Poor crystallinity
Hydrothermal reactions	Narrow size distribution Good control of size Scalable	Harsh reaction conditions Unwanted surface oxidation
High temperature decomposition	Good control of particle size and shape Narrow size distribution Good crystallinity High yield	Complicated and harsh experimental procedure Furthers step needed to obtain water stable suspension
Micro-emulsion	Good control of particle size and shape Homogeneous particle size distribution	Poor yield Complicated purification methods for surfactant separation Large quantity of solvent required

Co-precipitation method is the most simple and conventional method to synthesis magnetite nanoparticles. Co-precipitation of Fe^{2+} and Fe^{3+} ions from aqueous salt solutions is done by fine controlling of the pH of a reaction medium by adding ammonium hydroxide or sodium hydroxide aqueous solution (Coey et al., 2013). Parameters affecting the production of magnetic nanoparticles including pH (Darminto et al., 2011), reaction temperatures (Karaagac et al., 2011;Tai et al., 2014), alkaline species and concentration (Tajabadi & Khosroshahi, 2012;Mascolo et al., 2013), iron salts molar ratio, ligands and

concentration (Jiang et al., 2011). The reaction mechanism for the formation of magnetite nanoparticles is shown as follow (Mahdavi et al., 2013):

$$Fe^{3+}+3OH^-\rightarrow Fe(OH)_3 \qquad \text{(Equation 2.9)}$$

$$Fe(OH)_3\rightarrow FeOOH+H_2O \qquad \text{(Equation 2.10)}$$

$$Fe^{2+}+2OH^-\rightarrow Fe(OH)_2 \qquad \text{(Equation 2.11)}$$

$$2FeOOH +Fe(OH)_2\rightarrow Fe_3O_4 +2H_2O \qquad \text{(Equation 2.12)}$$

In this procedure, hydroxides of ferrous and ferric ions, ferrous hydroxide [$Fe(OH)_2$] and goethite (α-FeOOH), are co-precipitated as precursors in an alkaline solution to obtain magnetite, the end product.

2.4 Stabilization of Magnetite Nanoparticles

Magnetite nanoparticles experience strong van der Waals and magnetic attractions, which make the particle dispersion unstable and particles prone to aggregation (Liu et al., 2008). To prevent aggregation or coagulation phenomena in colloidal systems, the magnetite nanoparticles have to be stabilized against coagulation due to electrostatic or steric repulsion forces (Koetz & Kosmella, 2007;Meerod et al., 2008).

Electrostatic stabilization is a pH sensitive method, attractive van der Waals forces are overcome by the repulsive electrostatic forces between absorbed ions and associated couterions at moderate inter-particle separation. Low molecular weight ions (e.g. citrate and hydroxide ions) was shown to strongly absorb on the surface of metallic nanoparticles and therefore it was used as their electrostatic stabilizer (Starov, 2011). For example, citrate stabilized magnetite nanoparticles was developed by Nigam et al. (2011) as an appropriate candidate for biomedical applications. However, electrostatic stabilization of metal nanoparticles is rather weak and the electrostatically stabilized sol can be

coagulated if the ionic strength of the dispersing medium is increased sufficiently (Schmid, 2011).

Steric stabilization is a much better stabilization approach as the aggregation of nanoparticles is prevented based on steric effects, by the addition of polymers and surfactants at the surface of the particles (Schmid, 2011). The adsorption of organic molecules with a long chain, usually referred as "organic ligands" or "polymer ligands" can prevent the coalescence of the particles. These ligands will a form barrier that prevent the close contact of particles. Therefore, steric stabilization is especially useful in the case of concentrated dispersions of metal nanoparticles (Starov, 2011). In addition, When polymer or organic molecules are attached to a charged particle surface, the magnetite nanoparticles can be stabilized by combined steric and electrostatic stabilization (Astruc, 2008).

In general, a suitable surface functionalization and choice of solvent are crucial to achieving sufficient repulsive interactions to prevent agglomeration so as to obtain a stable colloidal solution and further expand the scope of application (Wu et al., 2009). The coating of magnetite nanoparticles (MNPs) can consist of long-chain organic ligands or inorganic/organic polymers, where these ligands or polymers can be introduced during (*in situ* coating) or after (post-synthetic coating) synthesis (Umut, 2013).

2.4.1 Polyethylene Glycol (PEG) Coating

Polyethylene Glycol (PEG) is one of the most frequently used synthetic polymers for surface modifications of MNPs, especially for biomedical applications (Ramimoghadam et al., 2015). PEG is a hydrophilic, highly water soluble, biocompatible, non-antigenic, and protein-resistant polymer. The solubility of PEG in water has been attributed to its hydration with bound water molecules, which increases with polymer molecular weight

(Huang & Nishinari, 2001). In addition, PEGs are FDA-approved excipients in numerous pharmaceutical formulations due to their biocompatibility property (Singh et al., 2014).
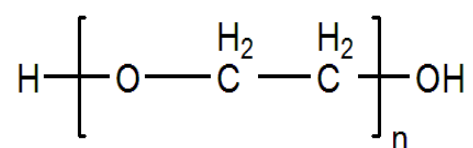
**Figure 2.11: Chemical structure of Polyethylene glycol**

In spite of all the aforementioned advantages, the synthesis of PEG-coated magnetite nanoparticles remains more or less complex, since it requires the use of modified PEG and special atmospheric conditions. Thus, the nanoparticle surface is modified using either a silane functionalized PEG (Barrera et al., 2009; Brullot et al., 2012), or by the additions of a primary surfactant (sodium oleate), followed by the addition of PEG, which acts as a secondary surfactant. Tables 2.9 present the summaries of research findings for PEG coated MNPs, which is focussed on the magnetic properties.

Table 2.9: Summaries of findings for PEG coated magnetite nanoparticles

| References	Findings
Zhao et al. (2010)	A core-shell structure with a diameter of 10-40 nm were prepared with sodium oleate and PEG 4000. The saturation magnetization of MNPs and PEG coated MNPs are 67.06 emu/g and 64.11 emu/g, respectively.
Jayanthi et al. (2013)	The surface functionalization of the as-synthesized magnetite nanoparticles with PEG 20,000 effectively controls the particle size and show enhanced magnetization values (60.06 emu/g).
Garc á-Jimeno and Estelrich (2013)	Ferrofluids was prepared with unmodified PEG (2000, 4000, 6000 and 10000 Da). The saturation magnetization of PEG 10000 Da coated MNPs is 55 emu g^{-1}.
J. Yang et al. (2014)	Saturation magnetization of as-synthesized MNPs decreased with increasing the molecular weight (400, 1000, and 2000) of PEG. Good size distribution and magnetic property are obtained with adding 4 g PEG 1000 while sealing the beaker.
Anbarasu (2015)	The saturation magnetization of the MNPs decreases from 62 to 51 emu/g, when PEG weight increases from 1 to 3 g.

2.4.2　Oleic Acid Coating

Oleic acid or oleate is the most often used surfactant in magnetite nanoparticles (MNPs) stabilization. Oleic acid, an unsaturated fatty acid with a cis-double bond in the middle can form a dense coating for effective stabilization than others saturated fatty acid like stearic acid. It is used to stabilize the magnetic nanoparticles with strong chemical bond between the carboxylic acid and the magnetite nanoparticles. Several authors have reported the magnetite nanoparticles coated or dispersed in oleic acid (Wang et al., 2010; Li et al., 2010). Mahdavi et al. (2013) modified the surface of MNAPs by oleic acid in order to control the particle size, prevent particles aggregation, and improve stability.
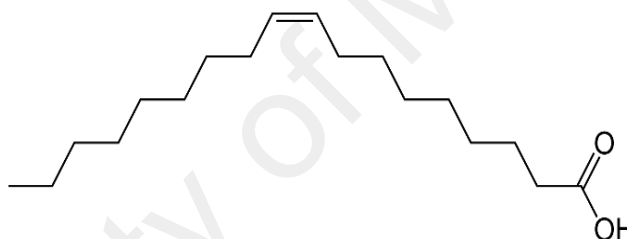
Figure 2.12: Chemical structure of oleic acid

Formation of water-based fatty acid coated magnetite particle dispersions is complicated by the non-polar nature of the hydrocarbon chain. Oleic acid, used for nonpolar dispersions, cannot form stable dispersions in water. Shimoiizaka et al. (1980), introduced the use of fatty acids to create iron oxide nanoparticles dispersible in water via the formation of a bilayer surfactant system. Since then oleic acid was used to produce aqueous dispersion of magnetite nanoparticles (Ingram et al., 2010). Bilayer oleic acid-coated magnetite nanoparticles can be well dispersed not only in nonpolar carrier liquids but also in polar medium with the adjustment of pH, while the single layer oleic acid-coated magnetite nanoparticles can be dispersed only in nonpolar medium. Therefore, bilayer oleic acid-coated magnetite nanoparticles have wider scope of applications than

single layer oleic acid-coated magnetite nanoparticles (Yang et al., 2010). Oleic acid is chemisorbed in the first layer due to the surface complex formation between the carboxylate (-COOH⁻) groups of Oleic acid and the FeOH sites on the surface of magnetite as assumed. A second layer of oleate anions can be adsorbed on the hydrophobic shell of oriented surfactant molecules via hydrophobic interaction. These oleate anions is negatively charged and it could provide electrostatic repulsion between colliding particles besides the steric hindrance of double layer (Hórvölgyi & Kiss, 2008). The schematic diagram of bilayer stabilized magnetite nanoparticles is presented as Figure 2.13.
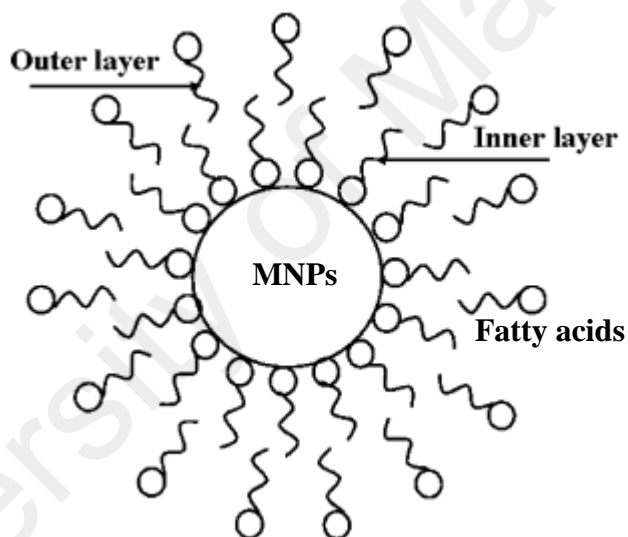
Figure 2.13: Bilayer stabilized magnetite nanoparticles by using fatty acids (Maity & Agrawal, 2007)

CHAPTER 3: MATERIALS AND METHODOLOGY

3.1 Introduction and Overview

This chapter presents experimental and characterization techniques which have been employed in this work. The content of this chapter is divided into two main sections. The first section introduces the raw materials, the last part presents the characterization.

3.2 Raw Materials and Chemicals Selections

3.2.1 Iron Chloride Tetrahydrate

Iron chloride tetrahydrate with chemical formula of $FeCl_2.4\ H_2O$, molar weight = 198.83 g/mol, density is 1.93 g/cm^3, was purchased from Merck.

3.2.2 Iron Chloride Hexahydrate

Iron chloride hexahydrate (ACS grade reagent), 97 % with chemical formula of $FeCl_3.6H_2O$, molar weight = 270.30 g/mol, density is 1.82 g/cm^3, was purchased from Sigma Aldrich.

3.2.3 Ammonium Hydroxide

Ammonium hydroxide (ACS grade reagent), 28.0-30.0% NH_3 basis was purchased from Sigma Aldrich.

3.2.4 Polyethylene Glycol (PEG)

Polyethylene glycol 600 with repeating unit of $HO(C_2H_4O)_n\ H$, average molecular mass = 570-630 g/mol and exhibits a density of 1.126-1.128 g/ml was purchased from Merck.

3.2.5 Oleic Acid

Oleic acid (extra pure) with chemical formula of $C_{18}H_{34}O_2$, molar weight = 282.46 g/mol and exhibits a density of 0.89-0.91 g/ml was purchased from Friendemann Schmidt.

3.2.6 Nitrile Butadiene Rubber Latex (NBRL)

The Nitrile Butadiene Rubber (NBR) latex with low acrylonitrile content grades and total solid content (T.S.C) = 43 % by dry weight was obtained from Harlatega Sdn. Bhd.

3.2.7 Compounding Chemicals

The compounding chemicals used to prepare nitrile latex films were provided by Hartalega Sdn. Bhd.

Table 3.1: Compounding chemicals and its functions

Compounding Chemicals	Chemical Formula	Molecular weight (g/mol)	Functions
Sodium Dodecyl Benzene Sulphonate (SDBS)	$C_{18}H_{29}NaO_3S$	348.48	Stabilizer
Zinc Dibutyldithiocarbamate (ZDBC)	$[(C_4H_9)_2NCS_2]_2Zn$	474.12	Accelerating agent
Sulphur	S	32.07	Crosslinking agent (covalent bond)
Zinc oxide	ZnO	81.38	Crosslinking agent (Ionic bond)
Titanium dioxide	TiO_2	79.87	Pigment
Aquawax	-	-	Antiozonant
Calcium nitrate	$Ca(NO_3)_2$	164.09	Coagulant
Teric acid	-	-	Mould release agent
Perfluorocarboxylic acid (PFCA)	$C_nF_{(2n+1)}CO_2H$	-	Surfactant

3.3 Methodology of Experiment

3.3.1 Synthesis of Magnetite Nanoparticles

In this stage, magnetite nanoparticles was primarily synthesized through co-precipitation method. Operational parameters such as final pH, precipitating agent concentration, iron salt concentration, and addition rate were optimized to produce the required size and magnetic properties for MNPs. Firstly, the desired final pH (6.5, 8.5 and 9.5) was achieved by the addition of 3.00 M of ammonium hydroxide. Then, the concentration of ammonium hydroxide was varied as 0.75 M, 1.50 M, 3.00 M and 6.00 M while the third parameter, total iron salts concentration was varied as 150 mM to 250 mM, 375 mM and 500 mM. Lastly, the addition rate of 1 ml/min, 5 ml/min, 10 ml/min and 20 ml/min were used to produce MNPs. After the reaction was completed, the solution was decanted, and the MNPs were washed with deionized water. This procedure was repeated three times, and then, the MNPs were separated by a permanent magnet and dried at room temperature.

3.3.2 Synthesis of Coated Magnetite nanoparticles

The synthesis of coated magnetite nanoparticles were carried out based on the reaction condition of MNPs with the highest saturation magnetization in previous section (stage 4.1). Coated MNPs were fabricated using in-situ coating technique, where coating agents (e.g., polyethylene glycol, oleic acid) with different loading amount were introduced into the iron salts solution before the addition of ammonium hydroxide solution. The loading amount of PEG was varied as 0.6 g, 0.8 g, 1.0 g, 2.0 g, and 3.0 g while the loading amount of oleic acid was varied as 0.3 g, 0.6 g, 0.9 g, 1.2 g and 1.5 g, respectively. After that, sedimentation test was carried out to evaluate the stability of MNPs in nitrile butadiene rubber latex.

3.3.3   Preparation of Nitrile Butadiene Rubber Films

The nitrile films preparation is divided into two main sections. In the first section, MNPs was incorporated into nitrile latex compound during the compounding process. Then, the formation of nitrile films by a series of dipping process was presented in the second section.

3.3.3.1   Nitrile Butadiene Rubber Latex Compounding Process

The first step of compounding process start with mixing tank cleaning Firstly, the mixing tank was brushed thoroughly to prevent contamination. 500 g of 43% total solid content (TSC) of nitrile butadiene rubber latex was filtered and transferred to the mixing tank. The nitrile butadiene rubber latex was stirred for 30 minutes (50 rpm stirring speed). Then, 12.9 g of Sodium Dodecyl Benzene Sulphonate (SDBS) was slowly added into the latex and continued by stirring process for an hour. After that, the pH of the latex was adjusted to pH 9.5 by adding ammonia solution.   Next, about 2.58 g of Dibutyldithiocarbamate (ZDBC), 5.01 g of sulphur, 4.66 g of Zinc oxide (ZnO) and 6.45 g of Titanium dioxide (TiO$_2$) were weighed and slowly added into the latex compound. It was stirred for 1 hour and stirred overnight at 30 rpm stirring speed. TSC of compounded latex was checked and diluted by DI water to 23%. In this stage, 5 phr of coated MNPs as well as 12.04 g of aquawax was added slowly into the compounded latex. It was stirred for 1 hour with stirring speed of 50 rpm and the final TSC and pH of the latex compound were checked and recorded. Figure 3.1 shows the overall flow process of latex compounding.

```
┌──────────┐     ┌──────────┐     ┌──────────┐     ┌──────────┐
│  Mixing  │ ──▶ │ Transfer │ ──▶ │ Add SDBS │ ──▶ │ Adjust pH│
│   Tank   │     │ latex to │     │          │     │          │
│ cleaning │     │mixing tank│     │          │     │          │
└──────────┘     └──────────┘     └──────────┘     └──────────┘
                                                          │
                                                          ▼
┌──────────┐     ┌──────────┐     ┌──────────┐     ┌──────────┐
│ Add TiO₂ │ ◀── │ Add ZnO  │ ◀── │   Add    │ ◀── │ Add ZDBC │
│          │     │          │     │ Sulphur  │     │          │
└──────────┘     └──────────┘     └──────────┘     └──────────┘
     │
     ▼
┌──────────┐     ┌──────────┐     ┌──────────┐     ┌──────────┐
│Check TSC │ ──▶ │   Stir   │ ──▶ │Dilute TSC│ ──▶ │ Add MNPs │
│  and pH  │     │ overnight│     │  to 23%  │     │          │
│          │     │ (30 rpm) │     │          │     │          │
└──────────┘     └──────────┘     └──────────┘     └──────────┘
                                                          │
                                                          ▼
                 ┌──────────┐     ┌──────────┐
                 │check final│ ◀── │   Add    │
                 │   TSC    │     │ Aquawax  │
                 └──────────┘     └──────────┘
```
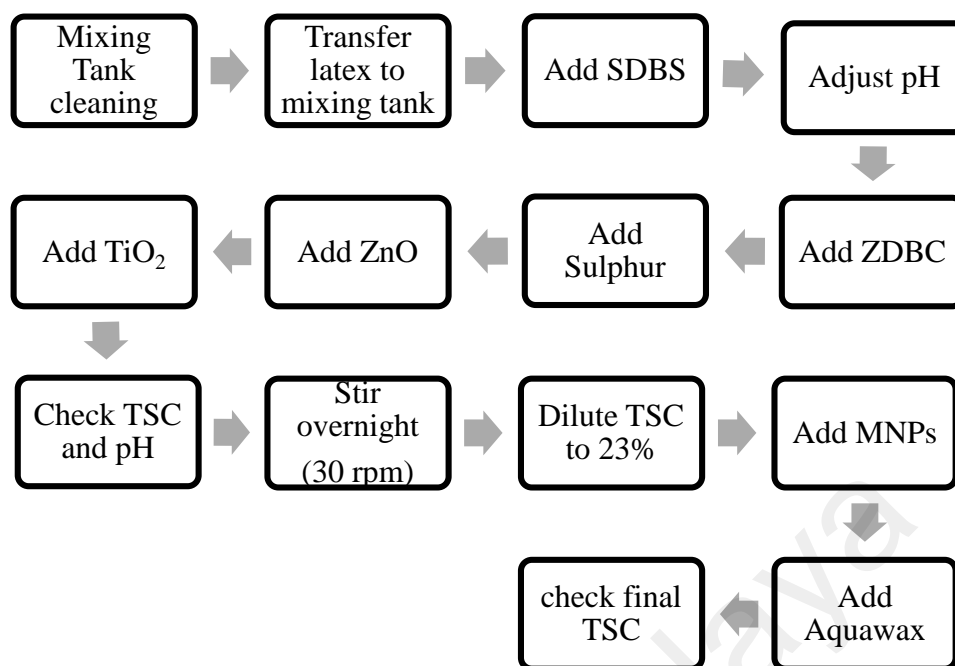
Figure 3.1: Flow chart of nitrile butadiene rubber latex compounding process

3.3.3.2 Dipping Process Of Nitrile Butadiene Rubber Latex Films

The first step of nitrile films dipping process start with former cleaning. Firstly, the former was brushed to ensure the surface of the former is smooth, consistent and free of dust. After the former was cleaned and dried, the former was immersed first into a coagulant and then in the latex compound for appropriate dwell time to give the desired latex film thickness. The coagulant comprises of 121.42 g calcium nitrate (CN), 6.25 g of perfluorocarboxylic acid (PFCA) and 0.50 g of teric acid into 371.83 g of water at 60 ℃, which causes a latex overcoat to gel. The latex concentrate was mixed with various compounding chemicals and then introduced into the dipping tank. When the thin latex film on each former was partially dried, it was leached in clean water (50 ℃) for 1 minutes to remove the water-soluble substances present in the latex film. The films were then dried and vulcanized. Drying and vulcanization or curing of the films were done in hot-air ovens, at temperatures of 125 ℃ for 20 minutes. The cured films were immersed in clean water tanks again to remove more water-soluble substances from the gloves. Dwell

time was set as 8, 4, 8 seconds for the former to dipping in, stopping, and dipping out, respectively. This process is similar to the wet-film leaching previously, but it was carried out on the dry latex films. Then, the former were dried in the oven at 100 °C for 5 minutes. The final operation on the nitrile film dipping process is the stripping process. In this stage, the latex films were removed off the former manually. Figure 3.2 shows the overall dipping process of nitrile butadiene rubber latex films.
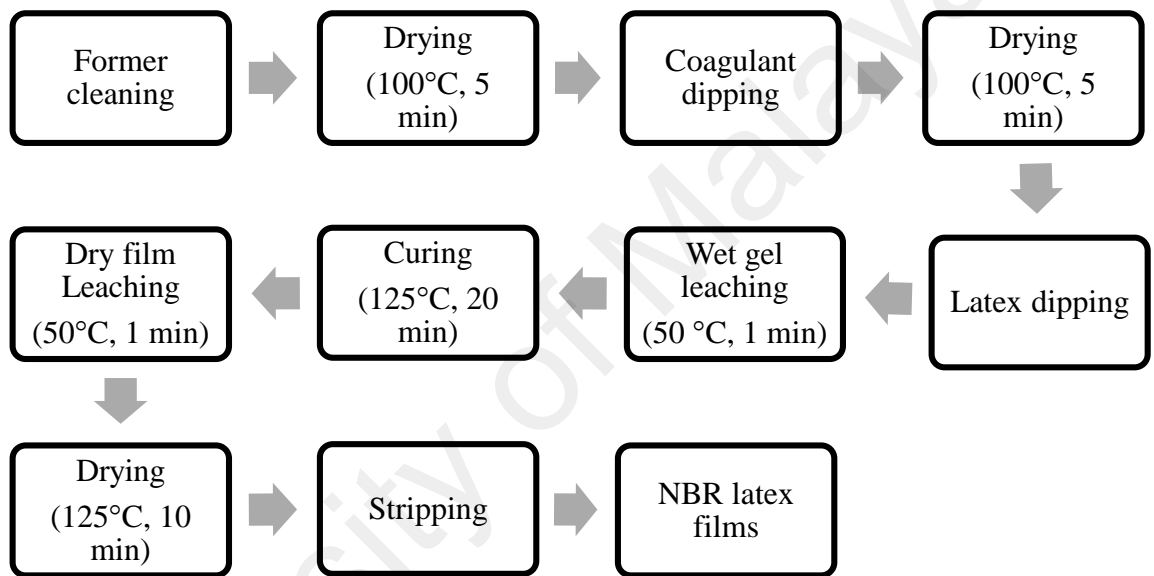
Figure 3.2: Flow chart of dipping process
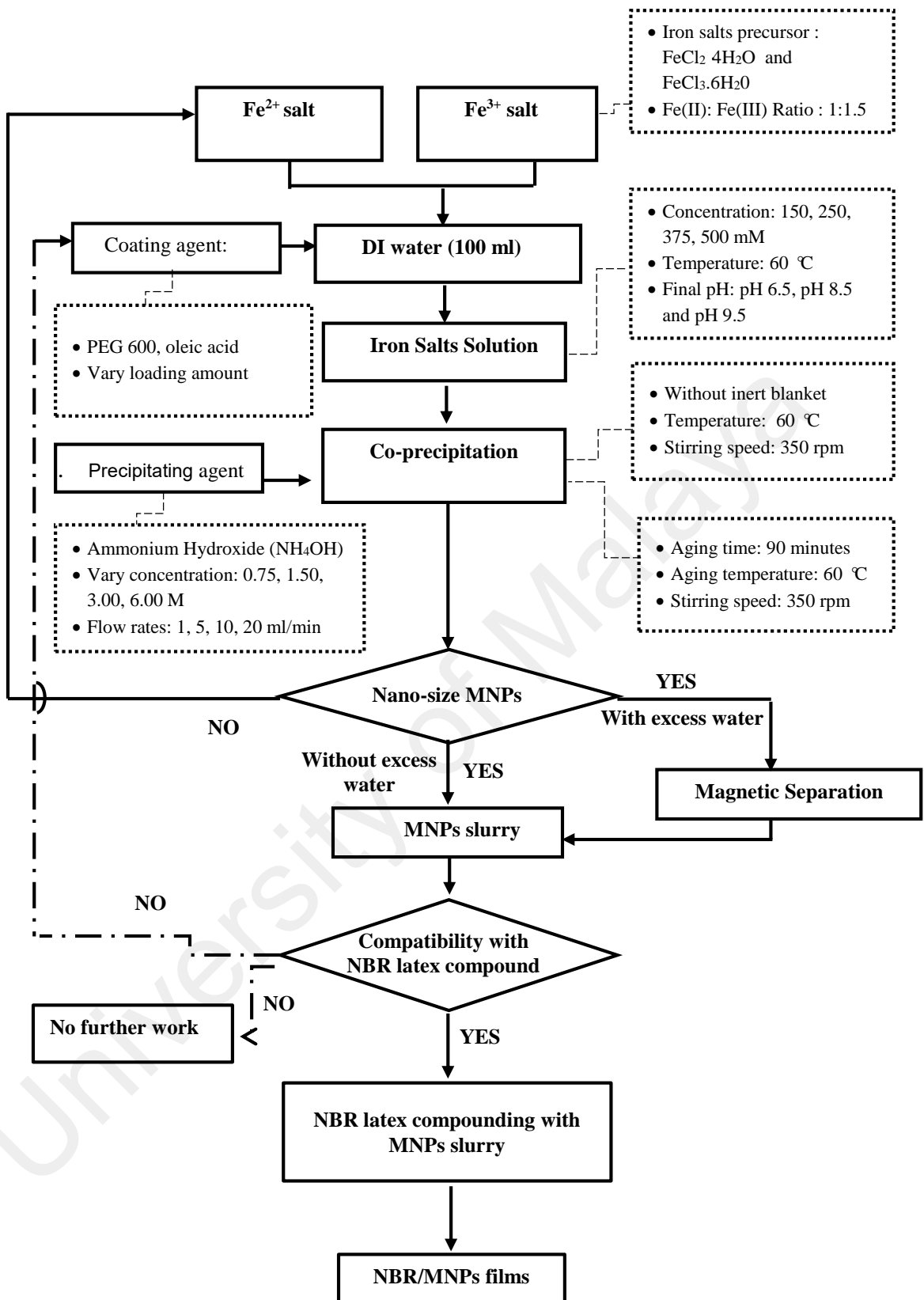
Figure 3.3: Overall flow chart of MNPs synthesis and incorporation into nitrile butadiene rubber latex compound

3.4 Characterization of Magnetite Nanoparticles and Nitrile Films

The structural, morphological, chemical, magnetic properties of uncoated and coated MNPs were characterized via various characterization techniques. The characterization techniques are Zeta sizer, X-ray diffraction (XRD), Fourier Transform infrared spectroscopy (FTIR), Raman spectroscopy, Thermogravimetric analysis (TGA), High-resolution transmission electron microscope (HRTEM), Field Emission Scanning Electron Microscopy (FESEM), and vibrating sample magnetometer (VSM). Lastly, the tensile properties, thermal stability, and morphology of nitrile butadiene rubber latex films were characterized via Universal Testing Machine (UTM), Thermogravimetric analysis (TGA) and Field Emission Scanning Electron Microscopy (FESEM), respectively.

3.4.1 Sedimentation tests

The colloidal stability of MNPs was evaluated by sedimentations tests and zeta potential. Sedimentations tests were performed to evaluate the colloidal stability of magnetite nanoparticles (MNPs) dispersed in water and nitrile butadiene rubber latex, at pH 10. For each tests, the nitrile butadiene rubber latex mixed with MNPs slurry was put in a sample vial and the evolution over time of the MNPs in these two medium was continuously monitored. 1.0 g of coated MNPs were weighed and dispersed in deionized water, with pH adjusted by ammonium hydroxide to pH 10. The MNPs slurry was sonicated for 60 minutes to prevent aggregation of MNPs. Then, the dispersion was mixed with nitrile butadiene rubber latex by manual stirring in order to obtain a homogeneous mixture. Lastly, the mixture was transferred to a sample vial and sediment of coated MNPs were observed and recorded at time 3 hours, 3 days, 7 days, 14 days and 21 days.

3.4.2 Zetasizer

Zetasizer instrument provides the ability to measure characteristics of particles or molecules in a liquid medium. The Zetasizer determines the particle size by first measuring the Brownian motion of the particles in a sample using Dynamic Light Scattering (DLS) and then interpreting a size from this using Stokes-Einstein relationship. The Particle Size measured in a DLS instrument is the diameter or radius of the sphere that diffuses at the same speed as the particle being measured. In the current study, Malvern Zetasizer Nano ZS was used to investigate zeta potential, number-based particle size distribution (PSD) and polydispersity (PDI) of MNPs.

The zeta potential is also a key indicator of the stability of colloidal dispersions. The magnitude of zeta potential indicates the degree of electrostatic repulsion between adjacent, similarly charged particles in dispersion. For molecules or particles that are small enough (nanoscale), a high zeta potential will confer stability, i.e., the solution or dispersion will resist aggregation. (Saraswathy et al., 2014). Details of the stability of suspensions with relation to zeta potential are summarized in Table 3.2.

Table 3.2 Stability of suspensions with relation to zeta potential
(Roch et al., 2005)

Zeta Potential (mV)	Stability Behaviour
0 to ±5	Aggregation and precipitation
±10 to ±30	Limited Stability
±30 to ±40	Moderate Stability
±40 to ±60	Good stability
±60 to ±80	Excellent stability
±81 to ±100	Extremely good stability

Approximately 0.001g of MNPs powder was weighed and dispersed in 5 ml of deionized water. Then, the pH of solution was adjusted to pH 10 by adding ammonium hydroxide (12 M). The solution was sonicated for 1 hour to ensure MNPs was dispersed well in deionized water. Next, dispersed solution was filtered and injected into a disposable

44

sample cell. Then, the sample cell was inserted into the instrument and the measurement start after the sensors have equilibrated. Finally, measurement was run and results were collected.

3.4.3   X-Ray Diffraction (XRD)

The crystallographic structure and phase of the MNPs was investigate by X-ray diffraction (XRD) analysis. This analysis were carried out using a Bruker D8 Advance diffractometer equipped with a quartz mono-chromator and Cu Kα radiation (λ= 0.154059 nm). Approximately 1 g of the sample was measured and placed into sample holder. The testing was carried out with a step size of 0.02 degrees and scan speed of 0.02 deg/sec in between 10° and 90° diffraction angle (2θ). One of the more frequent applications of XRD analysis is to determine the crystallite size. There are several studies on the determination of the crystallite size from the XRD patterns. From the XRD result, crystallite size can be determined by using Debye Scherrer's equation (Equation 3.1).

$$D= \frac{K\lambda}{\beta cos\theta}$$ (Equation 3.1)

where K is the shape factor, λ is the x-ray wavelength, β is the line broadening at half of the maximum intensity of each peak, and θ is the Bragg angle. D is the mean diameter of the ordered domains. The Debye-Scherrer equation can be used to obtain a rough estimate of the nanoparticle size.

3.4.4   Fourier Transform Infrared Spectroscopy (FTIR)

In the current study, Fourier transform infrared (FTIR) was used to identify the MNPs and coating agent (PEG 600, oleic acid) functional groups, and the functional group linked between MNPS and coating agent. FTIR spectra were recorded in the range 4000 cm^{-1} and 400 cm^{-1} at a resolution of 4 cm^{-1} for each set of coated MNPs samples. However, FTIR spectroscopy is also useful as a means of identification for iron oxyhydroxides,

showing Fe-O-H stretching and bending vibrations for each phase in the range of 1000 cm⁻¹ to 400 cm⁻¹ (Schwertmann & Cornell, 2008; Vikram et al., 2015). Therefore, FTIR spectra were recorded in the range of 1200 cm⁻¹ to 400 cm⁻¹ for the uncoated MNPs. Approximately 0.3 mg of MNPs was mixed with 4 mg of KBr and moulded to form pellet. Pellet was placed in the FTIR and IR radiation was passed through it. FTIR spectrum was collected with labelled peaks.

3.4.5   Raman Spectroscopy

Raman spectroscopy provides information about molecular vibrations that can be used for sample identification and quantitation. Raman spectra of samples were obtained with a Renishaw inVia Raman microscope with 514 nm laser as excitation source in the frequency range of 100-1800 cm⁻¹. To obtain the MNPs Raman spectra, approximately 0.05 g of sample was placed into the sample holder, and the testing was carried out with 0.02 mV laser power and 180 seconds of exposure time. Obtained Raman spectra was analysed and phases of MNPs was determined.

3.4.6   Thermogravimetric Analysis (TGA)

Thermogravimetric analysis (TGA) was conducted using a Mettler Toledo, TGA/SDTA-851ᵉ under nitrogen atmosphere. Thermal stability in terms of decomposition temperature and weight loss of a specimen was measured by monitoring the weight change that occurs as the specimen is heated. Approximately 4-5 mg of specimens was prepared and put into an alumina cup. After that, the specimen cup was heated from 30 ºC to 800 ºC at a heating rate of 10ºC/min under nitrogen gas (flow rate of 50 ml min⁻¹). A thermogram, which is a curve of the percentage of weight change against the specimen temperature was plotted. This technique was used to investigate the coating efficiency of coating agent on the surface of MNPs. TGA is beneficial in

quantifying the amount of the organic matter exchanged on the surfaces of the particles, thus generating an idea of the success or extent of ion exchange process. Thus, TGA provides an efficient tool to determine the organophilization of the particle surface. Mass loss due to high-temperature dihydroxylation of the iron oxide and evaporation of physisorbed water has to be subtract from the total weight loss to obtain information on the mass loss corresponding to the organic layer (Mittal, 2012).

3.4.7 High Resolution Transmission Electron Microscopy (HRTEM)

The high resolution transmission electron microscope (HRTEM) is probably the most powerful technique for characterizing nanomaterials. By using HRTEM, we can image particles in the nanometer size scale. High resolution transmission electron microscopy (JEM-2100F) with accelerating voltage 200 kV was used to visualize the morphology of the MNPs. During sample preparation, the MNPs was dispersed in ethanol (95 %). Then, the sample was sonicated for 1 hour. Finally, the dispersion of MNPs was allowed to slowly dry on 300 mesh copper grid. The sample need to be prepared at least three day before the measurement in order to ensure the sample is fully dry. This step is crucial to prevent the electrical contact while the reading is measured. All imaging and size calculations were carried out using Image J version 1.48 (National Institutes of Health, USA) with the scale bar as a unit of reference. The counting was performed on 100 particles for each sample.

3.4.8 Field Emission Scanning Electron Microscopy (FESEM)

FESEM is the abbreviation of Field Emission Scanning Electron Microscope. FESEM is used to visualize very small topographic details on the surface or entire or fractioned objects. In this research, morphology of the MNPs and nitrile butadiene rubber films were investigated using scanning electron microscope (HITACHI SU 8030). The samples were

mounted onto sample holder using double sided electrically conducting carbon adhesive tapes to prevent surface charge on the specimens when exposed to the electron beam. The tensile fractured surfaces of nitrile butadiene rubber films were pre-sputtered with platinum. The FESEM micrographs were obtained under conventional secondary electron imaging conditions with acceleration voltage of 5 kV.

3.4.9 Vibrating Sample Magnetometer (VSM)

The magnetic properties (hysteresis loop) of the dried nanoparticles were assessed using vibrating sample magnetometer (VSM, LakeShore 7400; Chicago, IL, USA) at 300 K. The main magnetotstatic parameters saturation magnetization, coercivity, and remanence are determined from magnetization curves measured on VSM at static magnetic fields with a strength of up to 10 kG. Approximately 0.05 g of MNPs powders were weighed and then placed in a sample holder for magnetic readings. The sample is placed between two electromagnets where a uniform magnetic field is generated. The sample is then physically vibrated sinusoidally at frequency of 70 Hz. By changing the strength of an external electromagnetic field the hysteresis curve of a material was obtained in the magnetic field from -10 kG to 10 kG.

3.4.10 Universal Testing Machine (UTM)

The produced nitrile butadiene rubber films was cut into desired dimension (Figure 3.5) in accordance to ASTM D412 standard using standard dumbbell die C. The thickness of each specimens was measured prior to testing. The specimens mounted on Tensile measurements, were tested at room temperature according to ASTM D412 with a computerized tensile tester (Instron 3345) with a load cell of 100 N. The crosshead speed was set at 500 mm/min. Tensile strength, elongation at break and modulus were collected.

Five specimens were used for each set of composite system. Each value obtained represented the average of five samples.

ASTMD-412-C、UL-62-C
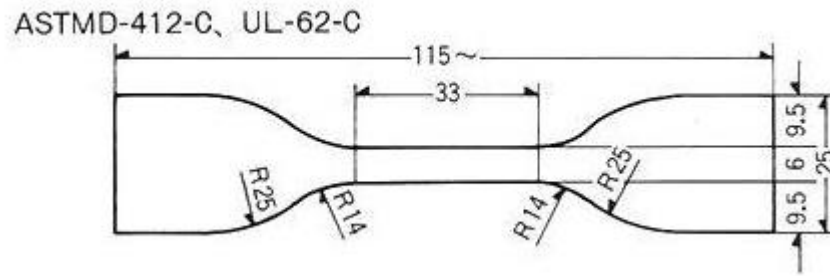
Figure 3.4: The dimension of nitrile butadiene rubber films specimen for tensile test

4.1 Introduction

This chapter presents the results obtained from the experiments conducted and the discussion of the analyses. There are three main sections in this chapter. The first section presents the synthesis and properties regarding to the formation of high saturation magnetization magnetite nanoparticles (MNPs) in the presence of ammonium hydroxide. The effect of final pH as well as the influence of the addition rate on MNPs are evaluated in detail. The second section of this chapter will illustrate the influence of coating agent's loading amount on the stabilization of MNPs in aqueous medium. Lastly, the third section of this chapter present the performance studies of MNPs loaded nitrile butadiene rubber latex films. This study aims to optimize the magnetic properties of as-prepared MNPs as well as improve their colloidal stability in nitrile latex.

4.2 Synthesis of Magnetite Nanoparticles (MNPs)

4.2.1 Zeta Potential and Hydrodynamic Size Analysis

Table 4.1 shows the hydrodynamic size and zeta potential measurement of MNPs synthesized with different reaction parameters, including final pH, ammonium hydroxide concentration, total iron salts concentration and addition rate of ammonium hydroxide. In general, all of the MNPs can be considered in stable form in a basic medium with negative surface charges around 30 mV and PDI values less than 0.3 (Cho et al., 2013).

Table 4.1: The hydrodynamic size and zeta potential of MNPs

Sample	Hydrodynamic size (nm)	Polydispersity index, PDI	Zeta Potential (mV)
a) Final pH			
pH 6.5	43.33	0.196	-32.7
pH 8.5	43.17	0.188	-30.3
pH 9.5	38.10	0.165	-29.8
b) Ammonium Hydroxide Concentration			
0.75 M	33.82	0.183	-33.9
1.50 M	35.33	0.167	-31.4
3.00 M	38.10	0.165	-29.8
6.00 M	47.42	0.151	-28.8
c) Total Iron Salts Concentration			
150 mM	38.10	0.165	-29.8
250 mM	38.99	0.202	-30.1
375 mM	42.96	0.214	-29.8
500 mM	49.09	0.228	-34.3
d) Addition Rate of Ammonium Hydroxide			
1 ml/min	47.82	0.245	-31.6
5 ml/min	42.96	0.214	-29.8
10 ml/min	38.99	0.202	-31.9
20 ml/min	37.14	0.146	-33.4

Interestingly, it could be noticed that hydrodynamic size of MNPs with 38.10 nm for the final pH of 9.5 was the smallest particle throughout the final pH window, suggesting that high hydroxide ion (OH^-) could facilitate the formation of small particle. The decrease in hydrodynamic size of MNPs is likely attributed to the high surface charges with increasing final solution's pH. This is in agreement with the results of Salazar et al. (2011), which reported that mean size of MNPs was decrease significantly at high pH. Furthermore, the size distribution width was reducing as the final pH increases, which indicating that MNPs particles produced at higher pH are smaller and more uniform. In Formation of large MNPs particle at low pH is due to continuous growth of the particles during the ageing phase associated with Ostwald ripening (Darminto et al., 2011). The mechanism of growth (Ostwald ripening) is caused by the change in solubility of nanoparticles dependent on their size. Due to the high solubility and the surface energy

of smaller particles within solution, these particles re-dissolve and in turn allow the larger particles to grow even more (Baumgartner et al., 2013).

Ammonium hydroxide was used as precipitating agent in the co-precipitation reaction of MNPs. According to Mascolo et al. (2013), the (OH⁻) concentration, which is related to the pH and base amount, is known to control the nucleation and growth of the magnetite nanoparticles and can influence the final properties of magnetite (particle size and saturation magnetization). Therefore, MNPs synthesized with different concentration of ammonium hydroxide was investigated in this part of experiment. The variations in hydrodynamic size, polydispersity index (PDI) and zeta potential of the MNPs with different concentration of ammonium hydroxide are presented in Table 4.1. The hydrodynamic size was increased when the concentration of ammonium hydroxide was increased from 0.75 M to 6.00 M under atmospheric condition. These results suggest that more reaction ingredients are available on the growth phase and therefore MNPs with large diameter (18 nm) could be synthesized under the high concentration of ammonium hydroxide (Tajabadi & Khosroshahi, 2012). The above-discussed statement is further confirmed by the polydispersity index (PDI) and zeta potential, which suggesting that high concentration of ammonium hydroxide can produce MNPs with larger diameter and more uniform size.

In order to understand the effect of total iron salts concentration on the hydrodynamic size, polydispersity index (PDI) and zeta potential of MNPs, the samples were synthesized with 150 – 500 mM. The result clearly shows that the hydrodynamic size of MNPs is dependent on the total iron salts concentration. Based on the results obtained, the hydrodynamic size of MNPs obviously increased with increasing salts concentration. However, it was observed that the PDI values increased with increasing salts

concentration. This result suggests that the size of MNPs prepared under higher iron salts concentration of 500 mM are less uniform as compared to the lower concentration one.

Lastly, the effect of addition rate of ammonium hydroxide on the hydrodynamic size of MNPs was investigated. Based on Table 4.1, the hydrodynamic size of MNPs appeared to be dependent on the addition rate of ammonium hydroxide into the mixture of iron chloride salts. It was noticed that the number average particle size of MNPs decreased from 53.32 nm to 37.14 nm, with the base addition rate from 1 ml/min up to 20 ml/min. It's a well-known fact that the fast addition of ammonium hydroxide solution into the reaction solution favour the continuous nucleation with respect to growth, thus enabling the formation of small particles (Mascolo et al., 2013). In additon, the nucleated particles had size distribution that varies with the supply rates during the nanoparticles growth. For this reason, the polydipsersity of MNPs was decreased from 0.245 to 0.146 at higher addition rates (Gnanaprakash et al., 2007).

4.2.2   X-ray Diffraction Analysis

In this part of experiment, XRD analysis was used to investigate the crystallite size of MNPs after synthesizing via different processing parameters. As shown in Table 4.2, the crystallite size of MNPs was determined by fitting of the magnetite (311) Bragg peak by Scherrer analysis with a pseudo-Voigt function (Baumgartner et al., 2013).

Table 4.2: Crystallite size of MNPs

Sample	Crystallite size, D_{XRD} (nm)
a) Final pH	
pH 6.5	17.7
pH 8.5	15.7
pH 9.5	12.3
b) Ammonium Hydroxide Concentration	
0.75 M	12.1
1.50 M	12.3
3.00 M	12.3
6.00 M	12.3
c) Total Iron Salts Concentration	
150 mM	12.3
250 mM	12.6
375 mM	13.6
500 mM	14.5
d) Addition Rate of Ammonium Hydroxide	
1 ml/min	14.1
5 ml/min	13.6
10 ml/min	10.8
20 ml/min	9.8

Based on Figure 4.1, the positions and relative intensities of all diffraction peaks fit well with those from the JCPDS card (19-0629) for magnetite with (220), (311), (400), (551) and (440) peaks at around $2\theta \approx 30°, 35°, 43°, 57°$ and $63°$, respectively. However, maghemite phase also has a crystal structure and lattice spacing similar to those of magnetite. For this reason, XRD characterization alone is insufficient to confirm the crystal structural forms of nanoparticles (Jiang et al., 2011).

It is noteworthy to mention that the crystallite size of the MNPs decreased with increasing final pH based on the XRD results obtained (Table 4.2). The decrease in crystallite size was as follows, 17.7 nm, 15.7 nm to 12.3 nm corresponding to sample synthesized at final pH increased from pH 6.5, pH 8.5 to pH 9.5, respectively. In addition, the broadening of peaks as a sign of smaller particle size could be observed from the XRD patterns as presented in Figure 4.1a. As a matter of fact, pH is known to control the nucleation and growth of the MNPs which eventually influences its particles size. During

co-precipitation process, the degree of supersaturation is higher at high pH, which promotes nucleation over growth. Thus, smaller particles were formed (Mascolo et al., 2013).

Nucleation and growth rates are controlled by supersaturation. Growth rate increases linearly with supersaturation, while nucleation increases exponentially (Lipták, 2013). According to classical nucleation theory, the nucleation rate J is typically described as Equation 4.1.

$$J = K_1 S \exp\left(-\frac{K_2}{\ln^2 S}\right)$$ **(Equation 4.1)**

Where $S = c/c_\infty$ is the degree of supersaturation, C is actual concentration of the substance in solution, C_∞ is normal equilibrium concentration of the substance in pure solvent, K_1 is a parameter determined by the kinetic aspect of nucleation, whose various expressions can be found in the literature, and K_2 is a parameter depend purely on the thermodynamic properties of the system (Vetter et al., 2013).

The corresponding experimental results on the influence of ammonium hydroxide concentration towards to the crystallite size of MNPs are presented in Table 4.2. It was found that the crystallite size of MNPs slightly increased from 12.1 up to 12.3 nm when increasing the ammonium hydroxide concentration (0.75 M to 1.50 M). Nevertheless, the crystallite size of MNPs did not have significant change when applying different ammonium hydroxide concentration. This statement is in the agreement of Arabi and Asnaashari Eivari (2014), which proposed that high concentration of a weak base (ammonium hydroxide) did not affect the nucleation rate and therefore, the crystallite size of MNPs did not increase significantly.

Figure 4.1c shows the XRD pattern of synthesized MNPs subjected to different iron salts concentration during reaction stage. It is worth noting that increment in the total iron

salts concentration resulted in a noticeble broadening and weakening of peaks. According to the literature, the broadening of XRD's peaks might be a sign of poor crystallization of the geothite structure or small particle size of MNPs (Karaagac et al., 2010). This finding might be attributed to the nucleation stage occurred when the concentration of reactant (iron salts) reached the supersaturation. Then, the nuclei start to grow via flocculation or aggregation of nuclei into larger particles. This infers that the reduction of iron salts concentration might be distrupted the nucleation and growth of MNPs (Jiang et al., 2011). Therefore, the crystalinity and crystallite size of synthesized MNPs formed decreased from 14.5 nm to 12.3 nm as the iron salts concentration decreased in the mixture.

Similary, there is no other impurity compouds could be detected from the MNPs sample when applying different addition rate of ammonium hydroxide into the iron salts mixture (Figure 4.1d). As the addition of ammonium hydroxide with increasing rate, the solution reached supersaturation state rapidly by nucleating the smaller particles at large numbers in unit volume. By referring to crystallization theory and homogenous nucleation equation, the nucleation rate was inversely proportional to the critical radius of the nucleated particle (Gnanaprakash et al., 2007). Based on the reults from XRD analysis, the crystallite size of MNPs was decreased from 14.1 nm to 9.8 nm when the base additon rate increased from 1 ml/min to 20 ml/min (Table 4.2).

In summary, it could be concluded that all samples have crystallite size less than the critical value 30 nm. Thus, they might exihibit superparamagnetic behavior. It has been reported that particles exhibited superparamagnetism behaviour when the size of single domain particles further reduces below a critical diameter and the coercivity becomes zero (Nyirő-Kósa et al., 2009;Cheng et al., 2010) .
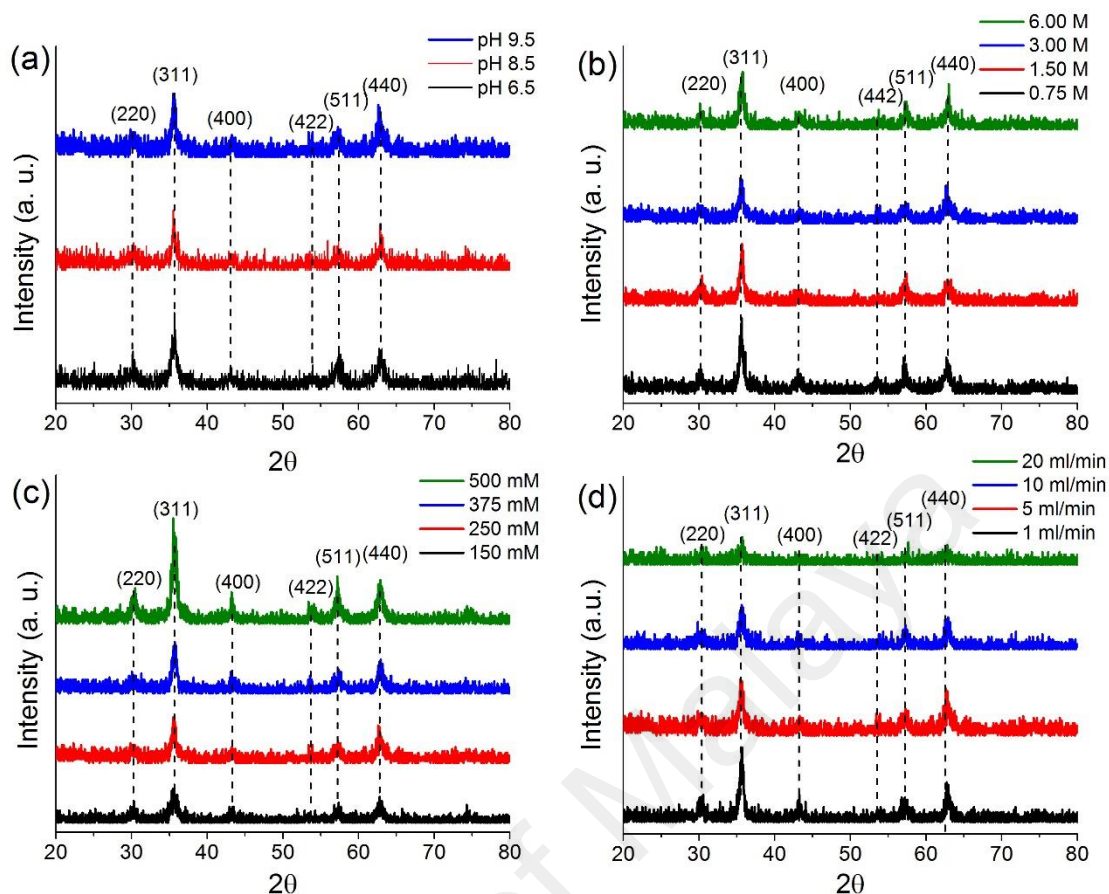
Figure 4.1: XRD pattern of MNPs optimized with different parameters (a) final pH, (b) ammonium hydroxide concentration, (c) total iron salts concentration, and (d) additon rate of ammonium hydroxide

### 4.2.3 Fourier Transform Infrared Spectroscopy (FTIR) Analysis

In this section, FTIR was done to gain further information about the structure of the synthesized MNPs. The transmittance peaks of magnetite were observed at about 449 cm^{-1} and 580 cm^{-1}, while maghemite peak was observed at 630 cm^{-1} for MNPs synthesized at final pH 9.5. However, in FTIR spectrum of MNPs synthesized at final pH 6.5 and final pH 8.5, these peaks weakened gradually and new transmittance peaks appeared at 799 cm^{-1} and 895 cm^{-1} indicate iron oxyhydroxide phase. Therefore, it shows that the MNPs synthesized with a lower final pH have an additional goethite (α-FeOOH) phase with main magnetite phase (Andrade et al., 2010). The inadequate of OH^{-} species (low pH condition) probably caused incomplete co-precipitation reaction during the

formation of MNPs, which producing intermediate compound from the MNPs. Similar findings with regards to goethite and maghemite are the most common impurity compounds that could be found in magnetite via co-precipitation methods were reported by the Gnanaprakash et al. (2007).

Meanwhile, the effect of ammonium hydroxide concentration on the information about the structure of synthesized MNPs was investigated in detail. From the results obtained, it was found that magnetite peaks were detected at 449 cm^{-1} and 580 cm^{-1} for all of the MNPs prepared using different ammonium hydroxide concentration. However, the highest intensity peak of the maghemite content could be detected from MNPs, which synthesizing with 6.00 M ammonium hydroxide as compared to the other samples. This is in agreement with the results of Tajabadi and Khosroshahi (2012),which reported the formation of non-magnetite layer on MNPs synthesized with high ammonium hydroxide concentration. The reasons might be due to magnetite phase of MNPs partly transformed into geothite phase at high pH (pH > 10) conditions. This conversion of magnetite to goethite passed through a maghemite intermediate and hence the maghemite phase was detected in the FTIR spectra of 6.00 M ammonium hydroxide sample (He & Traina, 2007).

The total iron salts concentration has significat effects on the structure of synthesized MNPs. It is noteworthy to mention that a shoulder peak for 500 mM sample can be observed at around 630 cm^{-1}, which indicates the maghemite phase that probably generate from surface oxidation of MNPs. Besides, the peaks of Fe-O (580-650 cm^{-1}) of all synthesized MNPs were widened with decreasing of iron salts concentration. This is in agreement with the results of Smolkova et al. (2015), which proposed that MNPs are very sensitive to oxidation due to their large surface area. All synthesized MNPs could be transformed into maghemite through oxidation process. As a result, magnetite and

maghemite mix-phase composition were observed in most of the synthesized samples. However, the co-precipitation reaction is said to be completed as there are no peaks located in the 790-890 cm⁻¹ region which belong to the intermediate of the reaction.

The current section discusses the effect of addtion rate of ammonium hydroxide into the iron salt mixture on the structure of synthesized MNPs. FTIR patterns from all of the synthesized MNPs at different loading rate exhibited one peak (580 cm⁻¹) only. This result indicates that the magnetite phase is still present dominantly and did not reveal any other phases in the FTIR patterns. In summary, the addition rate variation of ammonium hydroxide into iron salts mixture did not affect the structure of the nanoparicles and the results is consistent with the XRD results discussed earlier.
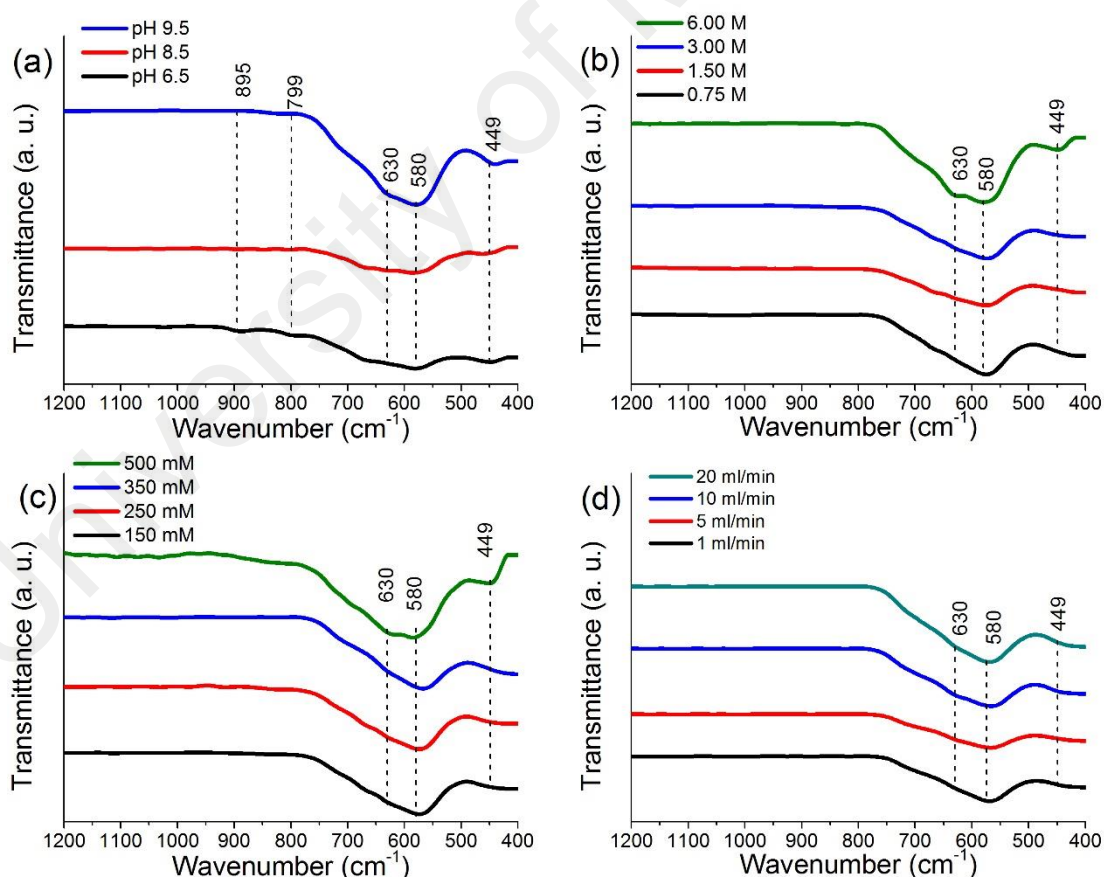
Figure 4.2: FTIR spectra of MNPs optimized with different parameters (a) final pH, (b) ammonium hydroxide concentration, (c) total iron salts concentration, and (d) additon rate of ammonium hydroxide.

4.2.4 RAMAN Analysis

In Raman spectroscopy, excessive exposure of the MNPs to laser radiation will generate hematite (Li et al., 2012). Therefore, the Raman spectra of MNPs were obtained by using a low power laser (0.20 mW). Indeed, Raman analysis has been used to determine and understand the structural changes of synthesized iron oxide samples upon different pH value.

Table 4.3: Raman frequencies (cm^{-1}) of the iron oxides
(Slavov et al., 2010;Li et al., 2012)

Iron oxides	Raman frequency (cm^{-1})
Magnetite	193 (W), 306 (W), 668 (S)
Maghemite	363 (S), 500 (S), 720 (S), 1400 (S)
Hematite	225 (S), 247 (W), 299 (S), 412 (S), 497 (W), 613 (M)
Goethite	400 (S)

S: Strong   M: Medium   W: Weak

Based on the Raman spectra obtained, it could be noticed that all synthesized samples containing magnetite and maghemite phases. The increment in Raman intensity of maghemite peaks at 720 cm^{-1} and 1400 cm^{-1} were observed when increasing the final pH from pH 6.5 to pH 9.5. According to Chourpa et al. (2005), they concluded that most of the band above 1100 cm^{-1} were not specific of magnetite-maghemite except for maghemite band at 1400 cm^{-1}. For the parameter of final pH, the goethite structure that was detected earlier in FTIR analysis disappeared in the Raman spectrum of MNPs synthesized with final pH 6.5. The reason might be due to the relatively small amount of goethite as compared to magnetite in sample. In overall, the comparison of maghemite content detected from the synthesized MNPs with the corresponding crystallite sizes is shown in Table 4.2. Interestingly, it can be seen that particle sizes of magnetite was reduced when the maghemite content was increased according to our MNPs results. However, the Raman's intensity of maghemite phase was decreased as the addition rate was increased from 1 ml/min up to 20 ml/min (Figure 4.3d). This result indicates that the

slower addition rate of ammonium hydroxide was prone to oxidation reaction than the

faster addition rate although it has bigger crystallite size of MNPs.
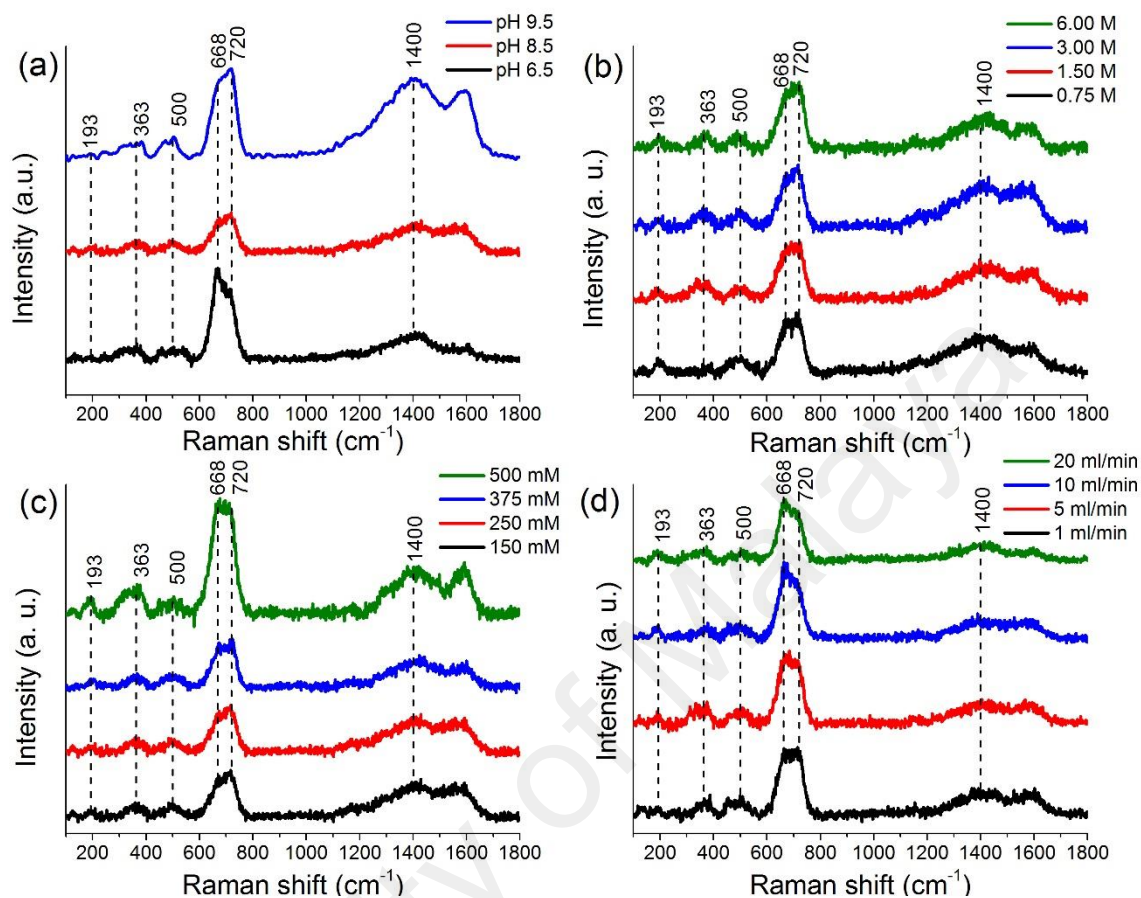
Figure 4.3: RAMAN spectra of MNPs optimized with different parameters (a) final pH, (b) ammonium hydroxide concentration, (c) iron salts concentration, and (d) additon rate of ammonium hydroxide.

4.2.5   HRTEM Analysis

Subsequently, corresponding HRTEM images of the selected synthesis parameter

(final pH) are presented in Figure 4.4. The Morphology and mean particle size of prepared

MNPs were further determined via HRTEM at $100,000\times$ magnification as presented in

Figure 4.4. Figure 4.4(a) shows the morphology of the goethite with rod-like particles as

indicated with arrows (dot-line). Based on Figure 4.4(a), there was obvious aggregation

of particles found on the as-synthesized MNPs. As a matter of fact, all rod-like particles

were identified earlier by FTIR as goethite, a by-product in co-precipitation process. The reaction occurred is depicted in equation below (Mahdavi et al., 2013):

$$Fe^{3+}+3OH^-\rightarrow Fe(OH)_3 \qquad \text{(Equation 4.2)}$$

$$Fe(OH)_3\rightarrow FeOOH+H_2O \qquad \text{(Equation 4.3)}$$
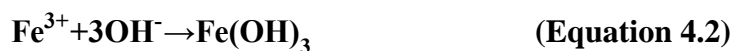
According to Equation 4.2, akaganeite was formed as a result of the hydrolysis of the ferric (Fe^{3+}) ion solution in the presence of Cl^- and highly acidic pH (Ahn et al., 2012; Bibi et al., 2012). Then, akaganeite was dissolved and evolved into mixture of goethite (minor component) and magnetite (major component) at higher pH (Figure 4.4a) as shown in Equation 4.3. According to Karaagac et al. (2010), goethite formation might be in amorphous phase as only magnetite phase were observed in XRD pattern (Figure 4.1a). It could be noticed that the content of magnetite phase was increased while goethite phase was disappeared from MNPs with pH up to 9.5 (Figure 4.4c). Thus, fine-tuning the pH of mixture for MNPs formation is important to develop a goethite free MNPs. All obtained results suggested that co-precipitation between Iron (II) ion and Iron (III) ion showed almost complete precipitation reaction at pH 8.5. As pH value increased to 9.5, it was found that smaller average size of MNPs with uniform spherical form (13.75 nm) could be synthesized. This result suggests that spherical MNPs with uniform size could be formed with the final pH of mixture must be above 9.5.
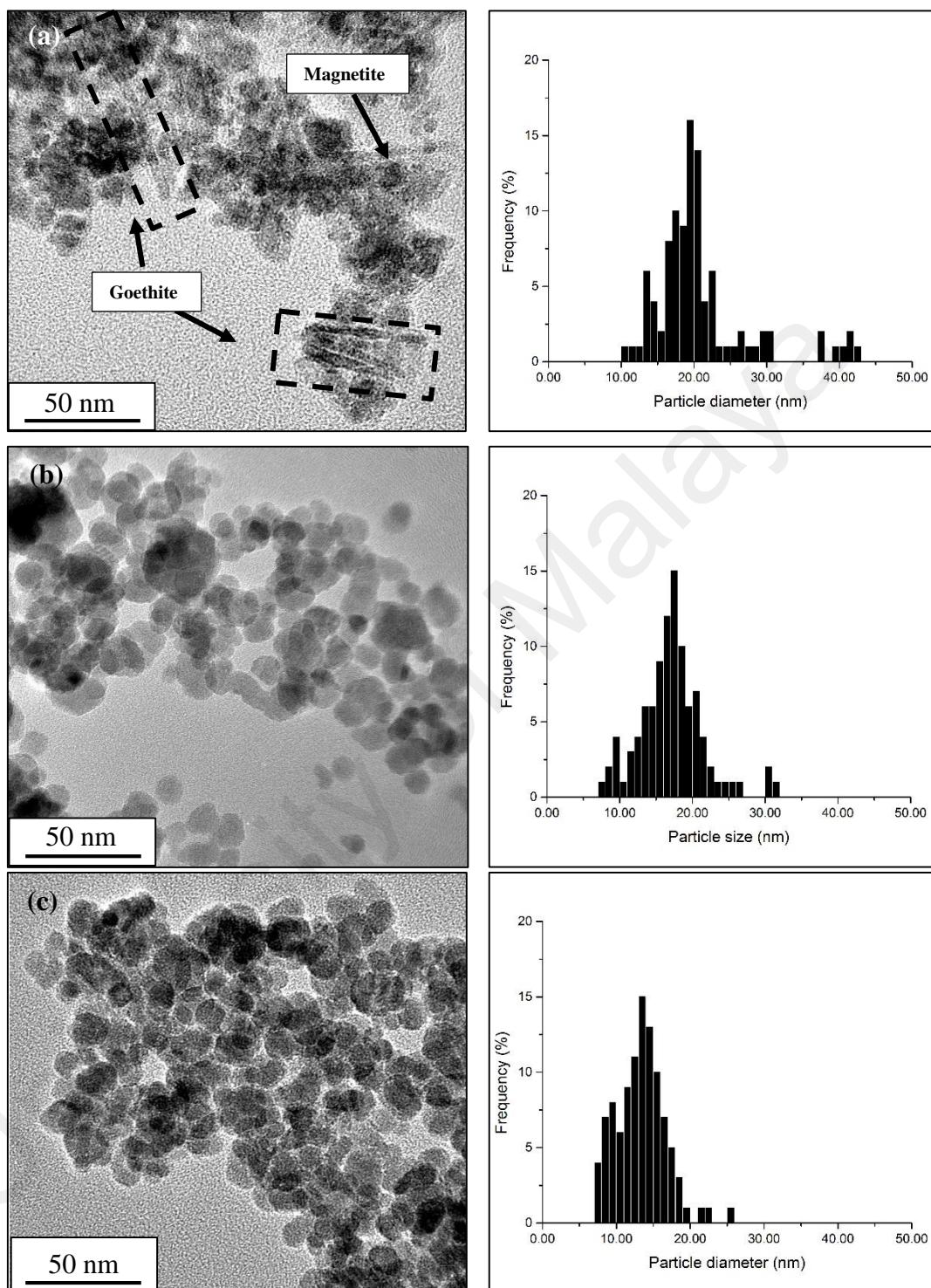
Figure 4.4: HRTEM images for final pH of (a) pH 6.5, (b) 8.5, and (c) pH 9.5 at 100,000 × magnification

4.2.6 Magnetic Properties Measurement

A vibrating sampler magnetometer (VSM) was used to measure magnetic properties of MNPs. The hysteresis curves of the synthesized samples from the above-mentioned list were measured and presented. Table 4.4 exhibits the saturation magnetization, coercivity and remanence of MNPs optimized with the parameters at room temperature.

Table 4.4: Magnetic properties of uncoated MNPs

Sample	Crystallite size (nm)	Saturation Magnetization, M_s (emu/g)	Coercivity, H_c (Oe)	Remanence, M_r (emu/g)
a) Final pH				
pH 6.5	17.7	31.90	3.29	0.19
pH 8.5	15.7	63.45	6.17	0.66
pH 9.5	12.3	65.04	11.97	1.21
b) Ammonium Hydroxide Concentration				
0.75 M	12.1	62.63	7.03	0.72
1.50 M	12.3	63.63	7.47	0.72
3.00 M	12.3	65.04	11.97	1.21
6.00 M	12.3	64.00	12.66	1.35
c) Total Iron Salts Concentration				
150 mM	12.3	65.04	11.97	1.21
250 mM	12.6	77.74	12.18	1.51
375 mM	13.6	80.23	14.71	1.79
500 mM	14.5	70.11	16.00	1.84
d) Addition Rate				
1 ml/min	14.1	77.90	12.21	1.37
5 ml/min	13.6	80.23	14.71	1.79
10 ml/min	10.8	69.91	11.37	1.16
20 ml/min	9.8	64.83	11.02	1.07

Hysteresis curves of the synthesized samples were further investigated and presented in Figure 4.5. As shown in Figure 4.5, saturation magnetization (Ms) obtained from hysteresis curve for the experiment set based on the final pH criteria clearly to shows that the Ms was increased from 31.90 emu/g to 63.45 emu/g, and then slighly increased back from 63.45 emu/g to 65.04 emu/g as the final pH was increased from pH 6.5 (acidity but close to neutral condition) to pH 9.5 (alkaline condition). In order to explain the change

of Ms, the structure of MNPs should also be taken into consideration as indicated by FTIR analysis. It could be noticed that the lowest saturation magnetization was obtained at final pH 6.5 which confirmed via FTIR and HRTEM micrograph that showed small portion of goethite that appeared within the synthesized MNPs. This reason might be attributed to the low pH values that prevent the precipitation to take place since the co-precipitation was completed at between pH 8 and pH 11 (Karaagac & Kockar, 2012). Therefore, in the following studies, MNPs with high saturation magnetization as well as uniform particle size were synthesized in such condition mentioned above to further study the effect of surface coating studies.
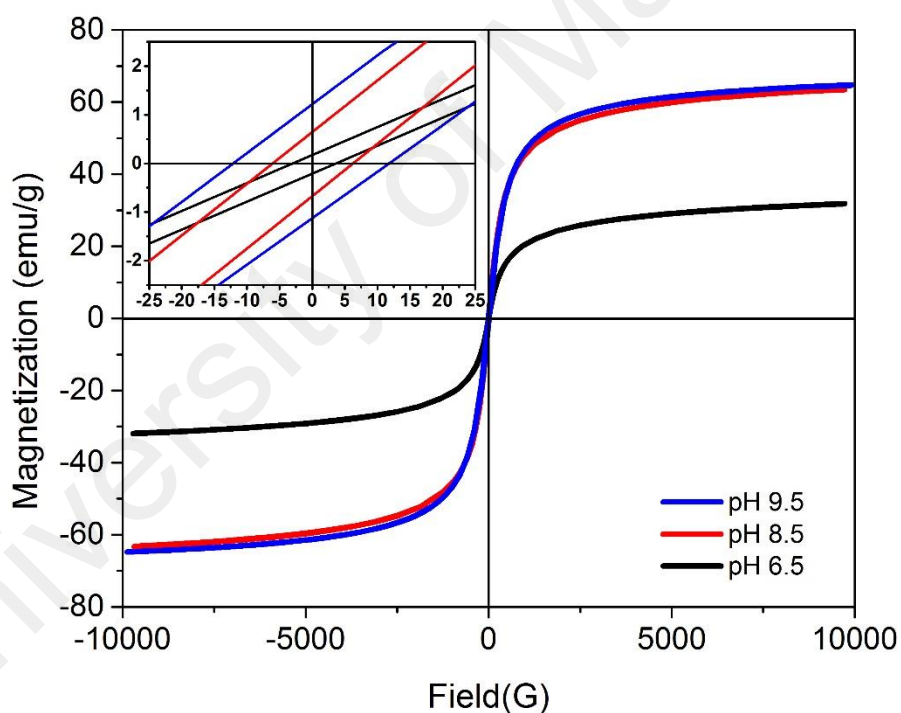
Figure 4.5: VSM hysteresis loop of the MNPs optimized with different final pH.

In this part of experimental works, magnetic properties measurement for the sample synthesized by controlling the ammonium hydroxide concentration was further studied. It was found that saturation magnetization of MNPs was slightly increased from 62.63

emu/g to 65.04 emu/g with increasing base concentration from 0.75 M to 3.00 M. However, the saturation magnetization of MNPs was slightly reduced from 65.04 emu/g to 64.00 emu/g when applied 6.00 M of ammonium hydroxide during coprecipitation process. It was a well- known fact that the saturation magnetization usually is related to the crystallite size of magnetic particles (Roca et al., 2007). Based on aformentioned discussion, the crystallite size of MNPs was not affected by the base concentration (Table 4.4). It was found that the influence of ammonium hydroxide concentration towards to the saturation magnetization was insignificant in our present study as the total increment was only 1.37 emu/g or 2.19 %. The reason might be due to the ammonium hydroxide used as precipitating agent is a weak base and increasing its concentration does not affect nucleation and growth rate (Arabi & Asnaashari Eivari, 2014).
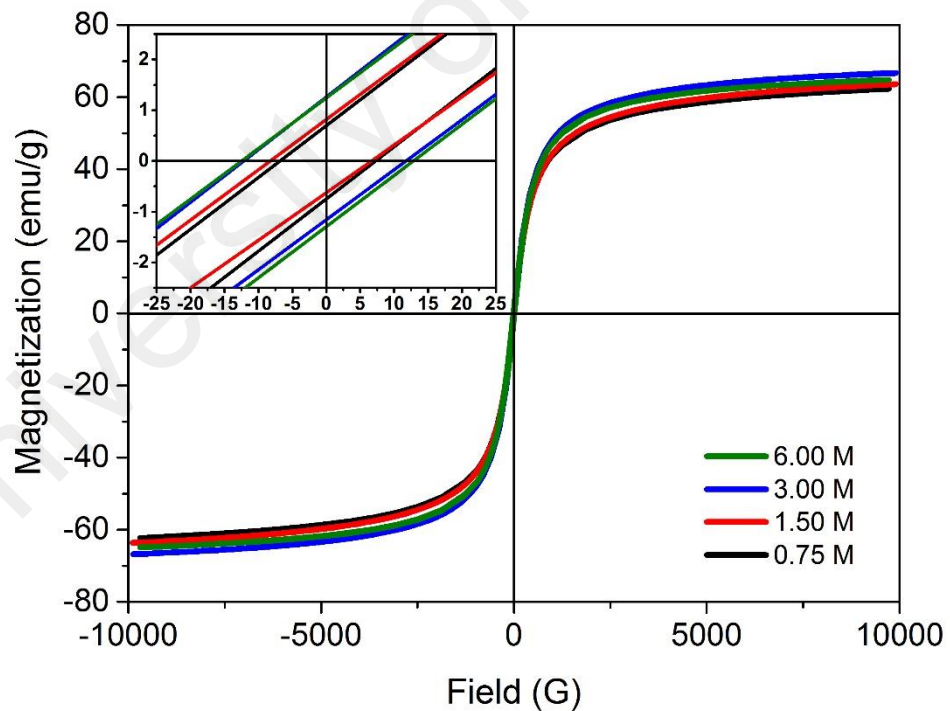
Figure 4.6: VSM hysteresis loop of the MNPs optimized with different ammonium hydroxide concentration.

The next batch of our experimental work showed that the saturation magnetization of particles were found to be stronger with increasing the total iron salts concentration up to 375 mM (as presented in Figure 4.7). Based on the VSM hysteresis loop, Ms reached a high value of 80.23 emu/g from 65.04 emu/g when the total iron salts concentration was increased from 150 mM to 375 mM. The increased of magnetic properties was due to larger crystallite of MNPs that produced by higher total iron salts concentration (Roca et al., 2007). However, MNPs produced with highest iron salts concentration (500 mM) showed decreased of Ms, which is 70.11 emu/g. According to Li et al. (2011), the reduction of saturation magnetization of sample with high iron salts concentration might be attributed to the particle aggregation problem, especially at higher total iron salts concentration therefore there was no improvement in the magnetic properties.
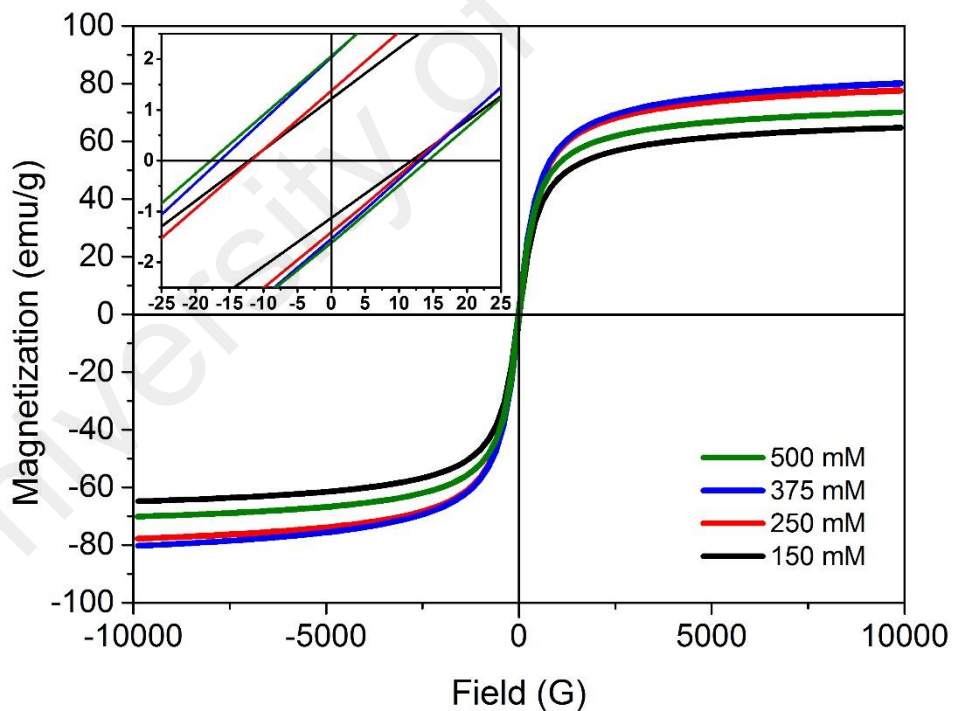
Figure 4.7: VSM hysteresis loop of the MNPs optimized with different total iron salts concentration.

In this study, the samples were produced by varying the addition rate of ammonium hydroxide from 1 ml/min up to 20 ml/min. Interesting, it could be noticed that the saturation magnetization was initially increased from 77.90 emu/g to 80.23 nm as the addition rate was increased from 1 ml/min to 5 ml/min (Figure 4.8). Nevertheless, the Ms value was dropped from 80.23 emu/g to 63.84 emu/g as increasing the addition rate to 20 ml/min. According to Gnanaprakash et al. (2007), the oxidation of ferrous ions to ferric ions is prone to happen on slower addition rate and this account to the formation of more non-magnetic compounds in the sample. Equation 4.4 explains the formation of goethite from the partial oxidation of ferrous hydroxide by the oxygen dissolved in the iron salts solution.

$$3Fe(OH)_2 + \frac{1}{2}O_2 \rightarrow 2FeOOH + H_2O \qquad \textbf{(Equation 4.4)}$$

In addition, longer reaction time is require to complete the MNPs synthesis for a slower addition rate. Hence, the synthesized MNPs was exposed to oxygen atmosphere in a longer duration. The reduction of saturation magnetization value for the slowest addition rate (1 ml/min) was due to oxidation, and the others samples (5-20 ml/min) were due to decrease in the crystallite size of the particles with increasing addition rate (Table 4.4).
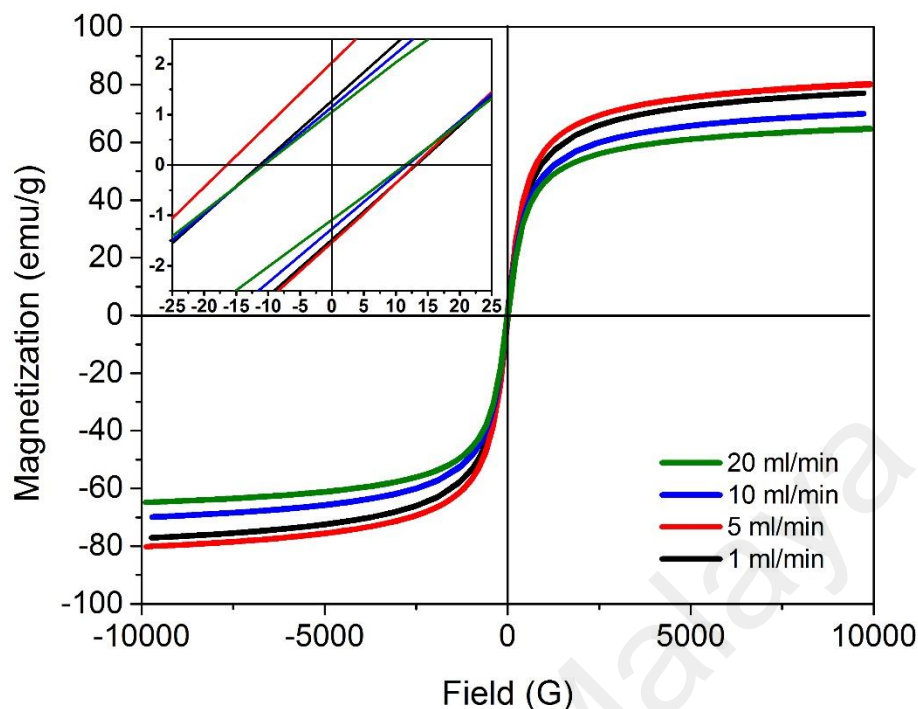
Figure 4.8: VSM hysteresis loop of the MNPs optimized with different addition rate.

Based on our reults, saturation magnetization values of all synthesized MNPs are much smaller than the bulk magnetite value, 92 emu/g (Mascolo et al., 2013). In fact, the reduction of saturation magnetization of synthesized MNPs can be related to its nano size of nanoparticles. In addition, the hysteresis loop of the synthesized MNPs exhibited a very low coercivity and remanence values as compared to the bulk magnetite. The typical characteristics of superparamagnetic behaviour were observed for all of the samples. However, the overall colloidal stability performance of MNPs is still poor in water and nitrile latex. These findings clearly indicate that coating with coating agent (e.g., PEG 600 and oleic acid) is a potential solution for MNPs agglomerations.

4.3 Synthesis of Coated Magnetite Nanoparticles

Based on aforementioned discussion, MNPs with hydrodynamic size less than 50 nm were successfully synthesized by applying co-precipitation methods. A maximum saturation magnetization (80.23 emu/g) was achieved by the reaction between 375 mM of total iron salts concentration and 3.00 M ammonium hydroxide (5 ml/min) at final pH of 9.5. Therefore, in the following studies, resultant magnetite nanoparticles (MNPs) were synthesized in such condition mentioned above to study the influence of coating agents (e.g., PEG 600 and oleic acid) loading on the stabilization of synthesized MNPs in nitrile latex (raw material for nitrile glove production) and further protection of MNPs against fast oxidation by oxygen. The aim of this section is to improve the colloidal stability of MNPs in nitrile latex.

4.3.1 Zeta Potential and Hydrodynamic Size Analysis

The surface charge on the uncoated and coated MNPs with potential organic stabilizer (e.g., PEG 600 and oleic acid) was characterized with the zeta potential, as shown in Table 4.5 alongside with the hydrodynamic diameters and size distributions.

Table 4.5: Hydrodynamic size, polydispersity index and zeta potential for uncoated MNPs, PEG coated MNPs, and oleic acid coated MNPs

Sample	Hydrodynamic size (nm)	Polydispersity index	Zeta Potential (mV)
a) Uncoated			
Optimized uncoated	42.96	0.214	-29.8
b) PEG 600			
0.6 g	44.12	0.200	-35.9
0.8 g	36.75	0.188	-41.1
1.0 g	35.59	0.178	-43.6
2.0 g	35.95	0.176	-45.6
3.0 g	32.29	0.168	-45.8
c) Oleic acid			
0.3 g	61.04	0.129	-50.2
0.6 g	57.75	0.136	-50.6
0.9 g	54.79	0.139	-52.2
1.2 g	48.21	0.154	-54.7
1.5 g	41.90	0.193	-58.1

It is worth noting that the addition of PEG 600 with MNPs resulted in a smaller hydrodynamic size and narrower size distribution, meanwhile the MNPs coated with oleic acid resulted in bigger and slightly broader size distribution. In addition to that, it could be observed that the zeta potential for uncoated MNPs sample of -29.8 mV was due to the OH^- ion associated with the surface at pH 10 medium as discussed in previous section, synthesis of MNPs. However, zeta potential of MNPs increased to the range of ~35 mV to ~46 mV after the addition of PEG 600. This indicates that the stability of synthesized MNPs could be further improved by applying PEG coating. On the other hand, the zeta potential value increased to -58.1 mV by adding oleic acid at the same pH medium. The reason might be attributed to the carboxylate ions in the outer layer of the bilayer, which promotes the stability of MNPs. When the charges of particles were increased significantly, the hydrodynamic size of the oleic acid coated with MNPs decreased from 61.04 nm to 41.90 nm which was attributed to the greater electrostatic repulsion (Ingram

et al., 2010). In overall, the PDI values of coated MNPs are lower than the uncoated MNPs (0.214), ranging from 0.129 to 0.200 reflecting good colloidal properties.

It's a well-known fact that nanoparticles can be stabilised by steric and electrostatic stabilization (Mahmoudi et al., 2011). A surface charge, which is measured as zeta potential will be developed when a solid emerges in a polar solvent or an electrolyte solution, (Cao & Wang, 2011). The higher the particles are equally charged, the higher is the electrostatic repulsion between the particles and the higher is the physical stability. The result clearly shows that the colloidal stability of MNPs was enhanced due to electrostatic stabilization. For this reason, the aggregation of magnetite nanoparticles in suspension due to the attractive van der Waals forces and strong magnetic dipole–dipole interactions between particles was prevented (Tombacz et al., 2006).

4.3.2   X-ray Diffraction Analysis

It is well known that surface morphology change of coated MNPs is closely related to crystal growth. Therefore, XRD analysis was conducted to investigate the effect of phase transformation for the coated MNPs. According to the Figure 4.9, the plotted XRD patterns of uncoated MNPs and PEG 600 coated MNPs were exhibited almost similar pattern. However, the diffraction peaks are weaker in term of peak's intensity and much broader for the MNPs modified by PEG 600. This observation further confirmed that the increasing of concentration of PEG 600 showed reduced crystallinity of the MNPs modified by PEG 600 (Anbarasu, 2015). The estimated crystallite size of uncoated MNPs was decreased accordingly when the concentration of PEG 600 was increased from 0.6 g up to 3.0 g. The PEG coated MNPs with increasing concentration exhibited decreased of crystallite size, that are approximately 13.60 nm, 12.30 nm, 11.90 nm, 10.70 nm, 10.40 nm, and 9.30 nm, respectively. These results further ascertain that the addition of the polymer PEG 600 plays a critical role in controlling the size of the MNPs.
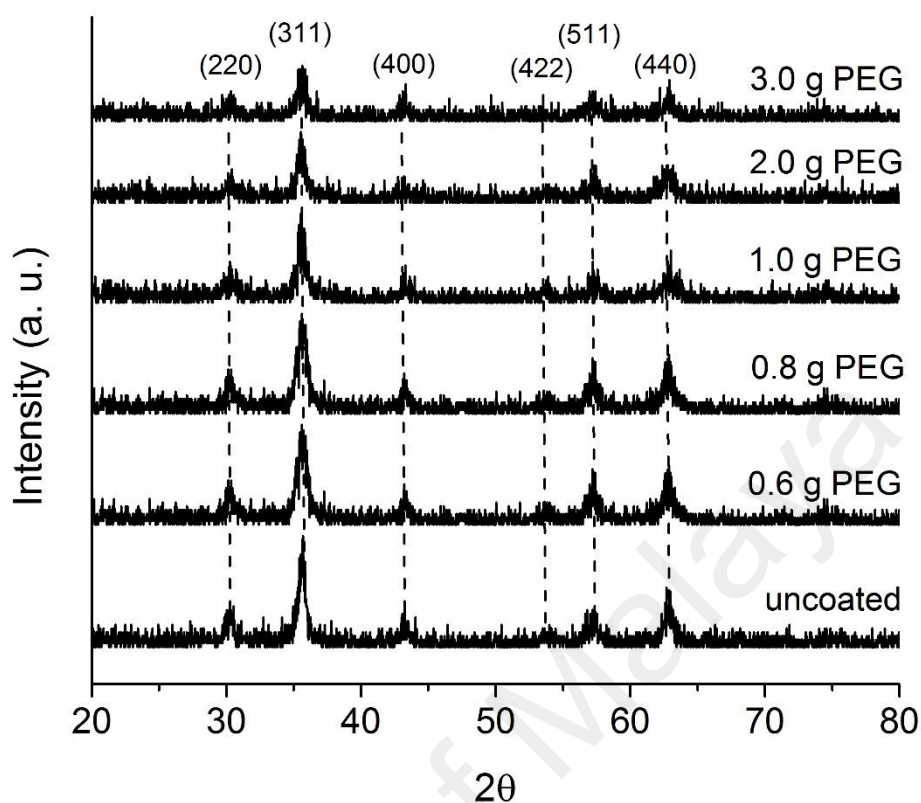
Figure 4.9: XRD pattern of MNPs with different loading of PEG 600

Interestingly, we could observed that the estimated crystallite size of oleic acid coated MNPs with different amount of 0.3 g, 0.6 g , 0.9 g, 1.2 g, and 1.5 g were about 10.40 nm, 10.40 nm, 10.3 nm, 9.70 nm, and 9.50 nm, respectively. Similarly, the crystallinity of synthesized MNPs decreased with increasing amounts of applied oleic acid (Figure 4.10). It could be noticed that the crystallite size of MNPs was decreased, which indicates from the obtained broadening peaks width (Ramimoghadam et al., 2015). On overall, it could be summarized that MNPs growth can be easily controlled via adding optimum amount of coating agents. The main reason might be attributed to the orientation of coating agents adsorbed on the surface of a particle and further increasing the retention of magnetic particles on the surface layer that will cause a decline in the diffusion rate and prevent the precipitation of particles during surface deposition. This condition will cause the surface

deposition rate slows down, which could effectively control the growth of magnetite nanoparticles (Li et al., 2011).
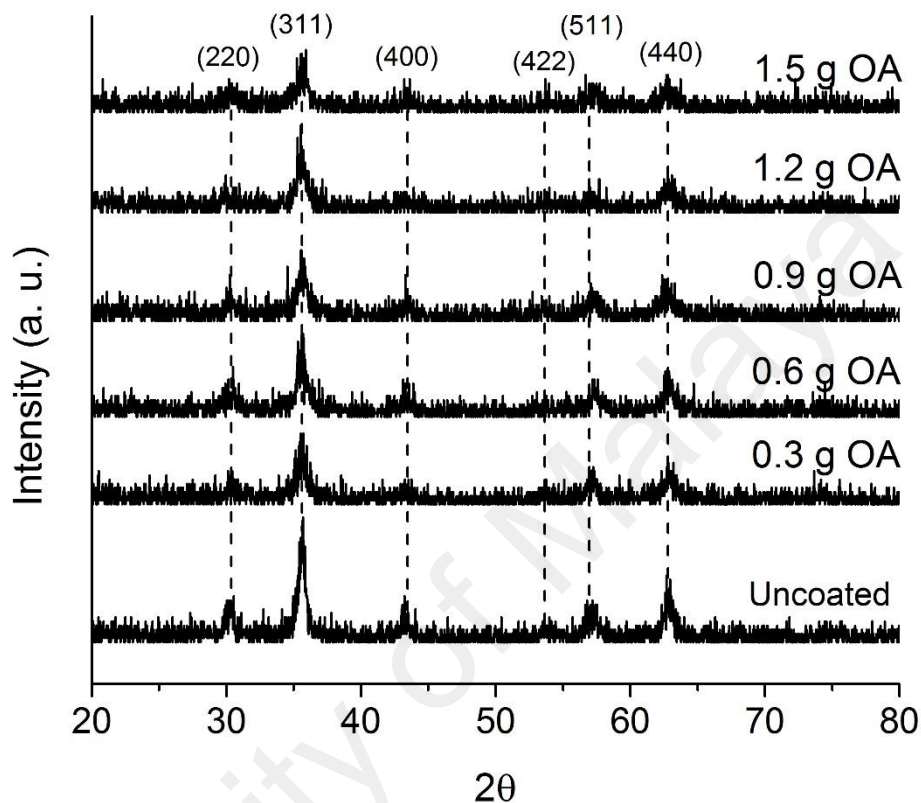
Figure 4.10: XRD pattern of MNPs with different loading of oleic acid

4.3.3 Fourier Transform Infrared Spectroscopy (FTIR) Analysis

In the present study, FTIR analysis was conducted to investigate the adsorption of the coating agents (e.g., PEG 600 and oleic acid) on the surface of synthesized MNPs. Figure 4.11 shows the FTIR spectra of synthesized MNPs coating with different amount of PEG 600. Four peaks at 430 cm^{-1}, 580 cm^{-1}, 1630 cm^{-1}, and 3400 cm^{-1} appeared in the spectrum of uncoated MNPs. As discussed earlier, the peaks at 430 cm^{-1} and 580 cm^{-1} were assigned to magnetite phase while the peaks at 1633 cm^{-1} and 3400 cm^{-1} were attributed to the stretching –OH vibration of water molecules. In PEG parameter, the peak obtained at ~1633 cm^{-1} was assigned to the stretching of –OH band and asymmetric carboxylate

(COO⁻) stretching vibration, while the peak at ~1403 cm⁻¹ was attributed to the vibration of –CH. The peaks corresponding to the bonds –CH, and -COO⁻ are the strong evidence to show that the synthesized MNPs surface has been coated with PEG (Anbarasu, 2015; Jayanthi et al., 2013). The characteristic peaks of PEG polymer at around 950 cm⁻¹ and 1080 cm⁻¹ that correspond to the C-C stretch and C-O-C stretch were disappeared in the FTIR spectrum of PEG coated MNPs samples. This result indicates that a dipole-cation binding between the ether group of PEG and the positive charge of MNPs (García-Jimeno & Estelrich, 2013).
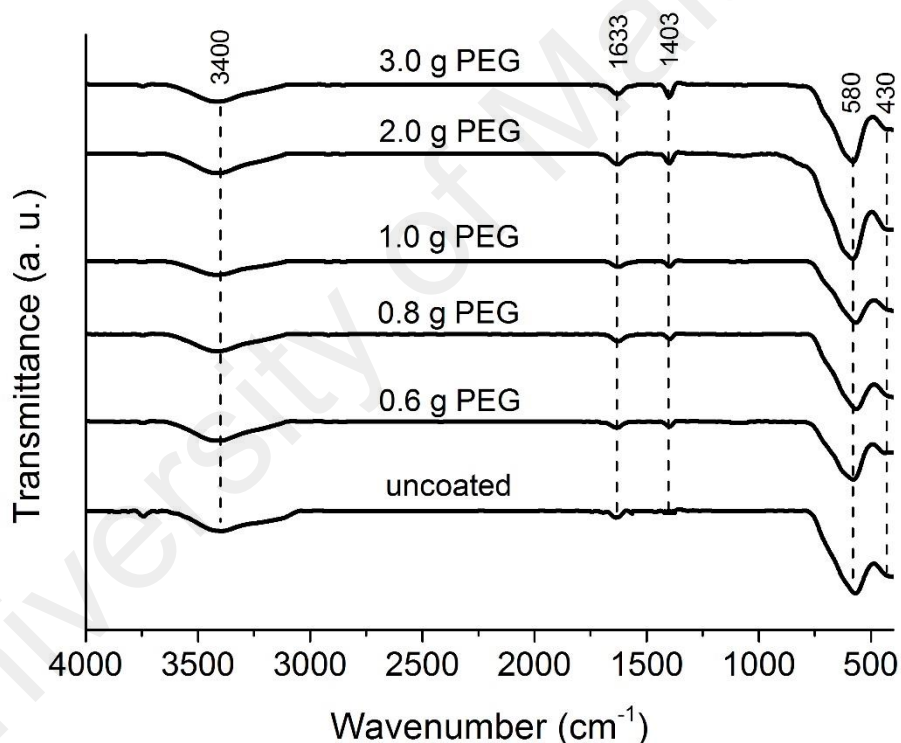
Figure 4.11: FTIR spectra of MNPs with different loading of PEG 600

Next, Figure 4.12 shows the FTIR spectra of the synthesized MNPs coated with oleic acid. It was found that additional six peaks could be detected at 1409 cm⁻¹, 1457 cm⁻¹, 1529 cm⁻¹, 1710 cm⁻¹, 2851 cm⁻¹, and 2923 cm⁻¹ after the surface modification of MNPs by oleic acid. Firstly, the peak at 1409 cm⁻¹ corresponded to the CH₃ umbrella mode of

oleic acid. Secondly, the peaks at 1457 cm^{-1} and 1529 cm^{-1} were attributed to the υ_{as} (-COO$^-$) and υ_s (-COO$^-$) stretch while the peak at 1710 cm^{-1} correlate to the C=O stretch in oleic acid. Thirdly, the peaks at 2851 cm^{-1} and 2923 cm^{-1} correspond to the asymmetric and symmetric CH$_2$ stretch in oleic acid (Li et al., 2010). Based on a literature in 2006, revealed that the wavenumber separation between the υ_{as} (-COO$^-$) and υ_s (-COO$^-$) stretch could be used to distinguish the type of the interaction between the carboxylate head and the metal atom (Zhang et al., 2006). As the loading amount was increased to 0.9 g, a peak appeared at 1710 cm^{-1} while the asymmetric (-COO$^-$) peak at 1457 cm^{-1} disappeared. Meanwhile, a similar finding was reported by Yang et al., in 2010 and they reported that the appearance of 1710 cm^{-1} peak confirmed the formation of bilayer oleic acid coating layer on MNPs (Yang et al., 2010). They also explained the disappearance of 1457 cm^{-1} peak by two reasons. First, the excessive addition of oleic acid might affect the interaction between carboxylate head and the Fe atom. Second, because the amount of oleic acid in bilayer coated structure was much more than that in single layer coated structure, the intensity of the band at 1409 cm^{-1} resulting from the CH$_3$ umbrella mode of oleic acid would be far greater than that of single layer oleic acid-coated ones. The wavenumber separation of 0.3 g OA sample and 0.6 g OA sample was lesser than 110 cm^{-1} and correspond to the chelating bidentate, where the interaction between the COO$^-$ group and the Fe atom was covalent (Rafiee et al., 2014).
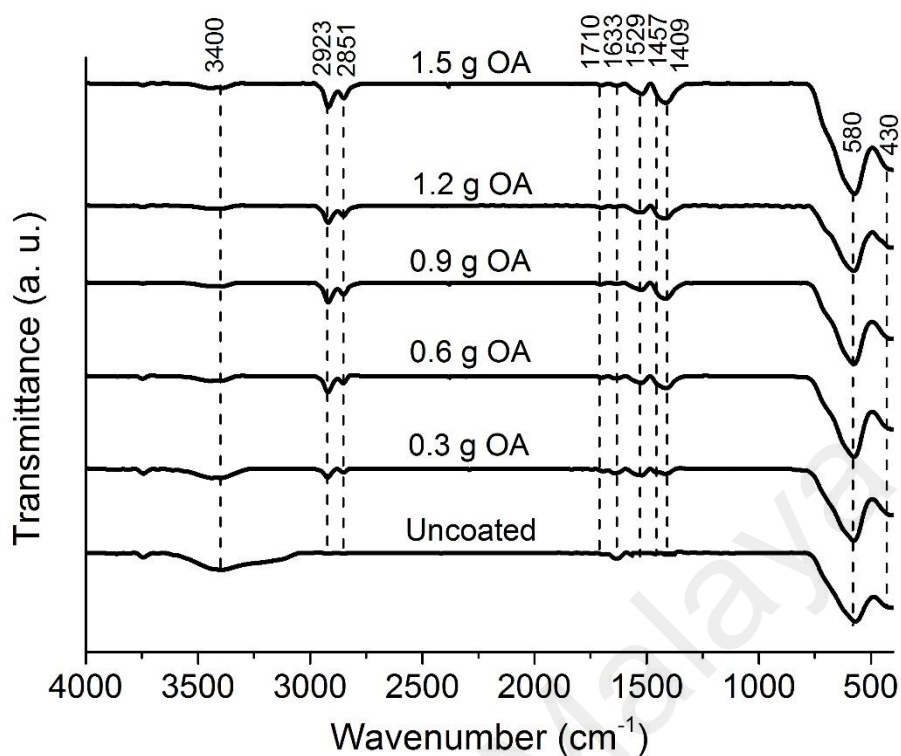
Figure 4.12: FTIR spectra of MNPs with different loading of oleic acid

4.3.4 Raman Analysis

In this study, Raman analysis has been used to determine and understand the structural changes of PEG coated MNPs, oleic acid coated MNPs, and uncoated MNPs upon different loading content. Based on Figure 4.13(a), the Raman spectra obtained from PEG coated MNPs and uncoated MNPS are almost identical. The obtained results clearly to infer that the PEG coating layer on MNPs were unable to prevent oxidation reaction that might be affected the purity of synthesized MNPs. In contrast, the shoulder peak of the oleic acid coated on MNPs at 720 cm^{-1} in Raman spectra was reduced after loading amount of oleic acid was more than 0.9 g (Figure 4.13b). This observation suggests that the oleic acid coating layer might reduce the oxidation reaction that trigger the phase transition of magnetite into maghemite phase. The hydrocarbon chains of oleic acid formed a hydrophobic shell around the MNPs core, which could provide the stability against oxidation to synthesized MNPs (Singh et al., 2014).
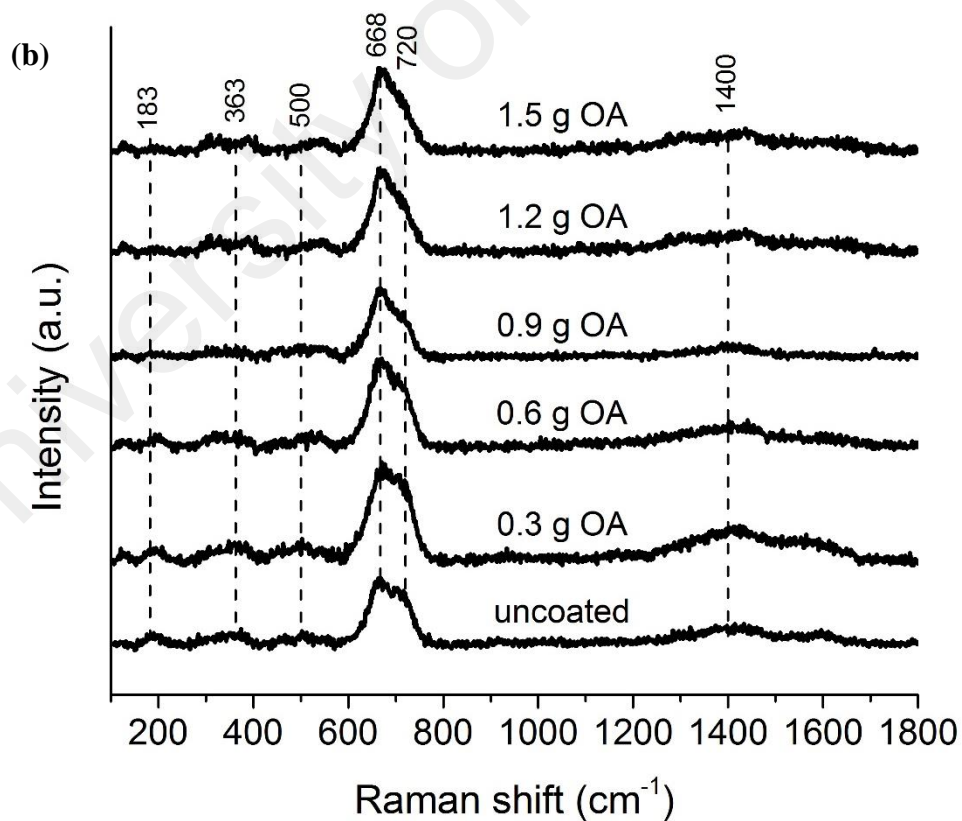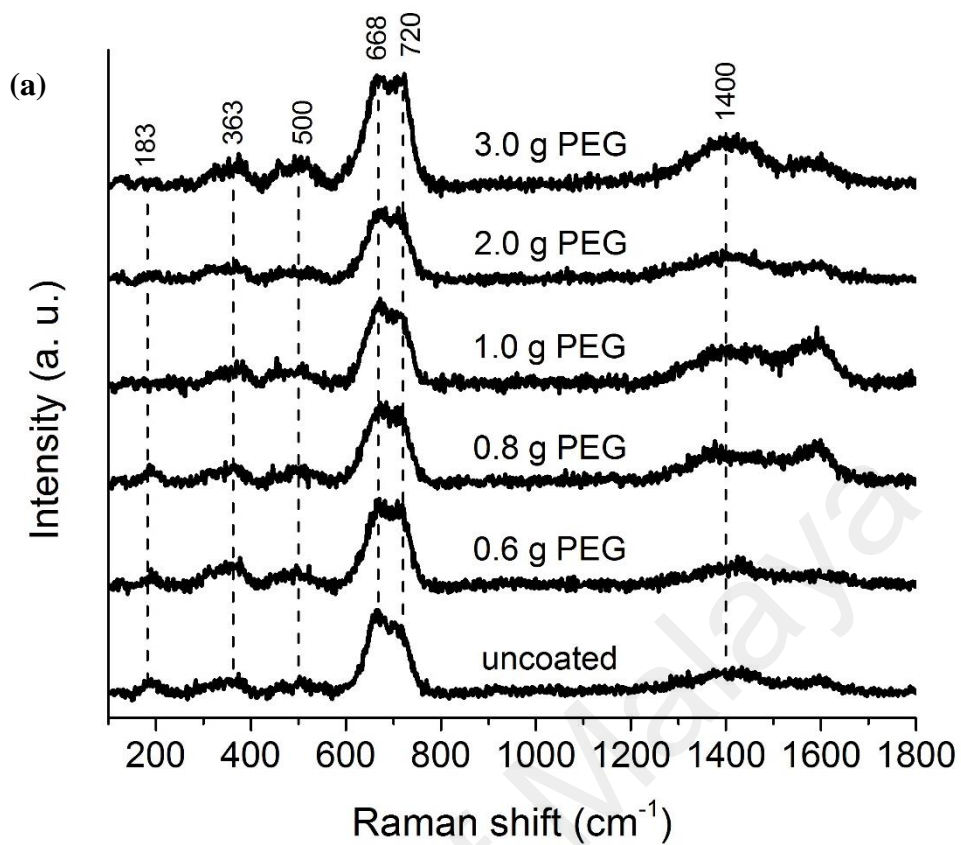
Figure 4.13: Raman spectra of MNPs with different loading of PEG 600 (a), and Oleic acid (b)

4.3.5 Thermogravimetric Analysis (TGA)

The TGA analysis was conducted to identify the coating formation and estimate the binding efficiency on the surface of MNPs. According to Hong et al. (2008), when the coating agent decomposed completely, the residual substance mostly is magnetic particles. Therefore, the coating efficiency of samples with different weight ratio of coating agent to MNPs could be calculated from the weight losses.

$$\text{Coating efficiency (\%)} = \frac{\text{Coating agent}}{\text{Phase transformation} + \text{Residue}} \times 100 \qquad \textbf{(Equation 4.5)}$$

Table 4.6: Results and analysis based on TGA curves of uncoated MNPs, PEG coated MNPs and oleic acid coated MNPs

Sample	Moisture (%)	Coating agent		Phase transformation		Residue (%)	Weight ratio (%)
		Derivative peak (℃)	Weight loss (%)	Derivative peak (℃)	Weight loss (%)		
Uncoated	1.35	262	3.68	-	-	94.97	-
PEG 600							
0.6 g	0.84	222, 273, 408	1.96	540	2.83	94.37	2.02
0.8 g	0.81	222, 272, 408	2.73	540	3.29	93.17	2.83
1.0 g	0.76	228, 281, 428	3.05	531	3.12	93.07	3.17
2.0 g	0.64	222, 276, 417	4.44	542	2.03	92.89	4.68
3.0 g	0.57	228, 275, 428	5.34	542	1.24	92.85	5.68
Oleic acid							
0.3 g	0.48	225, 356	8.16	680	5.79	85.57	8.93
0.6 g	0.41	252, 362	9.71	709	9.54	80.34	10.80
0.9 g	0.33	258, 367	13.09	717, 752	11.62	74.89	15.13
1.2 g	0.40	252, 362	13.74	722, 759	11.70	74.16	16.00
1.5 g	0.38	255, 357	13.83	718, 757	12.06	73.73	16.12

Figures 4.14 and 4.16 show the TGA curves of the uncoated MNPs, PEG coated MNPs, and oleic acid coated MNPs samples. The transition temperatures and the corresponding percentage weight loss of all samples were summarized in Table 4.6. According to Figure 4.14 and 4.16, a slight weight loss at temperature below 100 ℃ could be noticed for all of the tested samples. In this manner, the weight loss of MNPs at below 100 ℃ is likely to be caused by the contained water (Wang et al., 2010). From Table 4.6, the moisture content found in all samples was about 0.33 % up to 1.35 % based on calculation. For uncoated MNPs, a weight loss of 3.68 % was observed at 100-600 ℃. The main reason might be attributed to the decomposition of hydroxyl group on the surface of MNPs (Liang et al., 2014).

The TGA curves for PEG coated MNPs showed a sharp fall over the range of temperature from 160 ℃ to 450 ℃ under the second stage of weight reduction as presented in Figure 4.16. This condition was believed due to desorption and subsequent evaporation of PEG (García-Jimeno & Estelrich, 2013). In fact, phase transformation from magnetite (Fe_3O_4) to maghemite (γ-Fe_2O_3) has occurred during this stage. However, the weight gain produced by this phase transformation could not be detected as it is concealed by the remarkable weight loss due to combustion of PEG. The third weight loss in between 450 ℃ to 800 ℃ was caused by the phase transition of MNPs. In this stage, the maghemite phase of MNPs produced during the combustion of PEG was successfully transformed into hematite (α-Fe_2O_3) phase. (García-Jimeno & Estelrich, 2013). Referring to Table 4.6, the coating efficiency of PEG (0.6 g, 0.8 g, 1.0 g, 2.0 g and 3.0 g) coated MNPs were 2.02 %, 2.83 %, 3.17 %, 4.68 % and 5.68 %, respectively
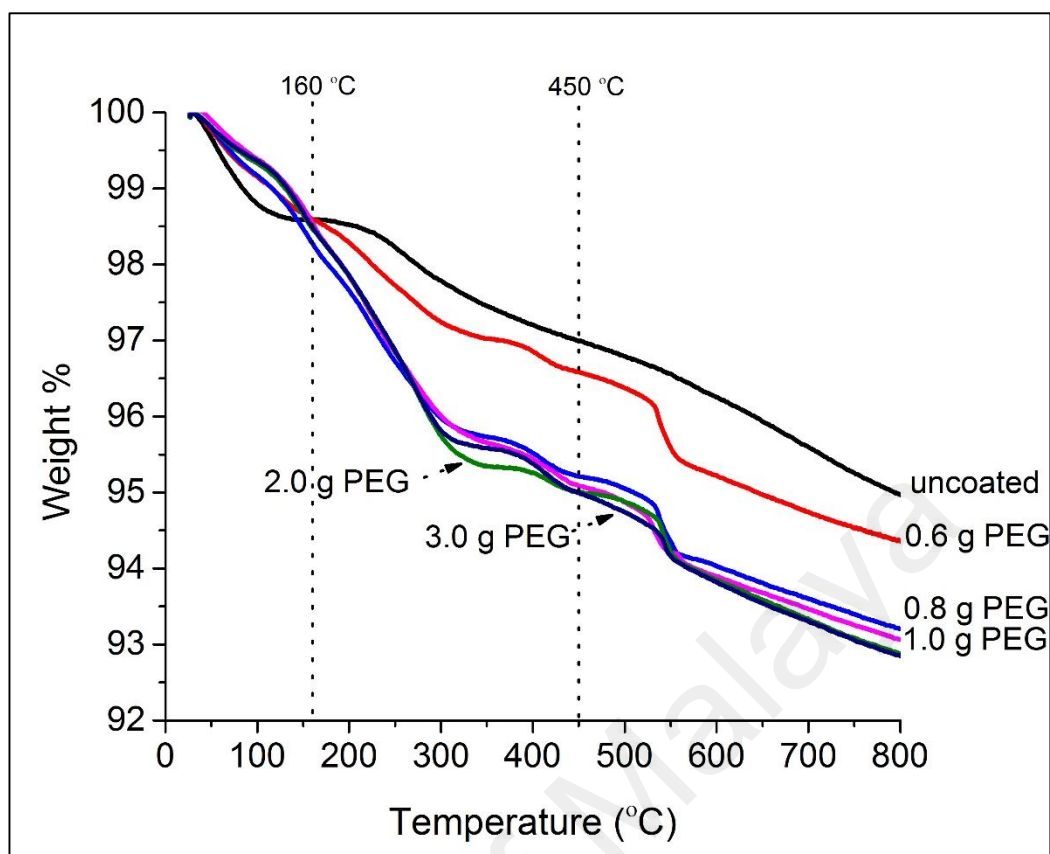
Figure 4.14: TGA curves of MNPs with different loading of PEG 600

As shown in Figure 4.15, all oleic acid coated MNPs samples exhibited two prominent weight loss stages at temperature below 600 ℃. The first and second weight loss at 100-600 ℃ corresponded to the decomposition of oleic acid (Wang et al., 2010). The first derivative peak was appeared at 252-258 ℃, which is around the boiling point of oleic acid (94-195 ℃/ 1.2 mmHg). The first weight loss indicated that the removal of free oleic acid molecules from the MNPs surface. However, first derivative of 0.3 g OA sample was found at the lower temperature (225 ℃), which suggests that less amount of free oleic acid molecules were appeared in the sample, which was in agreement with above discussed FTIR results. This indicates the formation of single layer oleic acid coated MNPs. Next, the second weight loss with derivative peak at 356-367 ℃ further affirmed that the strong binding force between oleic acid molecules and MNPs (Mahdavi et al., 2013). Lastly, third weight loss for oleic acid coated MNPs could be observed at

81

temperature above 600 ℃ with derivative peaks at 680-759 ℃, which were assigned to the reduction of MNPs by carbon dioxide gases produced during oleic acid degradation (Liang et al., 2014). According to Mahdavi et al. (2013), synthesized MNPs was reduced from magnetite phase to iron (II) oxide (FeO) phase because Iron (II) oxide is thermodynamically stable at temperature above 570 ℃. In addition, the fifth derivative peak appeared at 752-759 ℃ was mainly due to deoxidation of iron (II) oxide as the TGA analysis was performed under nitrogen gas atmosphere. In short, the results of TGA demonstrated that oleic acid existed on the surface of MNPs and their coating efficiency were about 8.93 %, 10.80 %, 15.13 %, 16.00 %, and 16.12 % for the loading amount of 0.3 g, 0.6 g, 0.9 g, 1.2 g and 1.5 g, respectively.
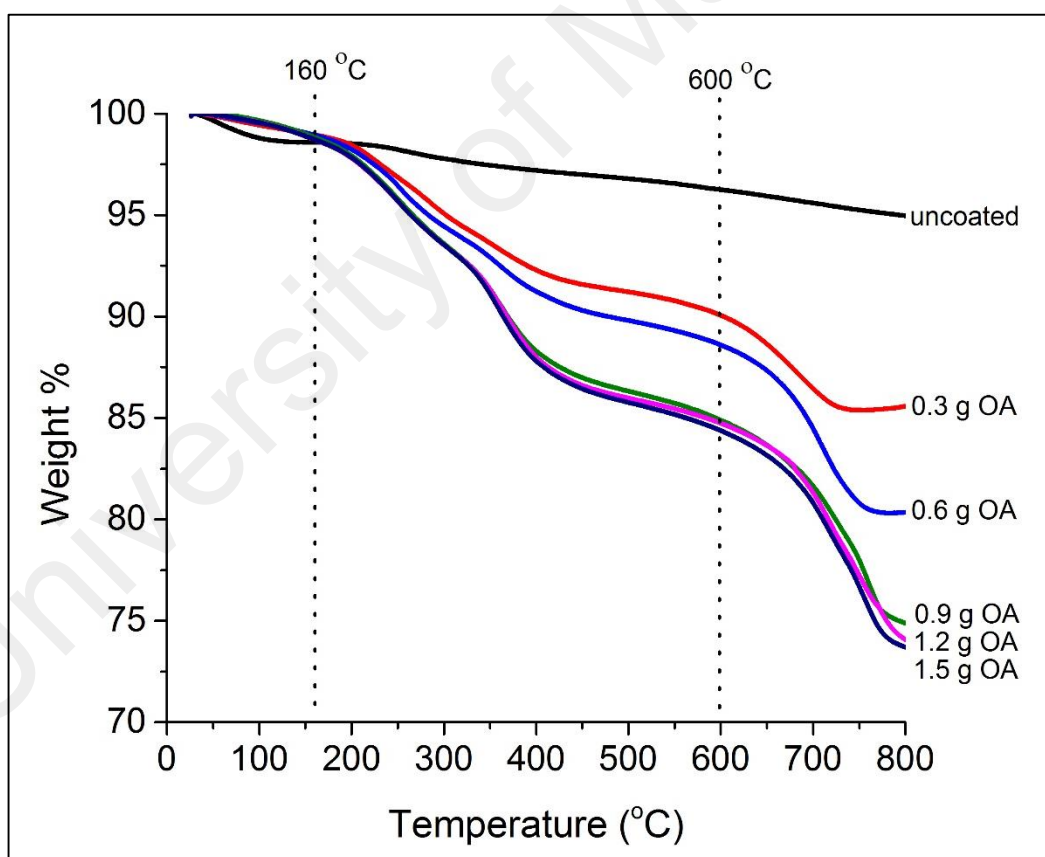
Figure 4.15: TGA curves of MNPs with different loading oleic acid

In addition, Yang et al. (2010) summarized that two steps weight loss occurred in between room temperature and 600 ℃ were attributed to the two kinds of bonding between carboxylate groups and Fe ions existed in the sample rather than a bilayer structure. A similar result was reported here, two step weight loss were observed in all oleic acid coated MNPs samples. Therefore, it can be said that there are two kinds of interaction in all the oleic acid coated MNPs samples (Figure 4.16).
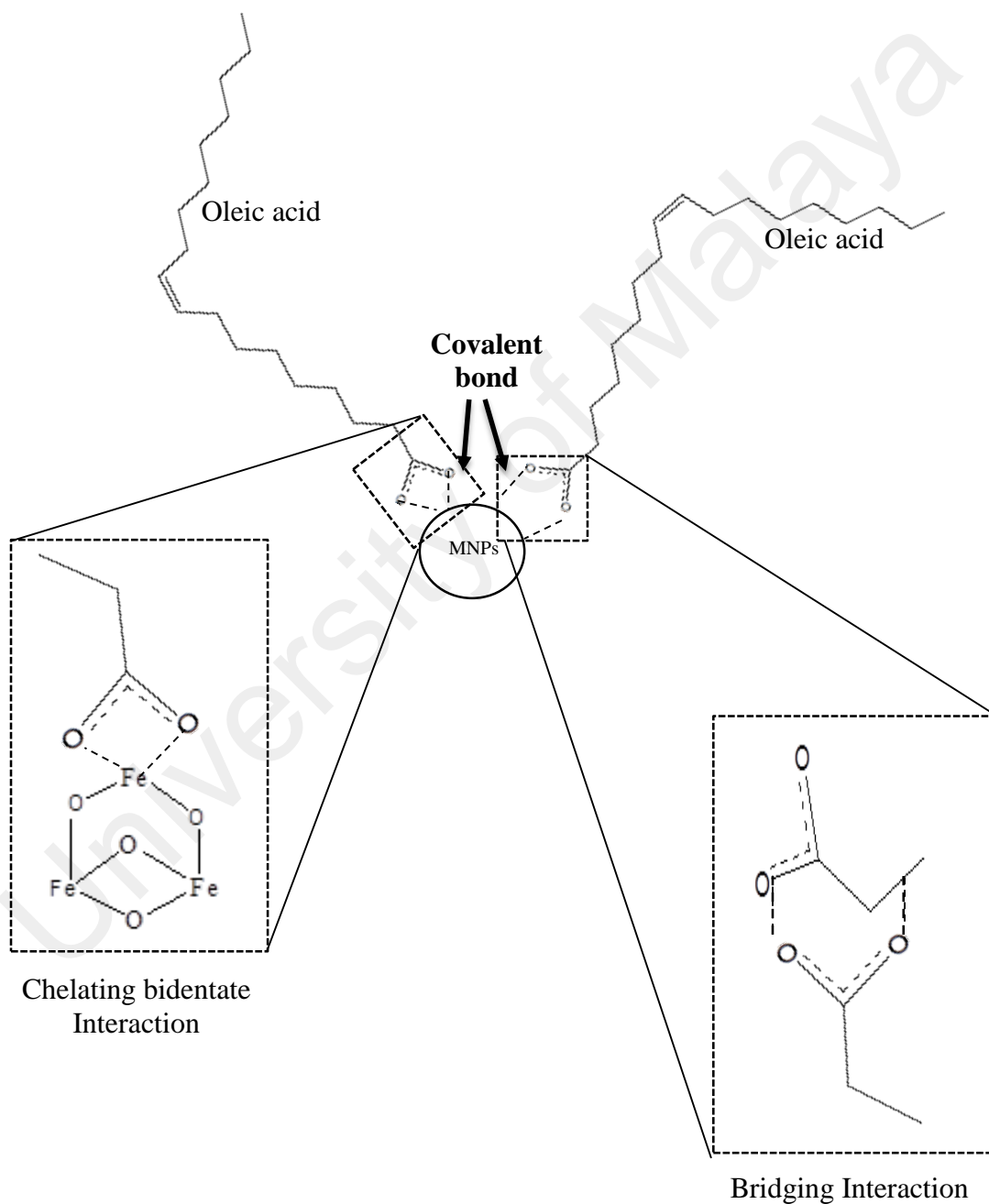
Figure 4.16: Proposed scheme for the interaction between oleic acid and MNPs

4.3.6 Observation

Sedimentation test was carried out to study the colloidal stability of coated MNPs in different mediums. Table 4.7 and 4.8 illustrates the stability of uncoated and coated MNPs in water (pH 10) after sonication for 30 minutes.

Table 4.7: Sedimentation of uncoated MNPs and PEG 600 coated MNPs in water (pH 10)

Duration	Loading amount (g)					
	0	0.6	0.8	1.0	2.0	3.0
0						
3 hours						
3 days						
7 days						
14 days						
21 days						

Table 4.8: Sedimentation of uncoated MNPs and oleic acid coated MNPs in water (pH 10)

Duration	Loading amount (g)					
	0	0.3	0.6	0.9	1.2	1.5
0						
3 hours						
3 days						
7 days						
14 days						
21 days						

Based on Table 4.7 and 4.8, uncoated sample started to sediment in day 3 and settled down fully in 7 days. The uncoated MNPs tend to precipitate rapidly due to strong magnetic dipole–dipole attraction between particles (Petcharoen & Sirivat, 2012). These magnetic interaction was known to exist for magnetite nanoparticles with particle size larger than 10 nm at room temperature (Dormann et al., 2012). By the addition of 0.6 g of PEG 600, the coated MNPs remained stable in basic medium even after 14 days.

Therefore, the colloidal stability of MNPs could be improved after the addition of optimum content of coating agents (PEG 600). However, there are no differences in the colloidal stability of MNPs coating as increased the loading amount of PEG 600.

Similarly, the colloidal stability of MNPs in basic medium improved after the surface modification of MNPs by oleic acid. However, the Oleic acid coated (0.3 g) MNPs shows lower stability than uncoated MNPs while the MNPs synthesized with higher loading amount of oleic acid result in a perfect colloidal suspension in water (basic). The oleic acid coated (0.3 g) MNPs was sediment faster than the uncoated sample and both of them settled down completely in 14 days. This result suggests that single layer (primary) coated MNPs was formed due to insufficient amount of oleic acid while the rest (sample 0.6-1.5 g OA) were coated by double layer (primary + secondary) of oleic acid (Yang et al., 2010). Therefore, the earlier MNPs sample was hydrophobic in nature while the later were hydrophilic.
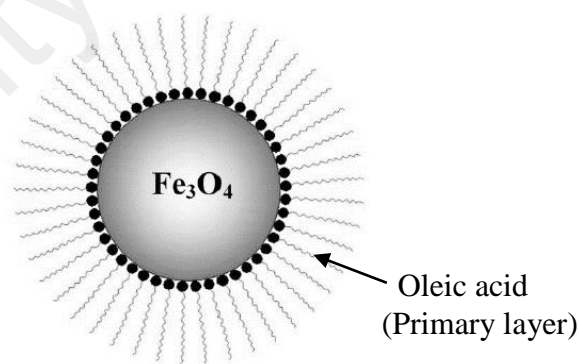
Figure 4.17: Schematic diagram of single layer oleic acid coated MNPs (Yang et al., 2010)

The primary coating layer is chemically absorbed on the surface of MNPs while the secondary coating layer is physically absorbed on the primary layer by forming interpenetration layer with the tails of the primary layer. Therefore, bilayer oleic acid coated MNPs can be well dispersed in polar liquid while the single oleic acid coated

MNPs can be dispersed only in non-polar liquid. However, Yang et al. (2010) revealed that bilayer oleic acid coated MNPs can be dispersed in both polar and non-polar liquid by increasing the pH of carrier liquids (Figure 4.18).
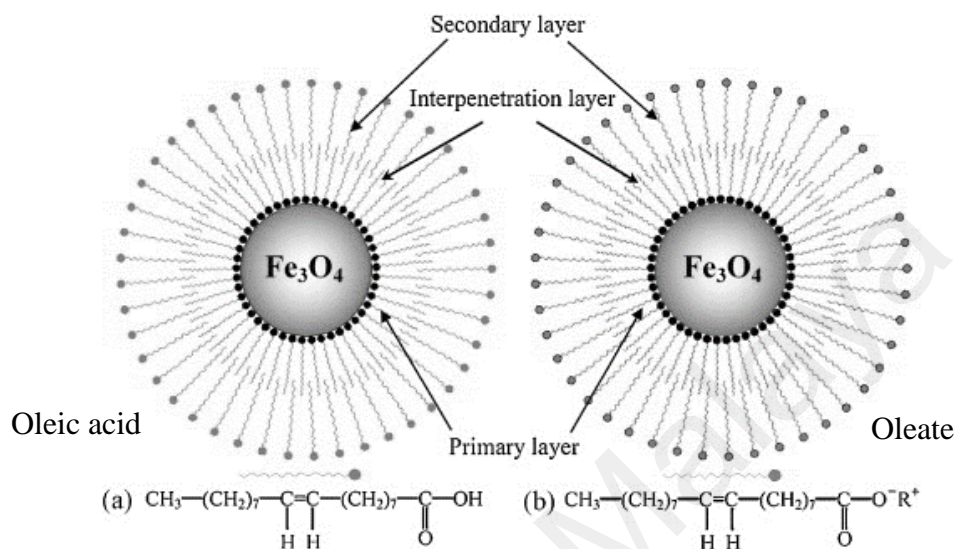

Figure 4.18: Bilayer oleic acid-coated MNPs nanoparticles: (a) oleic acid as the secondary layer, and (b) oleate as the secondary layer (Yang et al., 2010)

When the bilayers were formed, it prevented particles aggregation relayed on hydrophobic interactions and steric repulsion (Yue-Jian et al., 2010). Therefore, oleic acid coated MNPs (except 0.3 g OA) showed better colloidal stability than PEG coated MNPs in basic medium. The well-dispersed MNPs in aqueous solution can be obtained from the surface modification of oleic acid as it possesses great suspension stability over 3 weeks.

The sedimentation of uncoated MNPs, PEG 600 coated MNPs, and oleic acid coated MNPs in nitrile butadiene rubber latex are shown in Table 4.9 and 4.10. Based on Table 4.9, the uncoated MNPs settled down completely in nitrile latex in less than 3 days. Unexpectedly, PEG coated MNPs showed similar stability in nitrile latex. This indicate that PEG coated MNPs are hydrophilic in nature and will only disperse in polar medium.

As the percentage of acrylonitrile (polar part) present in the nitrile latex was very low (18 % to 24 %), the compatibility between PEG and nitrile latex was poor.

On the other hand, MNPs with oleic acid of more than 1.2 g successfully stabilized in the latex compound up to 21 days (Table 4.10). This result showed the stabilization of MNPs could be prolonged with the right loading amount of oleic acid. Although 1.5 g OA shows the optimum stability in this sedimentation test, when the loading amount is higher than 1.2 g, it posed difficulty in the separation and washing step as it was highly stable in the reaction medium. For this reason, 1.2 g OA MNPs was selected as the best sample.
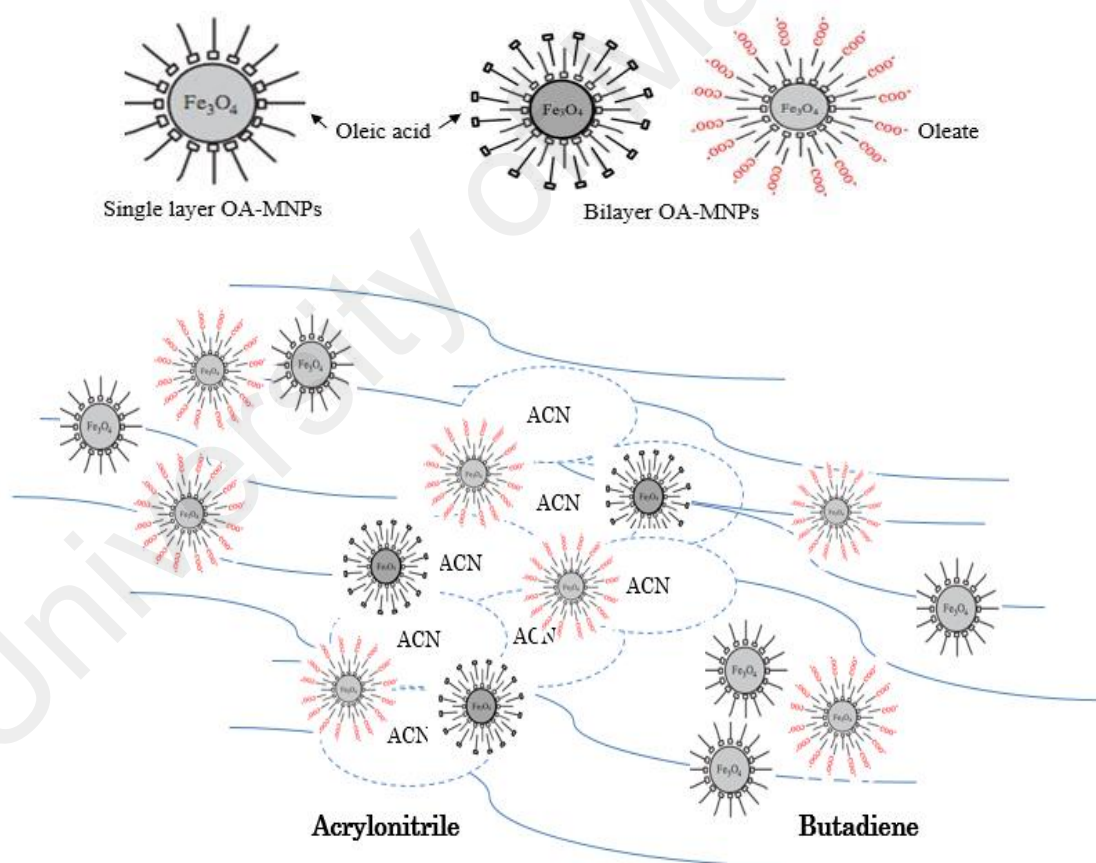
Figure 4.19: Schematic diagram of oleic acid coated MNPs in nitrile latex

Table 4.9: Sedimentation of uncoated MNPs and PEG 600 coated MNPs in nitrile butadiene rubber latex

Duration	Loading amount (g)					
	0	0.6	0.8	1.0	2.0	3.0
0						
3 hours						
3 days						
7 days						
14 days						
21 days						

Table 4.10: Sedimentation of uncoated MNPs and oleic acid coated MNPs in nitrile butadiene rubber latex

Duration	Loading amount (g)					
	0	0.3	0.6	0.9	1.2	1.5
0						
3 hours						
3 days						
7 days						
14 days						
21 days						

90

4.3.7   Morphological Analysis

In the present study, FESEM was used to study the surface morphology of the optimized PEG coated MNPs, Oleic acid coated MNPs, and uncoated MNPs sample. Figure 4.20 shows the FESEM images of uncoated MNPs, PEG (1.0 g) coated MNPs and Oleic acid (1.2 g) coated MNPs. The FESEM images confirmed the uncoated MNPs are non-uniform spherical while PEG coated MNPs are smaller and highly uniform in size. The particles of uncoated MNPs tend to aggregate by formation of strong magnetic dipole-dipole interactions in order to reduce the surface energy of its high surface area to volume ratio (Jaramillo Tabares et al., 2009). The agglomeration of MNPs was reduced when the PEG coated on the surface of MNPs (Jayanthi et al., 2013).

Figure 4.20c shows the FESEM images of oleic acid coated MNPs. From Figure 4.20c, it can be observed the adhesion between the MNPs due to the excess oleic acid. The oleic acid agglomerated into larger particle sizes due to combination of the oleic acid layer on the surface of MNPs (Li et al., 2011). Agglomeration of oleic acid coated MNPs was happened during the drying process for electron microscopy (Mahl et al., 2011). In addition, Petcharoen and Sirivat (2012) reported that the oleic acid may form micelles around the MNPs and a small amount of the nuclei might be trapped inside the micelles. These nuclei undergo self-assembly later and result in a larger particle sizes.
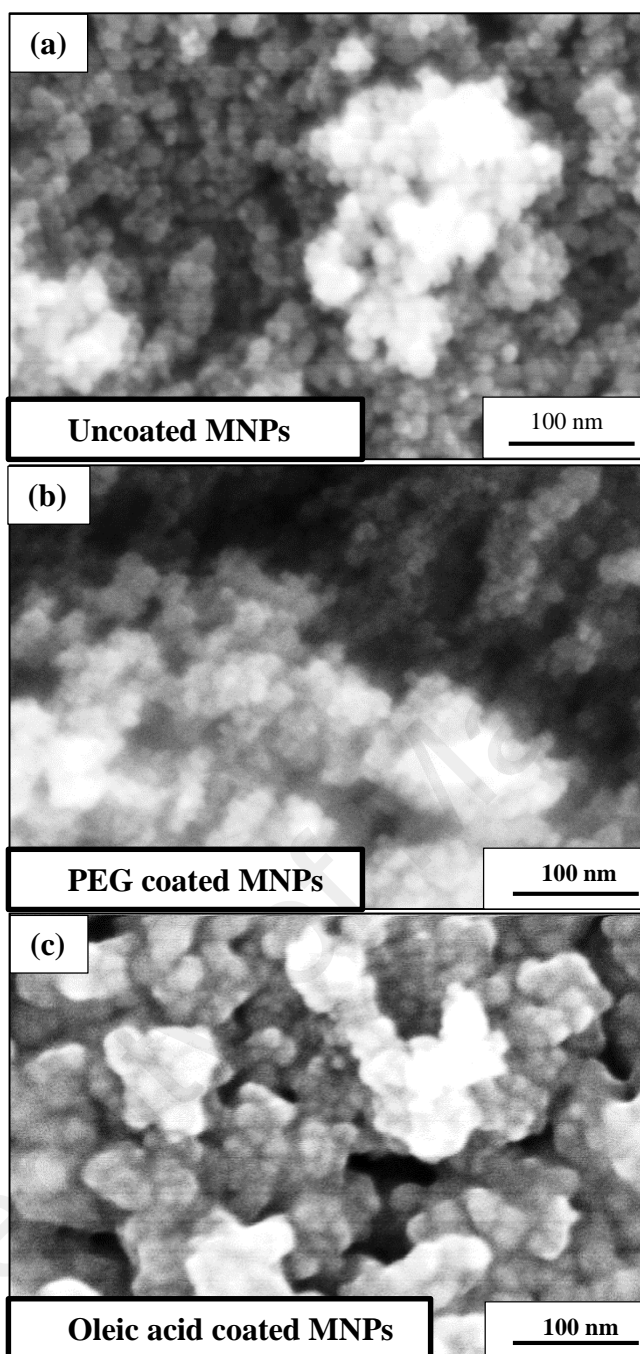
Figure 4.20: FESEM images of (a) uncoated MNPs, (b) PEG 600 coated MNPs and (c) Oleic acid coated MNPs at 250,000×magnification

The Energy dispersive x-ray spectroscopy (EDS) allowed the determination of the chemical composition of the samples. According to Martíñez-Mera et al. (2007), maghemite has an atomic stoichiometric ratio of 60.00 % O and 40.00 % Fe, while it is 43.00 % O and 57.00 % Fe in magnetite phase.

In this study, the uncoated MNPs obtained has an atomic stoichiometric ratio of 58.18 % O and 41.82 % Fe (Table 4.11). Moreover, by referring the O/Fe atomic ratio of the uncoated MNPs (1.39), it was closer to the theoretical atomic ratio for the magnetite (1.33) than maghemite (1.50). Thus, the EDS results confirmed that the prepared MNPs consist of high purity magnetite. As shown in Figure 4.21, the peaks at 0.8 keV, 6.3 keV, and 6.8 keV are related to the binding energies of Fe (Mahdavi et al., 2013). In addition, the existence of Oleic acid and PEG functionality on the surface of MNPs were confirmed by the peak at 0.2 keV, which correspond to C. It suggests that Fe, O and C are the main component in the coated MNPs.

Table 4.11: Elemental composition of MNPs

Sample	Element	Weight %	Atomic %	Atomic ratio
Magnetite (theoretical value)	O	27.52	57.00	1.33
	Fe	72.48	43.00	
Maghemite (theoretical value)	O	30.00	60.00	1.50
	Fe	70.00	40.00	
Uncoated MNPs	O	28.50	58.18	1.39
	Fe	71.50	41.82	
PEG 600 (1.0 g) coated MNPs	C	15.24	31.80	1.63
	O	26.99	42.28	
	Fe	57.77	25.92	
Oleic acid (1.2 g) coated MNPs	C	14.93	32.71	1.30
	O	23.16	38.11	
	Fe	61.91	29.18	
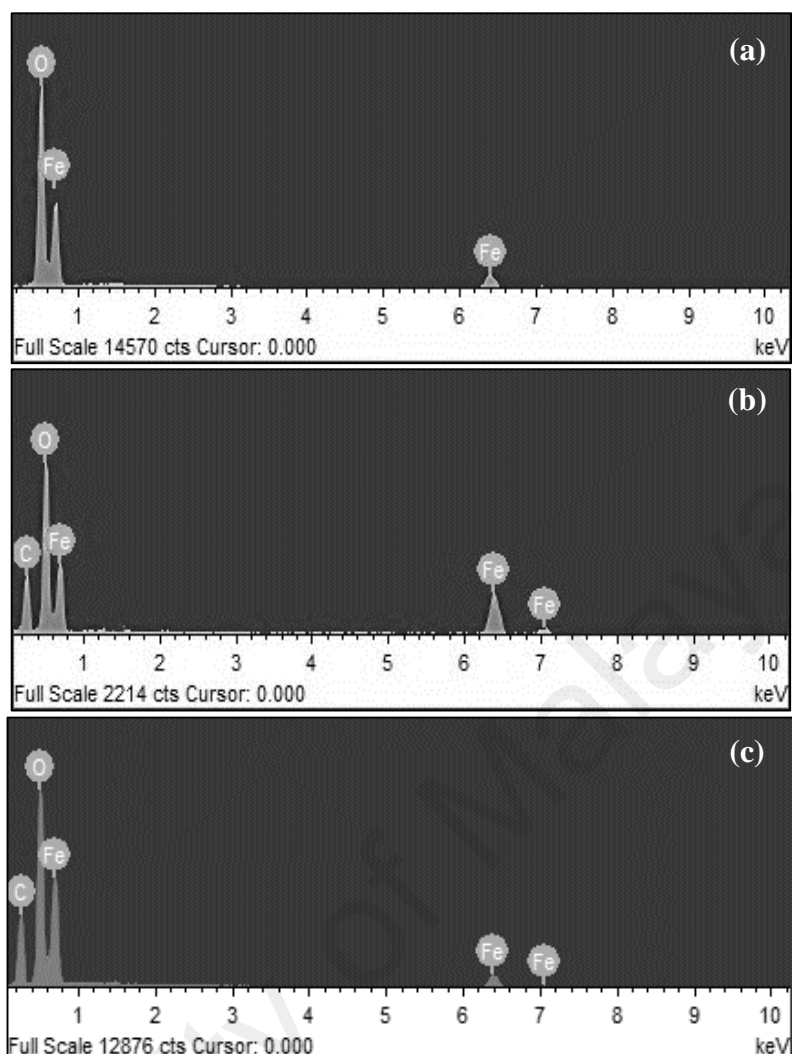
Figure 4.21: EDS spectra of (a) uncoated MNPs, (b) PEG coated MNPs, and (c) Oleic acid coated MNPs

Figure 4.22 shows the images obtained by high resolution transmission microscopy (HRTEM) for three samples, uncoated MNPs, PEG (1.0 g) coated MNPs and Oleic acid (1.2 g) coated MNPs. From Figure 4.22, round shaped particles were observed for the uncoated MNPs. According to Nyirő-Kósa et al. (2009), the shape changes correlated with the crystallite size and the samples with crystal size of smaller than ~25 nm is said to contain irregular and round shaped.

By the addition of PEG which acts as stabilizer and dispersing agent, MNPs produced are well-defined and had homogeneous shape with small particle size, about 14.12 nm ± 2.33 nm (Figure 4.22b). In the same ways, oleic acid is used to prevent the agglomeration

of MNPs. The smallest particle size was about 10.25 nm ± 3.05 nm (Figure 4.22c) while the average size of optimized uncoated MNPs was about 15.54 nm ± 3.50 nm (Figure 4.22a). The coating agent of PEG and oleic acid were not visible under HRTEM.
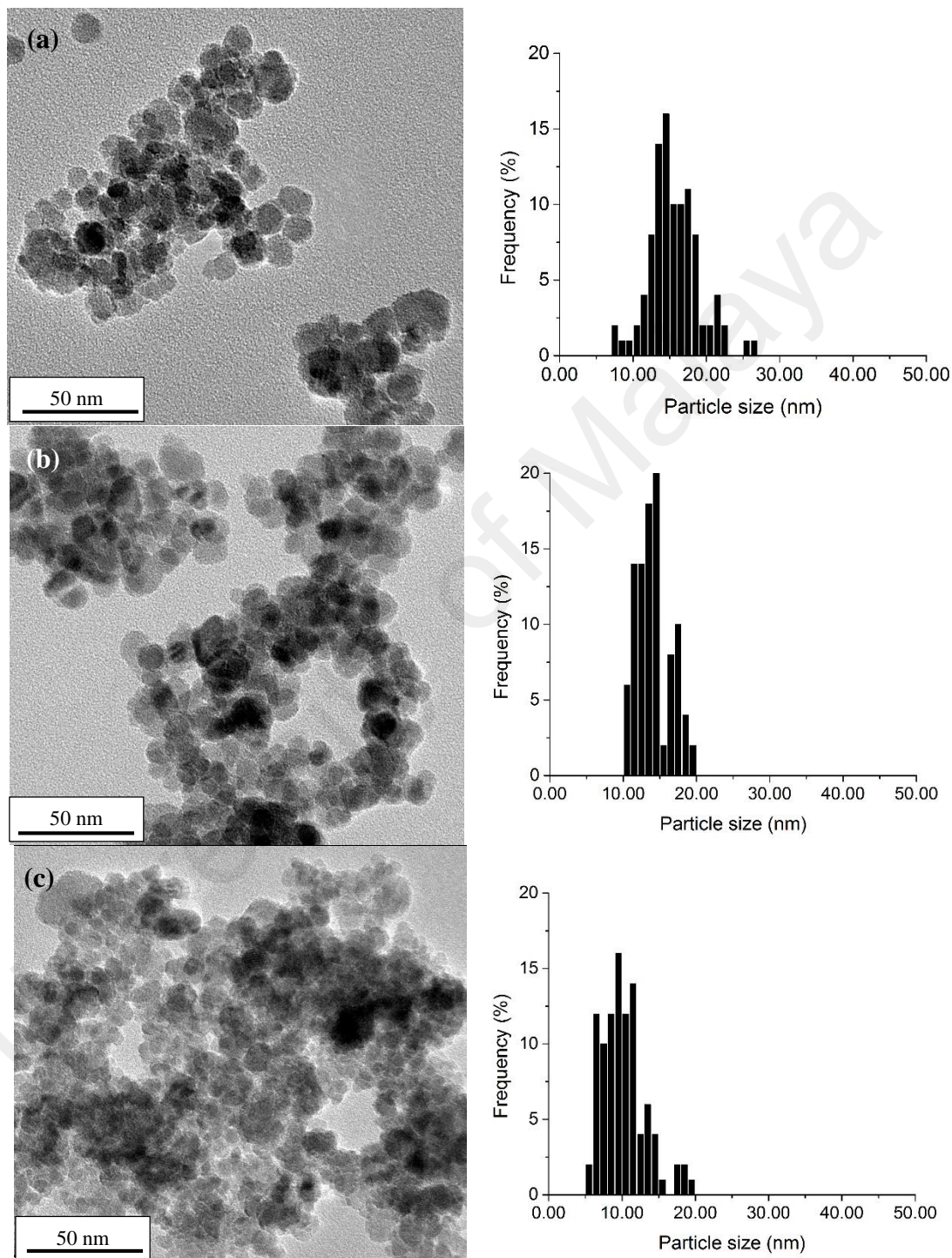
Figure 4.22: HRTEM images of (a) uncoated MNPs, (b) PEG 600 coated MNPs and (c) Oleic acid coated MNPs at 100,000× magnification

4.3.8　Magnetic Properties Measurement

Vibrating sampler magnetometer measurement of the magnetic properties of the samples at room temperature are shown in Table 4.12.

Table 4.12: Magnetic properties of uncoated MNPs, PEG coated MNPs and Oleic acid coated MNPs

Sample	Crystallite size (nm)	Saturation Magnetization, M_s (emu/g)	Coercivity, H_c (Oe)	Remanence, M_r (emu/g)
a) Uncoated				
Optimized uncoated	13.6	80.23	14.71	1.79
b) PEG 600				
0.6 g	12.3	66.56	4.55	0.52
0.8 g	11.9	65.01	3.95	0.40
1.0 g	10.7	64.12	4.75	0.50
2.0 g	10.4	63.76	4.45	0.45
3.0 g	9.3	63.24	4.05	0.40
c) Oleic acid				
0.3 g	10.4	68.55	8.57	1.07
0.6 g	10.4	65.16	6.47	0.80
0.9 g	10.3	64.65	4.41	0.52
1.2 g	9.7	54.53	2.98	0.31
1.5 g	9.5	51.61	3.11	0.29

From previous section, it can be clearly seen that the uncoated MNPs have saturation magnetization (Ms) of 80.23 emu/g at 10 kOe and a coercivity of 14.71 Oe, which are close to the bulk value of magnetite about 85−100 emu/g and 115−150 Oe, respectively. The Ms of PEG coated sample gradually decreased from 66.56 emu/g to 63.24 emu/g as the PEG loading amount increased from 0.6 g to 3.0 g. These values of saturation magnetization were much larger than the result reported by Anbarasu (2015) (51-62 emu/g). In addition, Anbarasu (2015) related the reduction of saturation magnetization of MNPs to the decreasing particle size. However, the existence of diamagnetic shell that encapsulated the MNPs might also be attributed to lower Ms values (Qu et al., 2010).
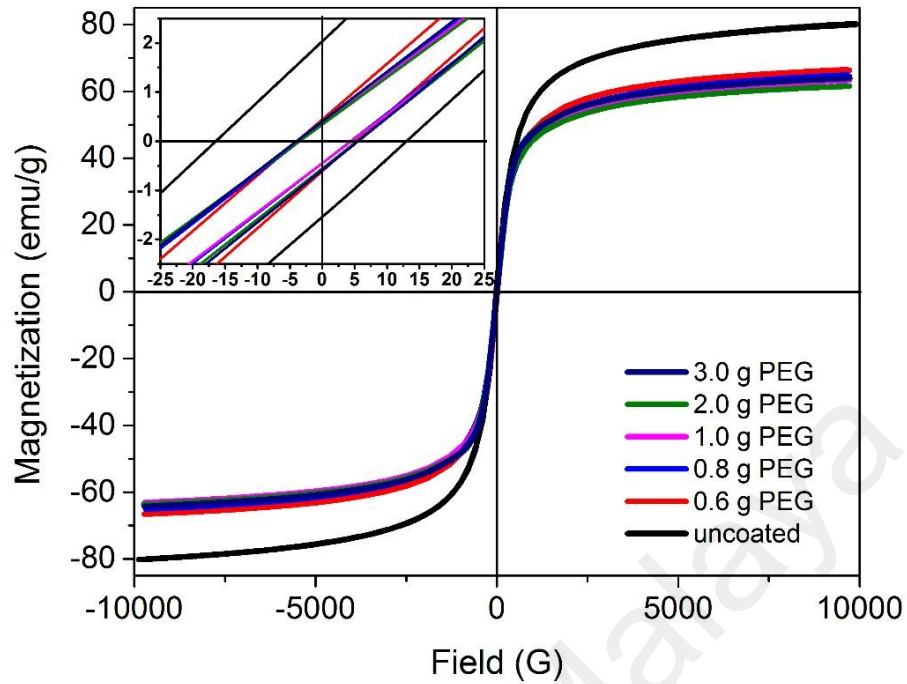
Figure 4.23: VSM hysteresis loop of the MNPs with different loading of PEG 600

Similarly, the saturation magnetization of MNPs decreased after the coating of oleic acid. It can be seen that the degree of reduction can be related to loading amount of oleic acid as the Ms decreased from 68.55 emu/g to 51.61 emu/g. In this case, the oleic acid coating layer, which protect the MNPs from oxidation, reduced the magnetic dipole-dipole interaction between the particles (Petcharoen & Sirivat, 2012). On overall, all of them showed superparamagnetic behaviour, with coercivity and remanence values less than 10 Oe and 2 emu/g, respectively.
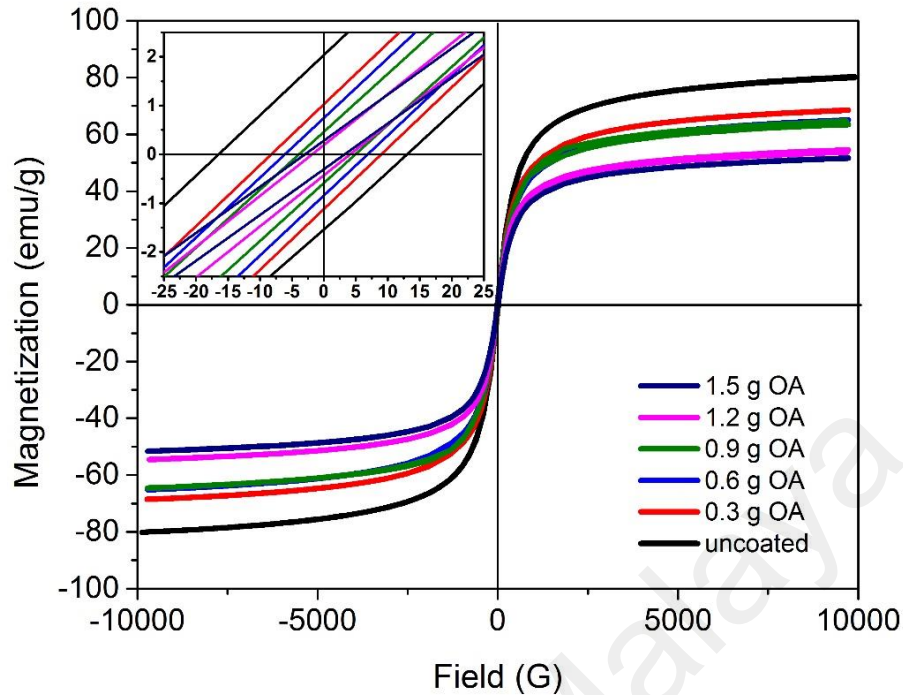
Figure 4.24: VSM hysteresis loop of the MNPs with different loading of oleic acid

4.4 Performance Studies of MNPs Loaded Nitrile Butadiene Rubber Latex Films

Based on previous discussion, oleic acid coated MNPs synthesized by *in situ* coating technique demonstrated a maximum colloidal stability. The colloidal suspension performance of oleic acid (1.2 g) coated MNPs was approximately 3 times higher (21 days) than the uncoated MNPs (3 days). Therefore, in the following studies, the as-synthesized oleic acid (1.2 g) coated MNPs with saturation magnetization of 54.53 emu/g was incorporated into the nitrile butadiene rubber latex compound to produce a nitrile butadiene rubber latex thin films. The aim of this section is to study the effect of MNPs on the tensile and magnetic properties of nitrile butadiene rubber films.

4.4.1   Tensile Properties

The effect of MNPs loading on the tensile properties of the nitrile butadiene rubber (NBR) latex films was shown in Table 4.13.

Table 4.13: Comparison of tensile properties between NBR and NBR/MNPs latex films

Tensile properties	NBR latex film	NBR/MNPs latex film
Modulus at 100 % (MPa)	1.833	1.388
Modulus at 300 % (MPa)	3.603	2.353
Modulus at 500 % (MPa)	7.904	4.420
Tensile Strength (MPa)	22.23	16.10
Elongation at break (%)	716.0	766.7

As shown in Table 4.13, the tensile strength, and modulus at 100 %, 300 % and 500 % of the NBR latex film reduced after the addition of MNPs. The incorporation of 5 part per hundred rubber (phr) of MNPs into NBR latex reduced the tensile strength from 22.23 MPa to 16.10 MPa, by 27.6 %. Similarly, the modulus at 100 %, 300 %, and 500 % reduced from 1.833 MPa, 3.603 MPa, 7.904 MPa to 1.388 MPa, 2.353 MPa, 4.420 MPa, respectively. In contrast, the elongation of NBR latex film increased from 716.0 % to 766.7 % after adding the MNPs. The non-reinforcing nature of MNPs was responsible for the drastic drop of tensile strength and modulus. The increased in elongation might due to the presence of excess oleic acid coated on the surface of MNPs (Figure 4.20c), which act as a plasticizer. The plasticizing effect of oleic acid is related to weak interaction between the MNPs and the NBR polymer matrix (Monticelli et al., 2012). Therefore, this result explained the lubricant effect of oleic acid on nitrile butadiene rubber latex film that significantly decreased the physical properties of latex film. In addition, plasticizer is not a popular additives for latex because they tend to migrate to the surface of a drying film even when they are compatible (Dzikowicz, 2014).
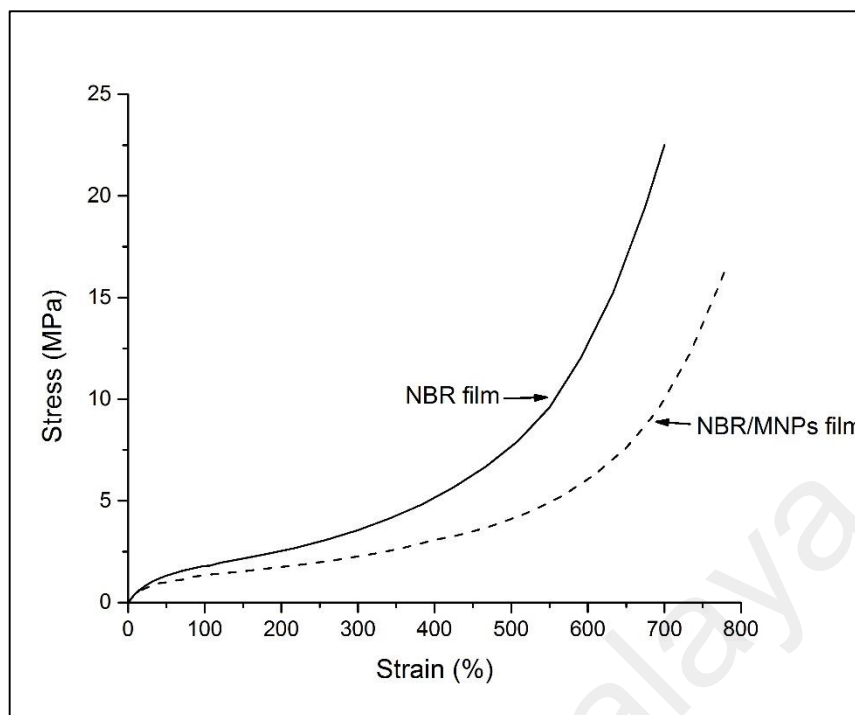
Figure 4.25: Stress strain curve of NBR and NBR/MNPs latex films

Figure 4.26 presents the field scanning electron (FESEM) micrograph of the tensile fractured surface of the tensile test samples at $2000\times$ magnification. NBR/MNPs latex film has a relatively rough fracture surface as compared to NBR latex film. This implies that the NBR latex film became more ductile after the addition of MNPs.
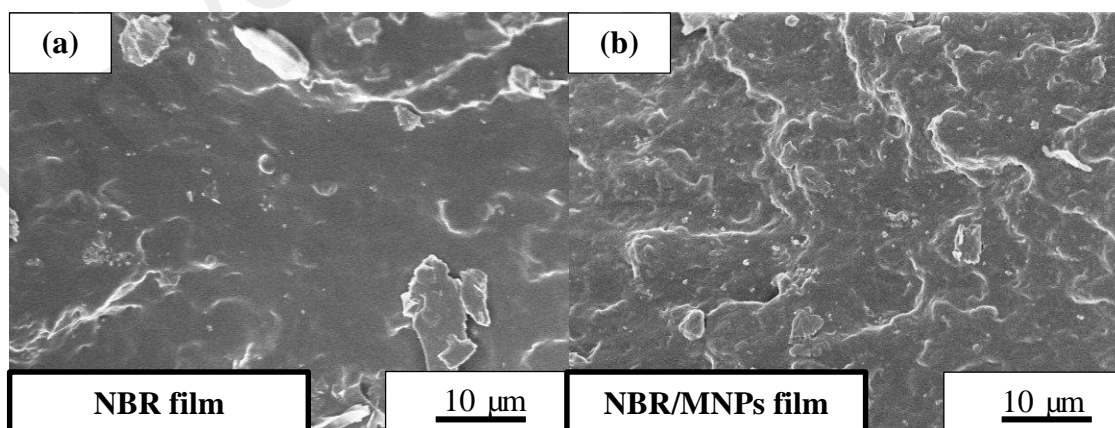
Figure 4.26: FESEM images of (a) NBR and (b) NBR/MNPs films tensile fractured surface ($2000\times$ magnification)

The dispersion of particle in the NBR latex was estimated based on the FESEM images of the tensile fractured surface. From Figure 4.27b, MNPs were poorly dispersed in the NBR matrix, as evidenced by the agglomeration of the MNPs within the nitrile butadiene rubber latex. These agglomerated clusters of MNPs not only reduced the contact between the NBR latex matrixes but also function as failure initiation sites which would lead to premature failure of materials (Thomas et al., 2013). Therefore, this result explained the poorer mechanical properties of nitrile butadiene rubber latex film after the addition of MNPs. However, the tensile properties of MNPs loaded nitrile butadiene rubber latex film are still in the acceptable range as the tensile properties of clean room and nitrile disposable glove available in market are in the range of 12-30 MPa (Phalen & Kee Wong, 2012). For this reason, oleic acid coated MNPs is the ideal candidate for metal detectable application.
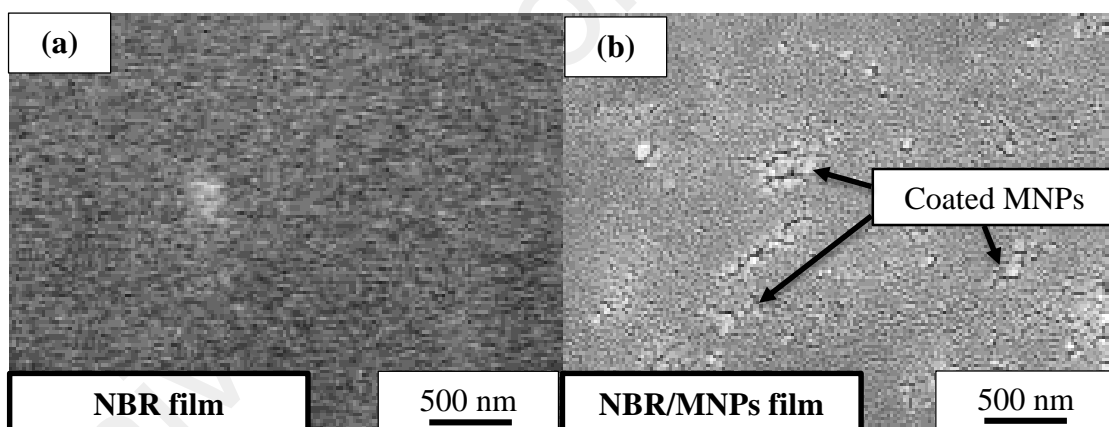
Figure 4.27: FESEM images of (a) NBR and (b) NBR/MNPs films tensile fractured surface (20,000 × magnification)

4.4.2 Thermogravimetric Analysis (TGA)

Thermogravimetric analysis has been carried out to understand thermal stability of the NBR/MNPs latex films. Typical weight loss thermogravimetry (TGA) curves of NBR and NBR/MNPs latex films are presented in Figure 4.28. As shown in Figure 4.28, the first weight loss of NBR latex film begins at 390.9 °C and reaches to maximum at 454.5

℃. However, the weight loss of NBR/MNPs latex film starts at 396 ℃ and reaches maximum at 456.7 ℃. This indicates that the NBR/MNPs latex film exhibited better thermal stability than that of NBR latex film.

Table 4.14: Measurement of degradation temperature and residue of NBR and NBR/MNPs latex films by TGA

Sample	Onset decomposition Temperature (℃)	Temperature at maximum weight loss (℃)	Residue (%)
NBR	390.9	454.5	10.90
NBR/MNPs	396.8	456.7	25.41

Table 4.14 summarizes the onset decomposition temperatures, temperature at maximum weight loss and residue of the samples at 800 ℃. The first weight loss was observed as a continuous weight loss starting at 390-397 ℃, which indicates the decomposition of the respective conducting polymer backbone and MNPs (Al‑Juaid et al., 2011). Besides, maximum thermal decomposition observed at 454-456 ℃ was due to the polymer matrix pyrolysis (Sagar et al., 2013). In addition, it is observed that the residue of NBR/MNPs latex film is higher than that of NBR latex film. The presence of residue at temperature above 500 ℃ might due to the presence of other compounding ingredients in the mix. At 800 ℃, 5 phr of MNPs incorporated in the nitrile butadiene rubber latex film has enhanced the thermal stability of the latex composites up to 33.1 % relative to the nitrile butadiene rubber latex film.
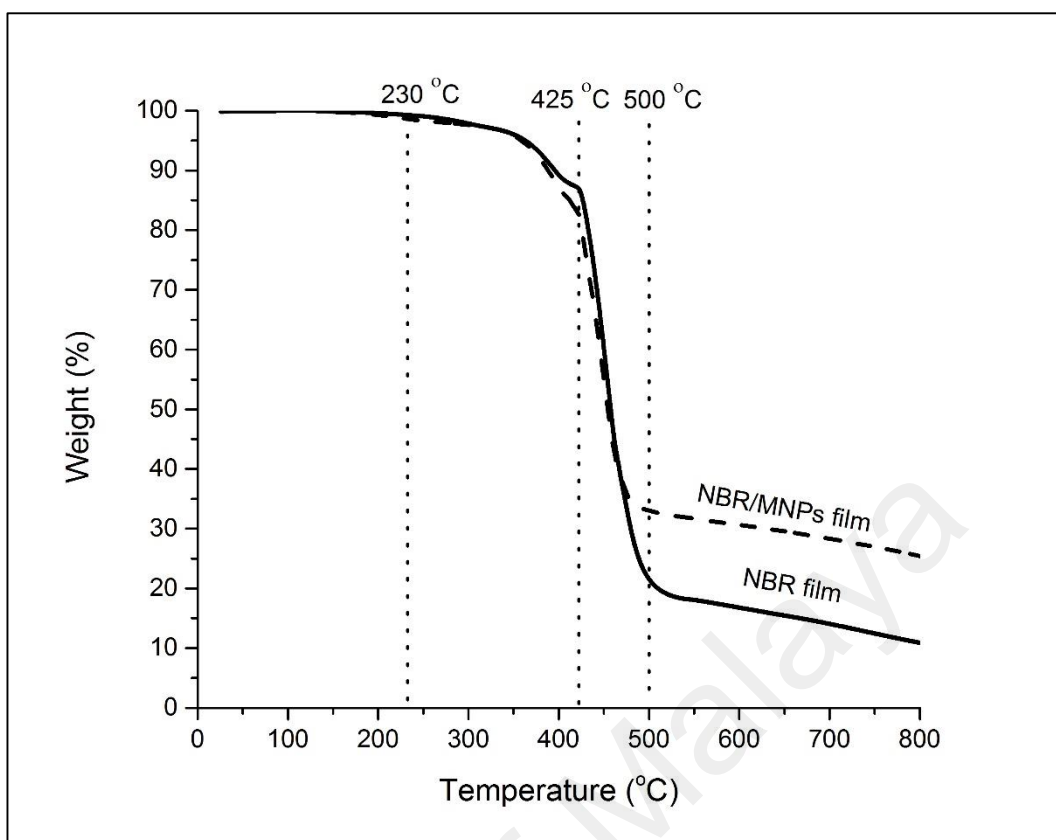
Figure 4.28: TGA curves of NBR and NBR/MNPs latex films

4.4.3 Magnetic Properties Measurement

Vibrating sampler magnetometer (VSM) measurement of NBR and NBR/MNPs latex films at room temperature are shown in Table 4.15. In order to prevent NBR films from sticking together, a dusting (talc) powder was applied on the surface of NBR latex films. After the removal of dusting powder, specimens were cut from the latex film and used to measure the magnetic properties of the films. These specimens were obtained from the positions shown in Figure 4.29.
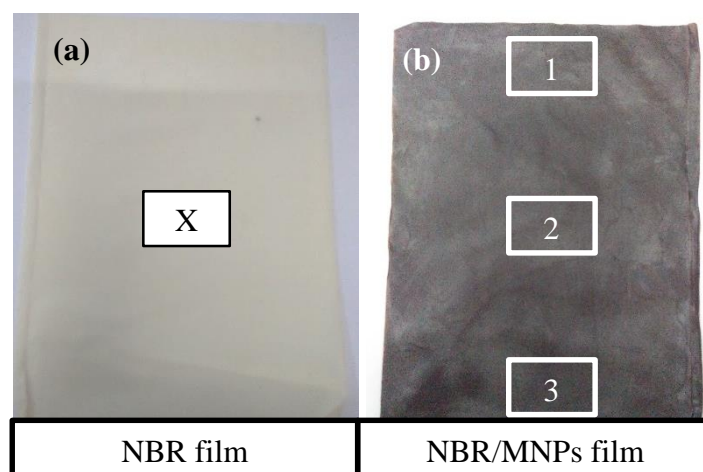
Figure 4.29: The specimens' location on (a) NBR film and (b) NBR/MNPs latex film

Table 4.15: Magnetic Properties of NBR and NBR/MNPs latex films

Magnetic Properties	NBR latex film	NBR/MNPs latex film			
		1	2	3	Average
Saturation Magnetization, M_s (emu/g)	0.19	1.83	1.85	1.87	1.85 ± 0.02
Coercivity, H_c (Oe)	44.97	5.78	4.85	4.02	4.88 ± 0.88
Remanence, M_r (emu/g)	8.64×10^{-3}	19.86×10^{-3}	20.08×10^{-3}	15.12×10^{-3}	18.35×10^{-3}

Significant different between hysteresis curves recorded for NBR and NBR/MNPs films can be seen in Figure 4.29. Based on Figure 4.29, NBR is a nonmagnetic material, which displayed diamagnetic behaviour (Reinholds et al., 2012). However, the NBR/MNPs latex film became a paramagnetic material, which does not retain the magnetic properties after the addition of superparamagnetic MNPs.

Table 4.15 shows the magnetic properties of NBR and NBR/MNPs latex films. From Table 4.15, higher values of saturation magnetization (Ms) and remanence (Mr) and lower values of the coercivity are the characteristic of NBR/MNPs latex film in comparison to NBR latex film. The Ms and Mr of NBR increased from 0.19 emu/g, 8.64×10^{-3} emu/g to 1.85 ± 0.02 emu/g, 18.35×10^{-3} emu/g, respectively. On the other hand, the coercivity, H_c

of the NBR latex film decreased from 44.97 Oe to 4.88 ± 0.88 Oe with the addition of MNPs. The presented results show the substantial difference between the NBR and NBR/MNPs latex films (Figure 4.30). It is obvious that NBR latex film incorporated with MNPs has improved magnetic properties. Lastly, when comparing between the sample position in NBR/MNPs latex film, it was found that the difference in Ms is only 0.04 emu/g or 2.2 %. This indicates that the MNPs was distributed homogeneously in NBR latex film and therefore it is appropriate for the metal detectable glove application.
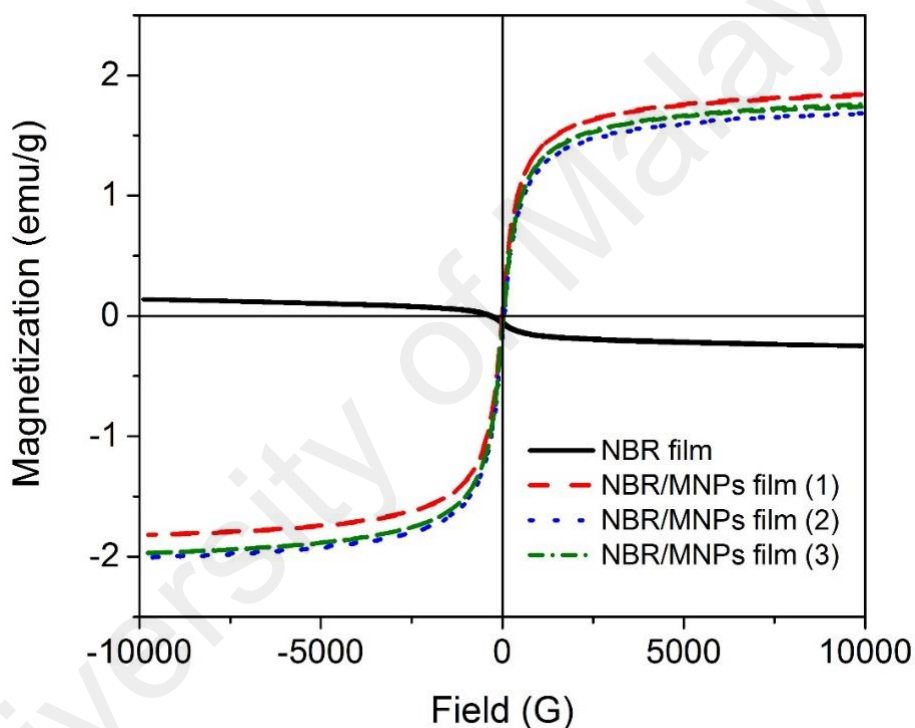
Figure 4.30: VSM hysteresis loop of NBR and NBR/MNPs films

CHAPTER 5: CONCLUSSION AND RECOMMENDATIONS

5.1   Conclusion

In summary, the objectives set for the thesis have been achieved. In the first stage of research study, the optimized conditions of reaction parameters to achieve optimum saturation magnetization were determined. The conclusions attained in this part of research work are summarised. Magnetite nanoparticles (<50 nm) with high saturation magnetization (80.23 emu/g) was successfully synthesized via precipitation technique by co-precipitating iron (II) and iron (III) chloride salts in the presence of 3.00 M ammonium hydroxide at final pH 9.5. Besides, it was found that increasing the final pH and total iron salts concentration increased saturation magnetization, but variation of ammonium hydroxide concentration did not change the saturation magnetization. In contrast, the saturation magnetization decreased from 80.23 emu/g to 64.83 emu/g when the addition rate of ammonium hydroxide increased from 5 ml/min to 20 ml/min. The reduction of saturation magnetization for these samples were due to decrease in the crystallite size of the particles with increasing addition rate.

Additional continuous efforts were made to further improve the dispersion stability of magnetite nanoparticles in aqueous media by modifying the magnetite surface using surface modifiers (e.g., polyethylene glycol, oleic acid) to generate an effective repulsive force in between particles. The zeta potential values of MNPs were reduced from -29.8 mV (uncoated) to -45.8 mV (PEG coated MNPs), and -58.1 mV (oleic acid coated MNPs). This indicates that stability of MNPs was improved by the coating. In addition, it was found that the resultant MNPs incorporated with oleic acid demonstrated a maximum stability in nitrile butadiene rubber latex. This colloidal suspension performance was approximately 7 times higher (21 days) than the uncoated MNPs and PEG coated MNPs (3 days). This is mainly attributed to the formation of oleate secondary

layer in the bilayer oleic acid coated MNPs that enabled the MNPs to be well dispersed in polar (acrylonitrile) and non-polar (butadiene) parts of the building block of nitrile latex. It is proposed that the bilayer oleic acid coated MNPs could be dispersed in polar and non-polar medium through adjusting the pH of medium by ammonium hydroxide.

Next, the oleic acid (1.2 g) coated MNPs were mixed into NBR latex during latex compounding process. Then, NBR/MNPs films were formed through a series of dipping process. It was found that the tensile strength, and modulus of the NBR latex film was reduced after the addition of MNPs. In contrast, the elongation of NBR latex film increased from 716.0 % to 766.7 % after adding the oleic acid coated MNPs. This increased of elongation might due to the presence of excess oleic acid coated on the surface of MNPs, which act as a plasticizer. Although the oleic acid coated MNPs loaded nitrile butadiene rubber latex film showed poorer mechanical properties but the tensile properties of these latex film are still in the acceptable range (12-30 MPa). For this reason, oleic acid coated MNPs is the ideal candidate for metal detectable application. TGA has been carried out to understand thermal stability of the NBR/MNPs latex film. It was found that the NBR/MNPs latex film exhibited better thermal stability than that of NBR latex film. 5 phr of oleic acid coated MNPs incorporated in the NBR latex film has enhanced the thermal stability of the latex composites up to 33.1 % relative to the NBR latex film. Lastly, the NBR latex film incorporated with oleic acid coated MNPs has improved magnetic properties. The saturation magnetization and remanence of NBR latex film increased from 0.19 emu/g, and 8.64×10^{-3} emu/g to 1.85 emu/g, and 18.35×10^{-3} emu/g, respectively. The coercivity of the NBR latex film decreased from 44.97 Oe to 4.88 Oe with the addition of oleic acid coated MNPs. In addition, it was found that oleic acid coated MNPs distributed homogenously throughout the nitrile butadiene rubber latex film. For this reason, oleic acid coated MNPs is the appropriate candidate to produce metal detectable glove.

5.2   Recommendations for Future Work

Magnetite glove that could be detected by using a standard metal detector is a key target for the development of effective inspection system for food and drug industry. In this work, the use of oleic acid coated MNPs was found to achieve 1.85 emu/g of magnetism for the nitrile butadiene rubber latex film. However, the mechanical properties of nitrile butadiene rubber latex film was impaired by the addition of oleic acid coated MNPs. Hence, the development of novel magnetic nano-materials is still a challenge. Several suggestions and recommendations should be noteworthy for further developments were proposed as follows:

i. To investigate the influences of oxidation on the magnetic properties and composition of MNPs. Oxidation reaction that trigger the phase transformation of magnetite phase of MNPs into maghemite phase will reduced the magnetic property of MNPs and further shorten the storage life of MNPs.

ii. The usage of others unsaturated fatty acid (e.g., palmitic-oleic acid, and linoleic acid) as coating agent in order to study their compatibility with NBR latex and influences on the magnetic properties of MNPs. These unsaturated fatty acid which fall under the same category with oleic acid could be used to stabilize the MNPs in NBR latex.

iii. To increase the concentration (phr) of coated MNPs in NBR latex compound to achieve higher magnetic properties. The saturation magnetization of NBR films could be improved by using higher loading amount of detectable agent, magnetite nanoparticles (MNPs).

REFERENCES

Ahn, T., Kim, J. H., Yang, H.-M., Lee, J. W., & Kim, J.-D. (2012). Formation pathways of magnetite nanoparticles by coprecipitation method. *The Journal of Physical Chemistry C, 116*(10), 6069-6076.

Akbarzadeh, A., Samiei, M., & Davaran, S. (2012). Magnetic nanoparticles: preparation, physical properties, and applications in biomedicine. *Nanoscale research letters, 7*(1), 1-13.

Al-Juaid, S. S., El-Mossalamy, E.-s. H., M Arafa, H., Al-Ghamdi, A. A., Daiem, A., & El-Tantawy, F. (2011). Novel functional nitrile butadiene rubber/magnetite nano composites for NTCR thermistors application. *Journal of Applied Polymer Science, 121*(6), 3604-3612.

Alex Duthie, P. E. (2012). *It's About Time: The Illusion of Einstein's Time Dilation Explained*: iUniverse.

Anbarasu, M., Anandan, M., Chinnasamy, E., Gopinath, V. & Balamurugan, K. (2015). Synthesis and characterization of polyethylene glycol (PEG) coated Fe_3O_4 nanoparticles by chemical co-precipitation method for biomedical applications. *Spectrochimica Acta Part A: Molecular and Biomolecular Spectroscopy*, 536-539. doi: 10.1016/j.saa.2014.07.059

Andrade, Â. L., Souza, D. M., Pereira, M. C., Fabris, J. D., & Domingues, R. Z. (2010). pH effect on the synthesis of magnetite nanoparticles by the chemical reduction-precipitation method. *Química Nova, 33*(3), 524-527.

Arabi, H., & Asnaashari Eivari, H. (2014). Applying a suitable route for preparation Fe_3O_4 nanoparticles by Ammonia and investigation of their physical and different magnetic properties. *International Journal of Nano Dimension, 5*, 297-303.

Astruc, D. (2008). *Nanoparticles and Catalysis*: Wiley.

Bakshi, A. V. B. U. A. (2009). *Field Theory*: Technical Publications.

Barrera, C., Herrera, A. P., & Rinaldi, C. (2009). Colloidal dispersions of monodisperse magnetite nanoparticles modified with poly (ethylene glycol). *Journal of Colloid and Interface Science, 329*(1), 107-113.

Baumgartner, J., Dey, A., Bomans, P. H., Le Coadou, C., Fratzl, P., Sommerdijk, N. A., & Faivre, D. (2013). Nucleation and growth of magnetite from solution. *Nature materials, 12*(4), 310-314.

Bibi, I. (2012). Mineralogy and Acid Neutralisation Mechanisms in Inland Acid Sulfate Environments.

Bououdina, M. (2014). *Handbook of Research on Nanoscience, Nanotechnology, and Advanced Materials*: IGI Global.

Brullot, W., Reddy, N. K., Wouters, J., Valev, V. K., Goderis, B., Vermant, J., & Verbiest, T. (2012). Versatile ferrofluids based on polyethylene glycol coated iron oxide nanoparticles. *Journal of Magnetism and Magnetic Materials, 324*(11), 1919-1925. doi: http://dx.doi.org/10.1016/j.jmmm.2012.01.032

Cao, G., & Wang, Y. (2011). *Nanostructures and Nanomaterials: Synthesis, Properties, and Applications*: World Scientific.

Carraher, C. E. (2012). *Introduction to polymer chemistry*: CRC press.

Carter, C. B., & Norton, M. G. (2007). *Ceramic materials: science and engineering*: Springer Science & Business Media.

Cheng, W., Tang, K., Qi, Y., Sheng, J., & Liu, Z. (2010). One-step synthesis of superparamagnetic monodisperse porous Fe_3O_4 hollow and core-shell spheres. *Journal of Materials Chemistry, 20*(9), 1799-1805.

Chikazumi, S., & Graham, C. D. (2009). *Physics of Ferromagnetism 2e*: OUP Oxford.

Cho, E. J., Holback, H., Liu, K. C., Abouelmagd, S. A., Park, J., & Yeo, Y. (2013). Nanoparticle characterization: state of the art, challenges, and emerging technologies. *Molecular pharmaceutics, 10*(6), 2093-2110.

Chourpa, I., Douziech-Eyrolles, L., Ngaboni-Okassa, L., Fouquenet, J.-F., Cohen-Jonathan, S., Soucé, M., … Dubois, P. (2005). Molecular composition of iron oxide nanoparticles, precursors for magnetic drug targeting, as characterized by confocal Raman microspectroscopy. *Analyst, 130*(10), 1395-1403.

Coey, J., Venkatesan, M., & Xu, H. (2013). Introduction to Magnetic Oxides. *Functional Metal Oxides: New Science and Novel Applications*, 1-49.

Connor, D. (2001). Gloves: Google Patents.

Corot, C., Robert, P., Idée, J.-M., & Port, M. (2006). Recent advances in iron oxide nanocrystal technology for medical imaging. *Advanced drug delivery reviews, 58*(14), 1471-1504.

Darminto, D., Cholishoh, M. N., Perdana, F. A., Baqiya, M. A., Cahyono, M. Y., & Triwikantoro, T. (2011). *Preparing Fe$_3$O$_4$ Nanoparticles from Fe^{2+} Ions Source by Co-precipitation Process in Various pH.* Paper presented at the American Institute of Physics Conference Series.

De Ricci, S., & Phalip, P. (1999). Contamination of food, drugs, agriculture product by tear of gloves which are made of plastic or elastomers and ferrite conducting and magnetic particles are uniformaly distributed through out the gloves, detected by metal detector: Google Patents.

Dzikowicz, B. (2014). Latexes. Retrieved from http://www.vanderbiltchemicals.com/e e_content/Documents/Technical/Latex_Bob_Dzikowicz_Web.pdf.

Estelrich, J., Sánchez-Martń, M. J., & Busquets, M. A. (2015). Nanoparticles in magnetic resonance imaging: from simple to dual contrast agents. *International journal of nanomedicine, 10*, 1727.

Faraji, M., Yamini, Y., & Rezaee, M. (2010). Magnetic nanoparticles: synthesis, stabilization, functionalization, characterization, and applications. *Journal of the Iranian Chemical Society, 7*(1), 1-37.

Feng, Y.-Z., & Sun, D.-W. (2012). Application of hyperspectral imaging in food safety inspection and control: a review. *Critical reviews in food science and nutrition, 52*(11), 1039-1058.

Filippousi, M., Angelakeris, M., Katsikini, M., Paloura, E., Efthimiopoulos, I., Wang, Y., …Van Tendeloo, G. (2014). Surfactant Effects on the Structural and Magnetic Properties of Iron Oxide Nanoparticles. *The Journal of Physical Chemistry C, 118*(29), 16209-16217.

Fojtik, A., Horák, D., Piksová, K., Trung, T. Q., & Škereň, T. (2009). Magnetic and Metallic Nanoparticles for Biomedical Application. *Nano Con.*

Gaca, M., & Zaborski, M. (2016). The properties of elastomers obtained with the use of carboxylated acrylonitrile-butadiene rubber and new crosslinking substances. *Polimery, 61*.

Galpaya, D., & Dona, G. (2009). *Processing Characteristics, Physical Properties and Morphological Study of Polypropylene (Pp)/Recycled Acrylonitrile Butadiene Rubber (rNBR) Blends [TN1-997].* Universiti Sains Malaysia.

Gao, J., Gu, H., & Xu, B. (2009). Multifunctional magnetic nanoparticles: design, synthesis, and biomedical applications. *Accounts of chemical research, 42*(8), 1097-1107.

García-Jimeno, S., & Estelrich, J. (2013). Ferrofluid based on polyethylene glycol-coated iron oxide nanoparticles: Characterization and properties. *Colloids and Surfaces A: Physicochemical and Engineering Aspects, 420*(0), 74-81. doi: http://dx.doi.org/10.1016/j.colsurfa.2012.12.022.

Getzlaff, M. (2007). *Fundamentals of Magnetism*: Springer Berlin Heidelberg.

Gnanaprakash, G., Mahadevan, S., Jayakumar, T., Kalyanasundaram, P., Philip, J., & Raj, B. (2007). Effect of initial pH and temperature of iron salt solutions on formation of magnetite nanoparticles. *Materials chemistry and Physics, 103*(1), 168-175.

Gnanaprakash, G., Philip, J., Jayakumar, T., & Raj, B. (2007). Effect of digestion time and alkali addition rate on physical properties of magnetite nanoparticles. *The Journal of Physical Chemistry B, 111*(28), 7978-7986.

Guimarães, A. P. (2009). *Principles of Nanomagnetism*: Springer Berlin Heidelberg.

Haddock, J. N., Hotchkiss, P., Jones, S., Kim, P., Kippelen, B., Marder, S., & Perry, J. (2006). Coated metal oxide nanoparticles and methods for producing same: WO Patent App. PCT/US2006/018,543.

Haff, R. P., & Toyofuku, N. (2008). X-ray detection of defects and contaminants in the food industry. *Sensing and Instrumentation for Food Quality and Safety, 2*(4), 262-273.

Hasany, S., Ahmed, I., Rajan, J., & Rehman, A. (2012). Systematic review of the preparation techniques of iron oxide magnetic nanoparticles. *Nanoscience and Nanotechnology, 2*(6), 148-158.

Haw, C., Mohamed, F., Chia, C., Radiman, S., Zakaria, S., Huang, N., & Lim, H. (2010). Hydrothermal synthesis of magnetite nanoparticles as MRI contrast agents. *Ceramics International, 36*(4), 1417-1422.

He, Y., & Traina, S. (2007). Transformation of magnetite to goethite under alkaline pH conditions. *Clay Minerals, 42*(1), 13-19.

Hong, R., Feng, B., Chen, L., Liu, G., Li, H., Zheng, Y., & Wei, D. (2008). Synthesis, characterization and MRI application of dextran-coated Fe_3O_4 magnetic nanoparticles. *Biochemical Engineering Journal, 42*(3), 290-300.

Hórvölgyi, Z., & Kiss, E. (2008). *Colloids for Nano- and Biotechnology*: Springer.

Huang, L., & Nishinari, K. (2001). Interaction between poly (ethylene glycol) and water as studied by differential scanning calorimetry. *Journal of Polymer Science Part B: Polymer Physics, 39*(5), 496-506.

Ida, N. (2015). *Engineering Electromagnetics*: Springer International Publishing.

Indira, T., & Lakshmi, P. (2010). Magnetic nanoparticles—A review. *Int. J. Pharm. Sci. Nanotechnol, 3*(3), 1035-1042.

Ingram, D. R., Kotsmar, C., Yoon, K. Y., Shao, S., Huh, C., Bryant, S. L., … Johnston, K. P. (2010). Superparamagnetic nanoclusters coated with oleic acid bilayers for stabilization of emulsions of water and oil at low concentration. *Journal of Colloid and Interface Science, 351*(1), 225-232. doi: http://dx.doi.org/10.1016/j.jcis.2010.06.048

Issa, B., Obaidat, I. M., Albiss, B. A., & Haik, Y. (2013). Magnetic nanoparticles: surface effects and properties related to biomedicine applications. *International journal of molecular sciences, 14*(11), 21266-21305.

Jangid, S., Barbar, S. K., & Roy, M. (2014). Structural, Electrical and Magnetic Properties of Pure and Substituted $BiFeO_3$ Multiferroics *Biosensors Nanotechnology* (pp. 433-505): John Wiley & Sons, Inc.

Jaramillo Tabares, B., Zuleta Gil, A. A., & Jaramillo Isaza, F. (2009). Effects of the synthetic method on the particle size and purity of magnetite. *Revista Facultad de Ingeniería Universidad de Antioquia*(50), 9-16.

Jayanthi, S. A., Sukanya, D., Pragasam, A. J. A., & Sagayaraj, P. (2013). The influence of PEG 20,000 concentration on the size control and magnetic properties of functionalized bio-compatible magnetic nanoparticles.

Jayanthy, T., & Sankaranarayanan, P. (2005). Measurement of dry rubber content in latex using microwave technique.

Jiang, W., Lai, K.-L., Hu, H., Zeng, X.-B., Lan, F., Liu, K.-X., …Gu, Z.-W. (2011). The effect of $[Fe^{3+}]/[Fe^{2+}]$ molar ratio and iron salts concentration on the properties of superparamagnetic iron oxide nanoparticles in the water/ethanol/toluene system. *Journal of Nanoparticle Research, 13*(10), 5135-5145.

John, R. (2014). *Solid State Physics,1e*: McGraw Hill Education.

Kandpal, N., Sah, N., Loshali, R., Joshi, R., & Prasad, J. (2014). Co-precipitation method of synthesis and characterization of iron oxide nanoparticlea. *J. Sci. Ind. Res, 73*, 87-90.

Karaagac, O., & Kockar, H. (2012). Effect of Synthesis Parameters on the Properties of Superparamagnetic Iron Oxide Nanoparticles. *Journal of superconductivity and novel magnetism, 25*(8), 2777-2781. doi: 10.1007/s10948-011-1264-8.

Karaagac, O., Kockar, H., Beyaz, S., & Tanrisever, T. (2010). A simple way to synthesize superparamagnetic iron oxide nanoparticles in air atmosphere: iron ion concentration effect. *Magnetics, IEEE Transactions on, 46*(12), 3978-3983.

Karaagac, O., Kockar, H., & Tanrisever, T. (2011). Properties of Iron Oxide Nanoparticles Synthesized at Different Temperatures. *Journal of superconductivity and novel magnetism, 24*(1-2), 675-678.

Kent, J. A. (2010). *Kent and Riegel's Handbook of Industrial Chemistry and Biotechnology: Vol. 1*: Springer Science & Business Media.

Khalil, M. I. (2015). Co-precipitation in aqueous solution synthesis of magnetite nanoparticles using iron(III) salts as precursors. *Arabian Journal of Chemistry, 8*(2), 279-284. doi: http://dx.doi.org/10.1016/j.arabjc.2015.02.008.

Klingender, R. C. (2008). *Handbook of Specialty Elastomers*: CRC Press.

Koetz, J., & Kosmella, S. (2007). *Polyelectrolytes and Nanoparticles*: Springer Berlin Heidelberg.

Laurent, S., Forge, D., Port, M., Roch, A., Robic, C., Vander Elst, L., & Muller, R. N. (2008). Magnetic iron oxide nanoparticles: synthesis, stabilization, vectorization, physicochemical characterizations, and biological applications. *Chemical reviews, 108*(6), 2064-2110.

Laurent, S., & Mahmoudi, M. (2011). Superparamagnetic iron oxide nanoparticles: promises for diagnosis and treatment of cancer. *International journal of molecular epidemiology and genetics, 2*(4), 367.

Lévy, F., Sheikin, I., Grenier, B., & Huxley, A. D. (2005). Magnetic field-induced superconductivity in the ferromagnet URhGe. *Science, 309*(5739), 1343-1346.

Lewis, S. (2014). 4 Primary Technologies For Detecting Foreign Bodies In Food. Retrieved May 11, 2015, from http://www.foodonline.com/doc/primary-technologies-for-detecting-foreign-bodies-in-food-0001.

Li, D., Jiang, D., Chen, M., Xie, J., Wu, Y., Dang, S., & Zhang, J. (2010). An easy fabrication of monodisperse oleic acid-coated Fe3O4 nanoparticles. *Materials Letters, 64*(22), 2462-2464. doi: http://dx.doi.org/10.1016/j.matlet.2010.08.025.

Li, J., Li, D., Zhang, S., Cui, H., & Wang, C. (2011). Analysis of the factors affecting the magnetic characteristics of nano-Fe3O4 particles. *Chinese Science Bulletin, 56*(8), 803-810.

Li, Y.-S., Church, J. S., & Woodhead, A. L. (2012). Infrared and Raman spectroscopic studies on iron oxide magnetic nano-particles and their surface modifications. *Journal of Magnetism and Magnetic Materials, 324*(8), 1543-1550.

Liang, J., Li, H., Yan, J., & Hou, W. (2014). Demulsification of Oleic-Acid-Coated Magnetite Nanoparticles for Cyclohexane-in-Water Nanoemulsions. *Energy & Fuels, 28*(9), 6172-6178.

Lipinski, T. M., & Tang, C. K. (2010). Thin, smooth nitrile rubber gloves: Google Patents.

Lipták, B. G. (2013). *Process Control: Instrument Engineers' Handbook*: Elsevier Science.

Liu, Y., Sellmyer, D. J., & SHINDO, D. (2008). *Handbook of Advanced Magnetic Materials: Vol 1. Nanostructural Effects. Vol 2. Characterization and Simulation. Vol 3. Fabrication and Processing. Vol 4. Properties and Applications*: Springer US.

Lowrie, W. (2007). *Fundamentals of Geophysics* (2nd ed.): Cambridge University Press.

Lu, L., Zhai, Y., Zhang, Y., Ong, C., & Guo, S. (2008). Reinforcement of hydrogenated carboxylated nitrile–butadiene rubber by multi-walled carbon nanotubes. *Applied Surface Science, 255*(5, Part 1), 2162-2166. doi: http://dx.doi.org/10.1016/j.apsusc.2008.07.052.

Lucas, D. M., Barclay, J., Loo, L. Y., Lai, H. M., & Wong, S. W. (2006). Magnetically detectable latex articles: Google Patents.

Mahdavi, M., Ahmad, M. B., Haron, M. J., Namvar, F., Nadi, B., Rahman, M. Z. A., & Amin, J. (2013). Synthesis, surface modification and characterisation of biocompatible magnetic iron oxide nanoparticles for biomedical applications. *Molecules, 18*(7), 7533-7548.

Mahl, D., Diendorf, J., Meyer-Zaika, W., & Epple, M. (2011). Possibilities and limitations of different analytical methods for the size determination of a bimodal dispersion of metallic nanoparticles. *Colloids and Surfaces A: Physicochemical and Engineering Aspects, 377*(1), 386-392.

Mahmoudi, M., Sant, S., Wang, B., Laurent, S., & Sen, T. (2011). Superparamagnetic iron oxide nanoparticles (SPIONs): development, surface modification and applications in chemotherapy. *Advanced drug delivery reviews, 63*(1), 24-46.

Maity, D., & Agrawal, D. (2007). Synthesis of iron oxide nanoparticles under oxidizing environment and their stabilization in aqueous and non-aqueous media. *Journal of Magnetism and Magnetic Materials, 308*(1), 46-55.

Majewski, P., & Thierry, B. (2007). Functionalized magnetite nanoparticles—synthesis, properties, and bio-applications. *Critical Reviews in Solid State and Materials Sciences, 32*(3-4), 203-215.

Marghussian, V. (2015). *Nano-Glass Ceramics: Processing, Properties and Applications*: Elsevier Science.

Martínez-Mera, I., Espinosa-Pesqueira, M., Pérez-Hernández, R., & Arenas-Alatorre, J. (2007). Synthesis of magnetite (Fe_3O_4) nanoparticles without surfactants at room temperature. *Materials Letters, 61*(23), 4447-4451.

Mascolo, M. C., Pei, Y., & Ring, T. A. (2013). Room Temperature Co-Precipitation Synthesis of Magnetite Nanoparticles in a Large pH Window with Different Bases. *Materials, 6*(12), 5549-5567.

Meerod, S., Tumcharern, G., Wichai, U., & Rutnakornpituk, M. (2008). Magnetite nanoparticles stabilized with polymeric bilayer of poly (ethylene glycol) methyl ether–poly (ε-caprolactone) copolymers. *Polymer, 49*(18), 3950-3956.

Merhari, L. (2009). *Hybrid nanocomposites for nanotechnology*: Springer.

Mittal, V. (2012). *Characterization Techniques for Polymer Nanocomposites*: Wiley.

Mohapatra, M., & Anand, S. (2010). Synthesis and applications of nano-structured iron oxides/hydroxides–a review. *International Journal of Engineering, Science and Technology, 2*(8).

Monticelli, O., Bocchini, S., Frache, A., Cozza, E. S., Cavalleri, O., & Prati, L. (2012). Simple method for the preparation of composites based on PA6 and partially exfoliated graphite. *Journal of Nanomaterials, 2012*, 25.

Mornet, S., Portier, J., & Duguet, E. (2005). A method for synthesis and functionalization of ultrasmall superparamagnetic covalent carriers based on maghemite and dextran. *Journal of Magnetism and Magnetic Materials, 293*(1), 127-134.

Murad, E., & Cashion, J. (2011). *Mössbauer Spectroscopy of Environmental Materials and Their Industrial Utilization*: Springer US.

Na, C. W., Han, D. S., Park, J., Jo, Y., & Jung, M.-H. (2006). Ferrimagnetic Mn2SnO4 nanowires. *Chemical communications*(21), 2251-2253.

Nano ferroferric oxide/natural composite magnetic latex and preparation method thereof. (2013).

NCPS Board. (2013). *Handbook on Rubber and Allied Products (with Project Profiles) (Photostate Edition)*: NIIR PROJECT CONSULTANCY SERVICES.

Neville, J. (2013). *Mosby's Pharmacy Technician Lab Manual Revised Reprint*: Elsevier Health Sciences.

Nigam, S., Barick, K., & Bahadur, D. (2011). Development of citrate-stabilized Fe_3O_4 nanoparticles: conjugation and release of doxorubicin for therapeutic applications. *Journal of Magnetism and Magnetic Materials, 323*(2), 237-243.

Nogi, K., Hosokawa, M., Naito, M., & Yokoyama, T. (2012). *Nanoparticle Technology Handbook*: Elsevier.

Nyirő-Kόsa, I., Nagy, D. C., & Pόsfai, M. (2009). Size and shape control of precipitated magnetite nanoparticles. *European Journal of Mineralogy, 21*(2), 293-302.

Petcharoen, K., & Sirivat, A. (2012). Synthesis and characterization of magnetite nanoparticles via the chemical co-precipitation method. *Materials Science and Engineering: B, 177*(5), 421-427.

Phalen, R. N., & kee Wong, W. (2012). Tensile Properties and Integrity of Clean Room and Low-Modulus Disposable Nitrile Gloves: A Comparison of Two Dissimilar Glove Types. *Annals of occupational hygiene, 56*(4), 450-457.

Poole Jr, C. P., Farach, H. A., Creswick, R. J., & Prozorov, R. (2007). 2 - Phenomenon of Superconductivity. In C. P. Poole, H. A. Farach & R. J. C. Prozorov (Eds.), *Superconductivity (Second Edition)* (pp. 23-59). Amsterdam: Academic Press.

Qi, H., Chen, Q., Wang, M., Wen, M., & Xiong, J. (2009). Study of self-assembly of octahedral magnetite under an external magnetic field. *The Journal of Physical Chemistry C, 113*(40), 17301-17305.

Qu, J., Liu, G., Wang, Y., & Hong, R. (2010). Preparation of Fe3O4–chitosan nanoparticles used for hyperthermia. *Advanced Powder Technology, 21*(4), 461-467. doi: http://dx.doi.org/10.1016/j.apt.2010.01.008.

Rafiee, E., Ataei, A., Nadri, S., Joshaghani, M., & Eavani, S. (2014). Combination of palladium and oleic acid coated-magnetite particles: Characterization and using in Heck coupling reaction with magnetic recyclability. *Inorganica Chimica Acta, 409, Part B*(0), 302-309. doi: http://dx.doi.org/10.1016/j.ica.2013.09.042.

Rajan, D. K., & Lekkala, J. (2013). Coercivity weighted Langevin magnetisation; A new approach to interpret superparamagnetic and nonsuperparamagnetic behaviour in single domain magnetic nanoparticles. *arXiv preprint arXiv:1308.2517*.

Rajasekar, R., Heinrich, G., Das, A., & Das, C. K. (2009). Development of SBR-nanoclay composites with epoxidized natural rubber as compatibilizer. *Journal of Nanotechnology, 2009*.

Ramesan, M. T., Alex, R., & Khanh, N. V. (2005). Studies on the cure and mechanical properties of blends of natural rubber with dichlorocarbene modified styrene–

butadiene rubber and chloroprene rubber. *Reactive and Functional Polymers, 62*(1), 41-50. doi: http://dx.doi.org/10.1016/j.reactfunctpolym.2004.08.002.

Ramimoghadam, D., Bagheri, S., & Hamid, S. B. A. (2014). Progress in electrochemical synthesis of magnetic iron oxide nanoparticles. *Journal of Magnetism and Magnetic Materials, 368*, 207-229.

Ramimoghadam, D., Bagheri, S., & Hamid, S. B. A. (2015). Stable Monodisperse Nanomagnetic Colloidal Suspensions: An overview. *Colloids and Surfaces B: Biointerfaces*.

Rapra Technology Limited. (2006). *Latex 2006: Frankfurt, Germany, 24-25 January 2006*: Rapra Technology.

Reinholds, I., Kalkis, V., & Maksimovs, R. D. (2012). The effect of ionizing radiation and magnetic field on deformation properties of high density polyethylene/acrylonitrile-butadiene composites. *Journal of Chemistry and Chemical Engineering, 6*(3), 242-249.

Ries, B. (2014). What food processors should know: metal detection vs. X-ray inspection. from http://www.thermoscientific.com/content/dam/tfs/ATG/EPD/EPD%20Do cuments/Application%20&%20Technical%20Notes/Checkweighers,%20Metal %20Detectors,%20and%20X%20ray%20Inspection/Metal%20Detectors/CAD-WhitePaper-MD-vs-XR.pdf.

Roca, A. G., Marco, J. F., Morales, M. d. P., & Serna, C. J. (2007). Effect of nature and particle size on properties of uniform magnetite and maghemite nanoparticles. *The Journal of Physical Chemistry C, 111*(50), 18577-18584.

Roch, A., Gossuin, Y., Muller, R. N., & Gillis, P. (2005). Superparamagnetic colloid suspensions: water magnetic relaxation and clustering. *Journal of Magnetism and Magnetic Materials, 293*(1), 532-539.

Roff, W. J., & Scott, J. R. (2013). *Fibres, Films, Plastics and Rubbers: A Handbook of Common Polymers*: Elsevier Science.

Sagar, S., Iqbal, N., Maqsood, A., & Javaid, U. (2013). Thermogravimetric, differential scanning calorimetric and experimental thermal transport study of MWCNT/NBR nanocomposites. *Journal of thermal analysis and calorimetry, 114*(1), 161-167

.

Santoyo Salazar, J., Perez, L., de Abril, O., Truong Phuoc, L., Ihiawakrim, D., Vazquez, M., …Pourroy, G. (2011). Magnetic iron oxide nanoparticles in 10− 40 nm range:

composition in terms of magnetite/maghemite ratio and effect on the magnetic properties. *Chemistry of Materials, 23*(6), 1379-1386.

Saraswathy, A., Nazeer, S. S., Nimi, N., Arumugam, S., Shenoy, S. J., & Jayasree, R. S. (2014). Synthesis and characterization of dextran stabilized superparamagnetic iron oxide nanoparticles for in vivo MR imaging of liver fibrosis. *Carbohydrate polymers, 101*, 760-768.

Sattler, K. D. (2010). *Handbook of Nanophysics: Principles and Methods*: Taylor & Francis.

Schmid, G. (2011). *Nanoparticles: From Theory to Application*: Wiley.

Schodek, D. L., Ferreira, P., & Ashby, M. F. (2009). *Nanomaterials, Nanotechnologies and Design: An Introduction for Engineers and Architects*: Elsevier Science.

Schwertmann, U., & Cornell, R. M. (2008). *Iron oxides in the laboratory*: John Wiley & Sons.

Singh, D., McMillan, J. M., Liu, X.-M., Vishwasrao, H. M., Kabanov, A. V., Sokolsky-Papkov, M., & Gendelman, H. E. (2014). Formulation design facilitates magnetic nanoparticle delivery to diseased cells and tissues. *Nanomedicine, 9*(3), 469-485.

Slavov, L., Abrashev, M., Merodiiska, T., Gelev, C., Vandenberghe, R., Markova-Deneva, I., & Nedkov, I. (2010). Raman spectroscopy investigation of magnetite nanoparticles in ferrofluids. *Journal of Magnetism and Magnetic Materials, 322*(14), 1904-1911.

Smolkova, I. S., Kazantseva, N. E., Parmar, H., Babayan, V., Smolka, P., & Saha, P. (2015). Correlation between coprecipitation reaction course and magneto-structural properties of iron oxide nanoparticles. *Materials chemistry and Physics, 155*(0), 178-190. doi: http://dx.doi.org/10.1016/j.matchemphys.2015.02.022.

Sonvico, F., Dubernet, C., Colombo, P., & Couvreur, P. (2005). Metallic colloid nanotechnology, applications in diagnosis and therapeutics. *Current pharmaceutical design, 11*(16), 2091-2105.

Spaldin, N. A. (2010). *Magnetic materials: fundamentals and applications*: Cambridge University Press.

Starov, V. M. (2011). *Nanoscience: Colloidal and Interfacial Aspects*: CRC Press.

Superior Glove Works ltd. (n.d.). Metal-Detectable Blue Vinyl Disposable Gloves. Retrieved May 6, 2015, from http://www.superiorglove.com/Keep_ Kleen_Disposable_Vinyl_Gloves_C112.html.

Tai, M., Lai, C., Hamid, S., Suppiah, D., Lau, K., Yehya, W., … Lim, Y. (2014). Facile synthesis of magnetite iron oxide nanoparticles via precipitation method at different reaction temperatures. *Materials Research Innovations, 18*(S6), S6-470-S476-473.

Tajabadi, M., & Khosroshahi, M. (2012). Effect of Alkaline Media Concentration and Modification of Temperature on Magnetite Synthesis Method Using $FeSO_4/NH_4OH$.

Tartaj, P., Morales, M. P., Veintemillas-Verdaguer, S., Gonzalez-Carreño, T., & Serna, C. J. (2006). Chapter 5 Synthesis, Properties and Biomedical Applications of Magnetic Nanoparticles. *Handbook of magnetic materials, 16*, 403-482.

Thomas, S., Chan, C. H., Pothen, L. A., Joy, J., & Maria, H. (2013). *Natural Rubber Materials: Volume 2: Composites and Nanocomposites*: Royal Society of Chemistry.

Tombacz, E., Majzik, A., Horvat, Z., & Illes, E. (2006). Magnetite in aqueous medium: coating its surface and surface coated with it. *Romanian Reports in physics, 58*(3), 281.

Umut, E. (2013). Surface Modification of Nanoparticles Used in Biomedical Applications.

Utkan, G., Sayar, F., Batat, P., Ide, S., Kriechbaum, M., & Pişkin, E. (2011). Synthesis and characterization of nanomagnetite particles and their polymer coated forms. *Journal of Colloid and Interface Science, 353*(2), 372-379. doi: http://dx.doi.org/10.1016/j.jcis.2010.09.081.

Varanda, L. C., Júnior, M. J., & Júnior, W. B. (2011). *Magnetic and multifunctional magnetic nanoparticles in nanomedicine: challenges and trends in synthesis and surface engineering for diagnostic and therapy applications*: INTECH Open Access Publisher.

Vetter, T., Iggland, M., Ochsenbein, D. R., Hänseler, F. S., & Mazzotti, M. (2013). Modeling nucleation, growth, and Ostwald ripening in crystallization processes: a comparison between population balance and kinetic rate equation. *Crystal Growth & Design, 13*(11), 4890-4905.

Vikram, S., Dhakshnamoorthy, M., Vasanthakumari, R., Rajamani, A., Rangarajan, M., & Tsuzuki, T. (2015). Tuning the Magnetic Properties of Iron Oxide Nanoparticles by a Room-Temperature Air-Atmosphere (RTAA) Co-Precipitation Method. *Journal of Nanoscience and Nanotechnology, 15*(5), 3870-3878.

Wahajuddin, S. A. (2012). Superparamagnetic iron oxide nanoparticles: magnetic nanoplatforms as drug carriers. *International journal of nanomedicine, 7*, 3445.

Wang, C. Y., Hong, J. M., Chen, G., Zhang, Y., & Gu, N. (2010). Facile method to synthesize oleic acid-capped magnetite nanoparticles. *Chinese Chemical Letters, 21*(2), 179-182.

Weston, S. (2014). Foreign body detection in food manufacture. Retrieved May 11, 2015, from http://www.foodbev.com/news/foreign-body-detection-in-food-manufactu#.VUiGtSGeDGc.

Whelan, A. (2012). *Polymer Technology Dictionary*: Springer Netherlands.

Williams, D. (2014). *Essential biomaterials science*: Cambridge University Press.

Wu, W., He, Q., & Jiang, C. (2009). Magnetic iron oxide nanoparticles: synthesis and surface functionalization strategies. *ChemInform, 40*(24), i.

Wu, W., Wu, Z., Yu, T., Jiang, C., & Kim, W.-S. (2015). Recent progress on magnetic iron oxide nanoparticles: synthesis, surface functional strategies and biomedical applications. *Science and Technology of Advanced Materials, 16*(2), 023501.

Yang, J., Zou, P., Yang, L., Cao, J., Sun, Y., Han, D., … Kong, X. (2014). A comprehensive study on the synthesis and paramagnetic properties of PEG-coated Fe3O4 nanoparticles. *Applied Surface Science, 303*, 425-432. doi: http://dx.doi.org/10.1016/j.apsusc.2014.03.018.

Yang, K., Peng, H., Wen, Y., & Li, N. (2010). Re-examination of characteristic FTIR spectrum of secondary layer in bilayer oleic acid-coated Fe 3 O 4 nanoparticles. *Applied Surface Science, 256*(10), 3093-3097.

Yue-Jian, C., Juan, T., Fei, X., Jia-Bi, Z., Ning, G., Yi-Hua, Z., … Liang, G. (2010). Synthesis, self-assembly, and characterization of PEG-coated iron oxide nanoparticles as potential MRI contrast agent. *Drug Development and Industrial Pharmacy, 36*(10), 1235-1244.

Zhang, L., He, R., & Gu, H.-C. (2006). Oleic acid coating on the monodisperse magnetite nanoparticles. *Applied Surface Science, 253*(5), 2611-2617.

Zhao, D.-L., Teng, P., Xu, Y., Xia, Q.-S., & Tang, J.-T. (2010). Magnetic and inductive heating properties of Fe3O4/polyethylene glycol composite nanoparticles with core–shell structure. *Journal of Alloys and Compounds, 502*(2), 392-395. doi: http://dx.doi.org/10.1016/j.jallcom.2010.04.177.

Zhao, F., Zhang, B., & Feng, L. (2012). Preparation and magnetic properties of magnetite nanoparticles. *Materials Letters, 68*(0), 112-114. doi: http://dx.doi.org/10.10 16/j.matlet.2011.09.116.

LIST OF PUBLICATIONS AND PAPERS PRESENTED

i.   Tai, M.F., Lai, C.W., S.B.A. Hamid, Suppiah, D.D., Lau, K.S., Yehya, W.A. ... & Lim, Y.S., Facile synthesis of magnetite iron oxide nanoparticles via precipitation method at different reaction temperatures. *Materials Research Innovations 2014; 18*(S6), S6-470-S6-473.

APPENDIX A: Published Paper (MATERIALS RESEARCH INNOVATIONS)

Facile synthesis of magnetite iron oxide nanoparticles via precipitation method at different reaction temperatures

M. F. Tai, C. W. Lai, S. B. A. Hamid[*], D. D. Suppiah, K. S. Lau, W. A. Yehya, N. M. Julkapli, W. H. Lee and Y. S. Lim

The nano-scale magnetite iron oxide particles have been synthesised by a facile precipitation method. Magnetite iron oxide nanoparticles were synthesised in a bath with electrolytes composed of 0·10 M of iron (II) chloride with 0·45 M of sodium hydroxide at different reaction temperatures under oxidising environment. In the present study, the influence of reaction temperatures (30, 45 and 80°C) on the morphology, particle size and crystallinity of the iron oxide particles were investigated in detail. Based on the Malvern Zetasizer analysis, the iron oxide particles with variable size from ~250 to ~70 nm could be achieved when increasing the reaction temperature up to 80°C. The magnetite phase of iron oxide particles was determined by using X-ray diffraction analysis. In addition, field emission scanning electron microscopy micrographs were further affirmed that our synthesised iron oxide particles were in nano-scale with a spherical shape. It was found that the high reaction temperature is helpful in controlling the formation of uniform magnetite iron oxide nanoparticles.

Keywords: Magnetite, Iron oxide particles, Precipitation, Particle size, Reaction temperature

Introduction

Today, development and design of nano-scale materials have gained a lot of attention because mechanical, chemical, electrical, optical, magnetic, electro-optical and magneto-optical properties of these materials are different from their bulk properties and depend on the particle size.[1] In this manner, magnetite iron oxide has exhibited great potential for their applications as catalytic materials,[2,3] wastewater treatment adsorbents,[4,5] pigments,[6] flocculants, coatings,[7] gas sensors, magnetic recording devices, magnetic data storage devices,[8] magnetic resonance imaging[9] and medicine applications.[10] Iron oxide nanoparticles have been comprehensively studied because of their non-toxicity, biocompatibility,[11] superparamagnetism, high coercivity and low Curie temperature properties. Several synthesis procedures have been developed for preparing magnetite nanoparticles, such as chemical co-precipitation,[12] sol–gel[13] and hydrothermal.

The precipitation technique is the simplest and most efficient chemical route to obtain iron oxide particles. However, it has difficulty in the control of particle size, size distribution and sometimes simultaneous the presence of different iron oxide phases such as magnetite and maghemite.[14,15] A wide variety of experimental factors such as pH, temperature, Fe^{2+}/Fe^{3+} molar ratio and stirring velocity affect the synthesis of iron oxide nanoparticles and their properties. In this study, a simple and efficient one-step precipitation method is reported to study the influence of reaction temperatures (30, 45 and 80°C) on the morphology, particle size and crystallinity of the iron oxide particles synthesised.

Experimental procedure

Ferrous chloride tetrahydrate ($FeCl_2 \cdot 4H_2O$, Sigma ≥99%) and sodium hydroxide (NaOH, Sigma ≥97·0%) were used for the synthesis of iron oxide nanoparticles. All chemicals used were of reagent grade and without further purification. The aqueous solution was prepared by dissolving 2·00 wt-% of $FeCl_2$ in 100 mL deionised water. Subsequently, 0·45 M of NaOH solution was added at a speed of 1·0 mL min^{-1} into the solution under vigorous stirring to reach a final pH 12. These reactions were carried in air medium for three different temperatures, i.e. 30, 45, and 80°C. It was observed that the solution became black because of the formation of Fe_3O_4 particles. The resultant black precipitate was isolated by centrifugation at 7000 rev min^{-1} and then removed by decantation. The precipitate was rinsed three times with deionised water and then dried in an oven at 50°C for 12 hours. Microstructure properties of

Nanotechnology & Catalysis Research Centre (NANOCAT), 3rd Floor, Block A, Institute of Postgraduate Studies (IPS), University of Malaya, 50603 Kuala Lumpur, Malaysia

*Corresponding author, email sharifahbee@um.edu.my

APPENDIX B: Raw data obtained from Universal Testing Machine

NBR film		NBR/MNPs film	
Strain (%)	Stress (MPa)	Strain (%)	Stress (MPa)
0	0.0020	0	0.0022
8.303	0.3909	6.611	0.2986
14.998	0.6214	14.996	0.5443
23.333	0.8479	23.333	0.7190
31.667	1.0300	31.667	0.8483
40.000	1.1715	40.000	0.9496
48.333	1.2922	48.333	0.9798
56.667	1.3993	56.667	1.0574
65.000	1.4899	68.000	1.1142
73.333	1.5748	73.333	1.1208
81.666	1.6474	81.666	1.2498
90.000	1.7186	90.000	1.2916
98.333	1.7859	98.333	1.3297
106.67	1.8076	106.67	1.3683
115.00	1.9089	115.00	1.401
123.33	1.9696	123.33	1.4337
131.67	2.0299	131.16	1.4677
140.00	2.0857	140.00	1.5019
175.00	2.3437	148.33	1.5315
216.67	2.6668	156.67	1.5655
258.33	3.0763	191.67	1.7073
300.00	3.5618	233.33	1.8942
341.67	4.1392	275.00	2.1134
383.33	4.8236	316.67	2.3676
425.00	5.6667	358.33	2.6799
466.67	6.6856	400.00	3.0741
508.33	7.9213	441.67	3.3968
550.00	9.5886	483.33	3.8710
591.67	12.083	525.00	4.4644
633.33	15.272	566.67	5.2376
675.00	19.476	608.33	6.2692
700.00	22.503	650.00	7.5884
701.67	1.0677	691.67	9.4813
705.00	-0.006	733.33	12.255
		775.00	15.961
		781.67	16.643
		783.33	1.8214
		786.67	0.0200

APPENDIX C: Thickness of tensile specimens

Sample		Thickness (mm)			
		1	2	3	Average
NBR Film	1	0.07	0.07	0.06	0.0633
	2	0.07	0.07	0.07	0.0700
	3	0.07	0.08	0.06	0.0700
	4	0.06	0.07	0.08	0.0700
	5	0.07	0.07	0.07	0.0700
NBR/MNPs Film	1	0.08	0.07	0.07	0.0733
	2	0.07	0.07	0.07	0.0700
	3	0.07	0.06	0.07	0.0667
	4	0.07	0.07	0.07	0.0700
	5	0.08	0.07	0.07	0.0733